POLITECNICO DI TORINO

College of Mechanical, Aerospace, Automotive and Production Engineering

Master's Degree in Aerospace Engineering

Master's Degree Thesis

Use of Lattice Structures in Topological Optimization – Case Study: PLT-2 TIR Mission Space Telescope Frame

Supervisors

Prof. Paolo Maggiore

Ing. Mauro Michetti

Ing. Emanuele Capuano

Ing. Alessandro Amorese

Candidate

Elia Starna

April 2021

"Earth is the cradle of humanity, but one cannot remain in the cradle forever."

~ Konstantin E. Tsiolkovsky

Acknowledgements

First of all, I would like to thank Maria Rita Stoppa, head of human resources at Leonardo S.p.A., who allowed this project to come to life. If it wasn't for her and the opportunity she gave me, I probably wouldn't be where I am now with a year of internship and ready for the world of work. Together with her I thank all the Leonardo and Altair engineers who followed me during this year and so Emanuele Capuano, Guglielmo Landi, Romano Iazurlo, Salvatore Cristofori, but above all Mauro Michetti and Alessandro Amorese who helped me in difficult times and taught me what it means to work and to do it together with a team of other people.

Then I have to say a few words for my family who supported me in this long journey that was the Politecnico, from the first day I came in Turin. I want to say thanks to my mother Paola and my father Paolo, who gave me strength every time I needed them and who believed in me even when I did not. Together with them also my little brother Davide, with whom we have always encouraged each other. They have been and will always be my strength. An important mention to the rest of my family too: my uncles, aunts, grandmothers and cousins.

Very important are also my friends, who made evenings and free moments unforgettable. I speak of my friends from Marche, whom I have known for many years now and we are like brothers and sisters, and of my new Turin friends, thanks to which these six years have passed very quickly between aperitifs, brunches, disco nights and evenings in company. In particular, I thank my friends from Cupramontana, so Donata, Irene, Mara and my best friend Arianna, my university mates Gianmarco and Federica, my dear friends Valentino and Leonardo and all the other: Federico B. and his sister Marta, Federico M., Andrea, Claudio, Manfredi, Francesco, Lucia, Riccardo, Alice and Laura.

Finally, I just have to thank my univeristy supervisor Paolo Maggiore and the Politecnico of Turin for teaching me so much despite the anxieties and difficulties experienced in the last six years.

Abstract

In the engineering sector, for some years now, it has been common to look for the best shape of a structure in terms of high mechanical performance. To do this, it is used what is commonly called optimization, that is a process through which a certain analysis software implements certain parameters set by the user and calculates, with regard to these constraints, the optimal shape of the structure considered, reorganizing the distribution of the material.

Aim of this thesis is to apply the optimization criteria to the mechanical frame of a space telescope. The initial geometry of PLATiNO Space Telescope, used for a preliminary feasibility study, has been used as case study with the objective to identify an optimized design solution in term of minimum mass and maximum stiffness (i.e.: maximize resonant frequencies).

The design process can summarized in the following steps:

- Analyse the original design to identify its structural performances (stress levels under the design static load and resonant frequencies); these performances have been used as baseline to assess the behaviour of the optimized design;

- Identify a working volume, the design space, that is the volume that the optimization tool can use to calculate the optimized geometry; verify the performance of the obtained solution and implement changes to reach the solution as much as possible. These changes consist in the introduction of manufacturing constraints to take into account the production process too;

- Fill the identified geometry with different type of lattice; optimization software identifies the best lattice solution, through the insertion of constraints and shape controls;

- Design the external ply to fully connect the lattice structure with the non-design space; structural performances of the optimized solution have been analysed and compared with the baseline to identify improvements;

- Find a way to transfer the optimized two-dimensional lattice geometry to a three-dimensional CAD or STL to manage additive manufacturing process.

The design activities have been carried out by the use of software tools from Altair HyperWorks 2020 suite:

- HyperMesh, a high-fidelity finite element modeling tool (a so called pre-post tool);
- Optistruct, an optimization-enabled structural FEM solver;
- HyperView, a comprehensive CAE Post-processing and Engineering Data Visualization

and from Altair Inspire 2020, that allows geometry creation and modification, as well as simplified FEM analysis.

All the activities relevant to this thesis, have been carried out in collaboration with personnel from Electronic Division of Leonardo S.p.A. and with the support of Altair staff.

Table of Contents

List of Tables

List of Figures

Acronyms

AM Additive Manufacturing

AoI Area of Interest

CAD Computer Aided Design

CAE Computer Aided Engineering

CFD Computational Fluid Dynamics

DoF Degree of Freedom

ET Evapotranspiration

FE Finite Element

FEM Finite Element Method

FP Focal Plane

GCOS Global Climate Observing System

GSD Ground Sample Distance

ID Identification Card

LB Lower Bound

LT Lattice Type

MOO Multi Objective Optimization

NVH Noise, Vibration and Harshness

SM Shutter's Motor

SST Sea Surface Temperature

STL Standard Triangle Language

TCL Tool Command Language

TIR Thermal Infrared

UB Upper Bound

UHI Urban Heat Island

VNIR visible and Near-Infrared

Chapter 1

State of Art

1.1 The Importance of Design in the Engineering Sector

First of all, let's start with what is meant by the word "Design": it aims to reconcile the technical, functional and economic requirements of a given product, so that the resulting shape is the synthesis of this design activity [1]. One of the tasks of an engineering designer is to come up with a design that is functionally "satisfying". This is often difficult to do, as there are so many different ways to define the "satisfaction" of a product. Before understanding how optimization fits into engineering design, it is useful to evaluate how "satisfaction" is measured at different levels of the industry [2].

Speaking of road transport vehicles, appearance, ride quality, safety and fuel economy are the most important factors in the design. Performance and costs, in most cases, determine the level of satisfaction. In the aerospace industry, performance is of paramount importance. Passenger safety regulations are among the strictest in the engineering world. Instead, fighter aircraft are subject to harsh environments and spacecraft can gain useful life with every ounce of weight lost. Products such as cell phones, stereos, watches, washing machines, etc., so-called "consumer goods", are usually designed for elegance and cost.

One thing that all manufacturing sectors have in common is the fact that designers are under increasing pressure in order to create better and better products in less time and at a lower price. And this, of course, is why optimization plays a vital role in product design.

Product development manages the creation of the product itself, taking into account different boundary conditions. In this way, the development processes include all the operations necessary to bring a new product to market. In the following figure, a typical product life cycle is summarized:

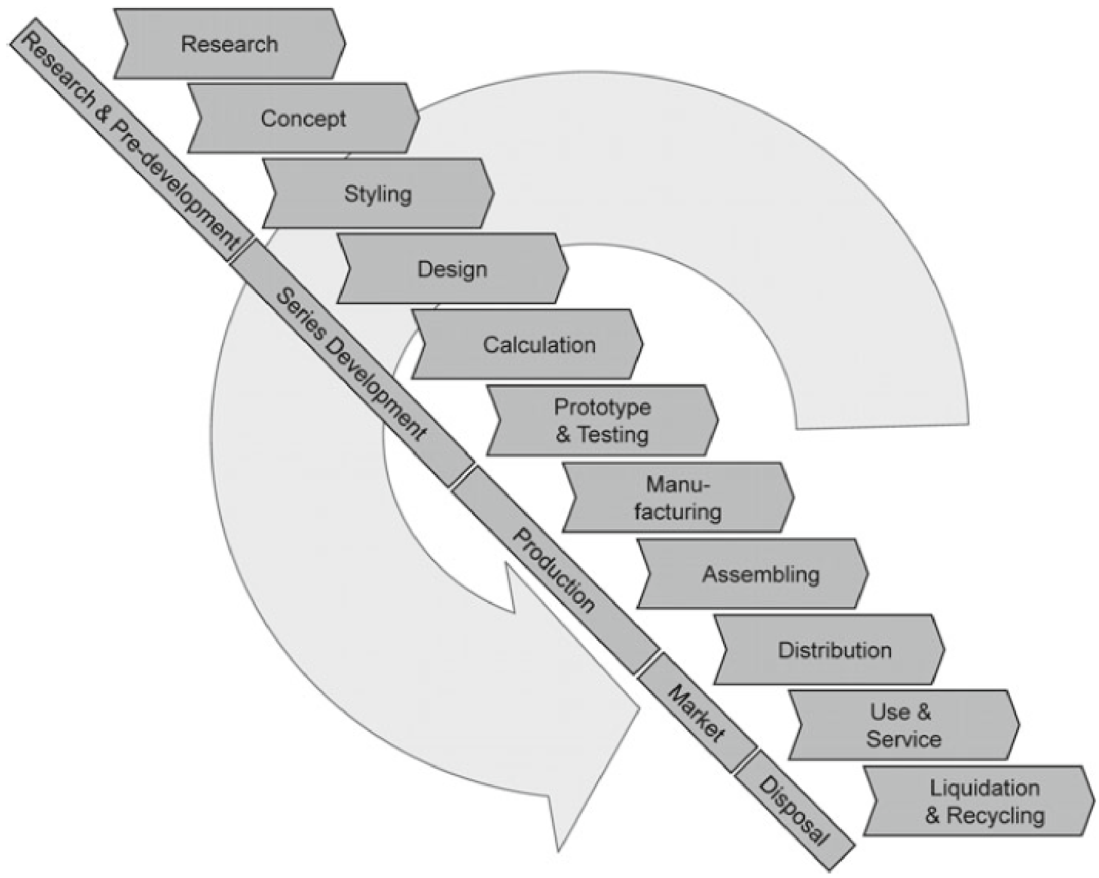

Figure 1.1: Typical product life cycle [3]

1. Firstly there is the research and pre-development phase in which the main characteristics of a new product are defined and evaluated;

2. The development phase includes styling, design and a detail engineering phase. This ends with the product testing phase, the duration of which depends on the type of product;

3. The processes related to production are developed and implemented later and the manufacturing phase of the product represents the last phase of the product creation cycle;

4. Finally, the marketing phases take place and then the distribution, use and disposal of the product (liquidation or recycling).

In this study, we deal with the development phase, starting from an already defined geometry and optimizing the structure in the best possible way, following the pre-established requirements. In the image below, we can see the conventional workflow for that phase:

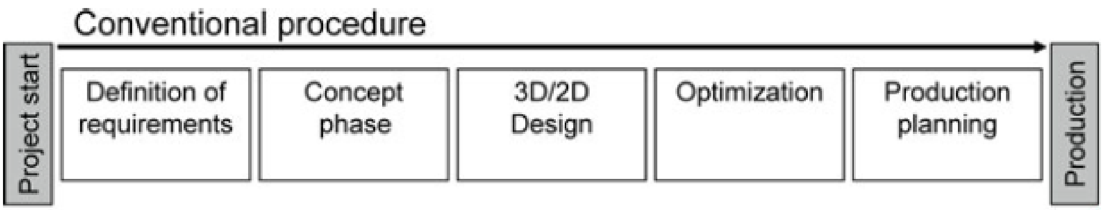

Figure 1.2: Conventional workflow of the development phase

What we must always remember, however, is that the workflow is not simply linear and consequential, since after the optimization phase it is very common to return to the design phase to make some changes to the structure. This is evident in the next image:

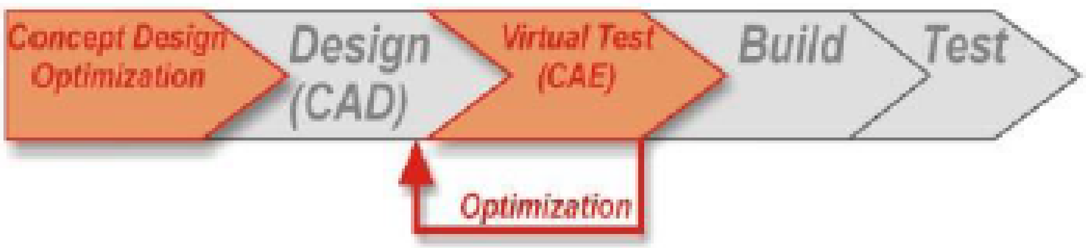

Figure 1.3: More realistic iterative and repetitive workflow

This way of doing is due to relatively recent advances in mechanics and software. In fact, this can suggest the most suitable design for specified conditions. In other words, thanks to these tools, it is possible to obtain an optimal design. It's important to know that a design optimization model consists of an analysis model (Finite Element Analysis) and an optimization model (Structural Optimization).

1.2 Methodology to Perform a Finite Element Analysis using FE solver

As we told in these lines, before we can start with the optimization process, an analysis model is defined and with it a FEM model too. To carry out a finite element analysis, there are three main steps to follow [4]:

1. Modeling, the pre-processing phase;
2. Solution;
3. Visualization of solution results, the post-processing phase.

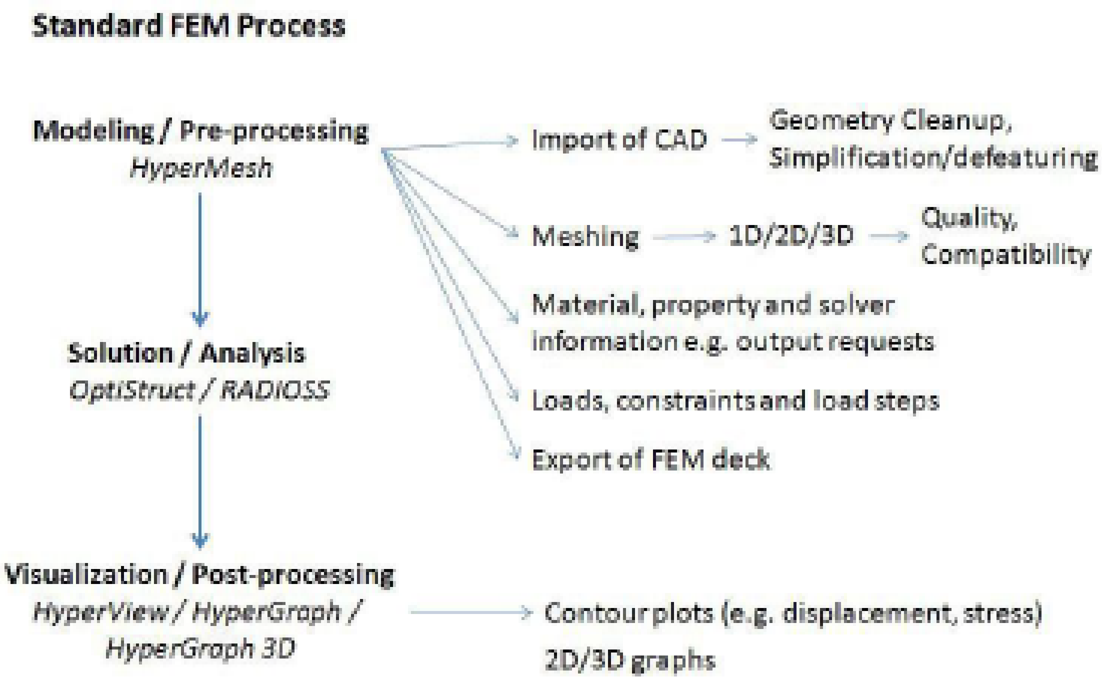

Figure 1.4: Finite element analysis phases definition

Since in this study we use Altair software, in the previous image, the corresponding tools to be used are indicated for each phase. Let's now analyze each of these three phases specifically.

1.2.1 Modeling (pre-processing)

First of all, to carry out any type of structural analysis, even for FEM analysis, we need a well-defined geometry, that is, a CAD model. In most cases, however, the CAD geometry imported into the modeling tool is not ready for meshing. Very often the geometry needs a preliminary cleaning due to the presence of

- inaccurate surfaces;
- non-continuous surfaces;
- redundant or multiple surfaces;
- surfaces too small to be sensibly measured;
- other geometry failures.

It is possible to see one of these problems, perhaps one of the most frequent, in the following image:

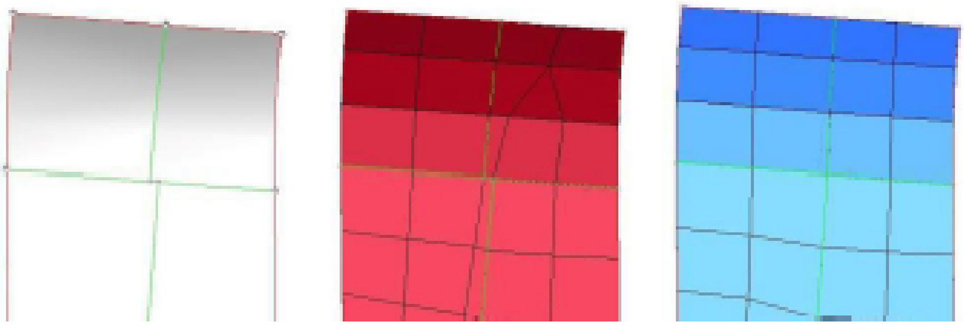

Figure 1.5: Geometry failure example

The image on the left shows the imported geometry. Here, the surface edges do not meet in a single point, i.e. there is very little lateral offset. Since the mesh is done with respect to surfaces, this small defect will automatically be considered during meshing, which will unfortunately result in poor quality elements. This can be seen very well in the image in the center, where we can see how the mesh is locally distorted. In the image on the right, however, we can see the updated and clean geometry, with the addition of the mesh.

Once we have fixed these defects and cleaned up the geometry as best as we can do, we need to ask ourselves if all the CAD information is really needed. So we need to understand if all the small fillets, small holes or even company logos often found in CAD data are necessary and really contribute to the final performance of the component.

Once the geometry has been modified to have well-defined surfaces and solids, a mesh is created to approximate that geometry. Based on the type of structure considered, a beam mesh (1D), a shell mesh (2D) or a solid mesh (3D) is created. This meshing phase is fundamental for finite element analysis, since the quality of the elements is directly reflected on the quality of the results obtained. At the same time, the number of elements (and consequently the number of nodes) affects the computation time. This is why 2D and 1D mesh is preferable to 3D mesh in some cases.

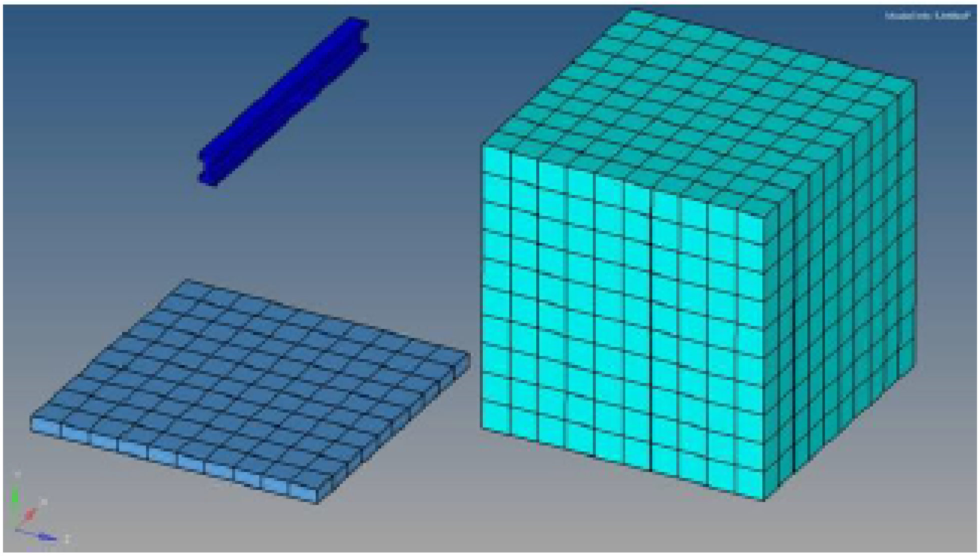

Figure 1.6: Mesh types: beam (1D), shell (2D) and solid (3D)

Although the meshing phase is a highly automated process, the quality of the mesh and the connectivity of the individual elements must be checked and modified if necessary. If necessary, these element defects may need to be improved by further modifying the geometry or individual elements through specific functions. Once the mesh has been defined, the elements are assigned material and property information.

The various loads and constraints are then added to the model to represent the load conditions to which the parts are subjected. We can define different load cases to represent different load conditions on the same model. The information relating to the type of analysis to be carried out is then also defined to indicate to the solver which results to export (static, modal analysis, etc.).

The FEM model (consisting of nodes, elements, materials, properties, loads and constraints) is then exported from HyperMesh. This model is a text file based on the specific syntax of the FEM solver. Most of the information stored in the analysis file is related to the definition of nodes (or grids). Each single node is defined by its nodal number (ID) and its coordinates along the three axes. Each element is therefore defined by its element ID and by the nodes that compose it.

1.2.2 Solution

During the solution phase of a simple linear static analysis or modal study, there is not much to do, also because it is a fully automated procedure. The default settings of the finite element program handle the problems related to this phase quite well. Usually if the solving process is interrupted by an error, this is due to errors made in the construction phase of the model. To name a few typical errors:

- Quality of the elements;
- Invalid material properties;
- Material properties not assigned to elements;
- Model not sufficiently constrained (the model shows rigid body movement due to external loads).

1.2.3 Visualizaion of Solution Results (post-processing)

Once the solution has been successfully determined, what is called post-processing of the simulation results is performed. Stresses, strains and deformations are tracked and examined to see how the structure responds to various load conditions. Based on the results obtained, we can make changes to the structure and run new analyzes to examine how these changes affected the part. This phase concludes the FEM analysis process.

As we will see in the following chapters, the process described above must be repeated several times, in an iterative way, because the simulation results may indicate the presence of errors or that the structure does not work as required.

1.2.4 Analysis Types

There are several types of analyzes that can be performed by Altair tools:

1. Linear static analysis;
2. Non linear analysis;
3. Dynamic analysis;
4. Instability analysis;
5. Thermal analysis;
6. Fatigue analysis;
7. Modal analysis;
8. CFD analysis;
9. Crash analysis;
10. NVH analysis.

Since in our study, we will deal exclusively with static and modal analyzes, let's see only these two in detail:

- Linear static analysis: in a linear analysis, the FE solver always follow a straight line from base to deformed state, as it is shown in the figure below

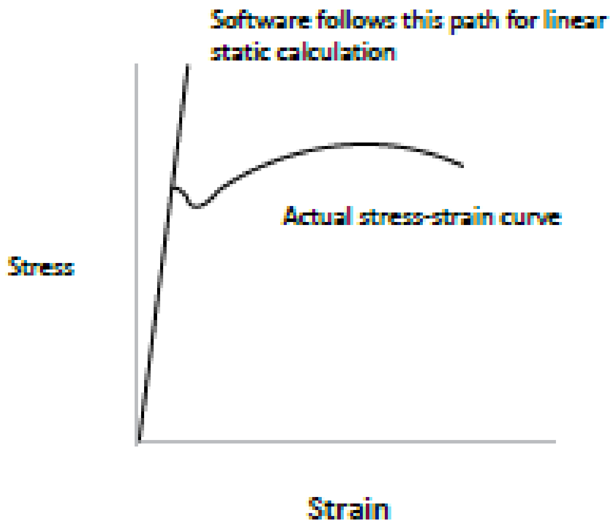

Figure 1.7: Stress and strain graph

The line in the graph represents the elastic behavior of a material, defined by Hooke's law

$$\sigma = E\varepsilon \tag{1.1}$$

where σ is the stress, ε is the strain and E is the Young's module.

For the static analysis, the FE solver needs to respect two conditions:

- the force is static, so there is no variation in time

$$\frac{dF}{dt} = 0; \tag{1.2}$$

- the equilibrium condition, so the sum of forces and moments is equal to zero

$$\sum F = \sum M = 0. \tag{1.3}$$

- Modal analysis: it is used to calculate the vibration modes and associated frequencies of a given structure. It is very important to know these frequencies, because if cyclic loads are applied at these frequencies, the structure can enter a state of resonance and lead to catastrophic failure. The equilibrium equation for a structure subjected to free vibration appears as an eigenvalue problem, with the following formulation:

$$[K - \lambda M]x = 0 \tag{1.4}$$

where K is the stiffness matrix of the structure and M is the mass matrix. Damping is neglected.

1.3 Optimization Process Overview

1.3.1 Optimal Design

From the previous chapters, it is clear that a designer must find the optimal design for his project. But how do you recognize an optimal design?

An "optimal" process, says the dictionary, is "the best and most favorable condition for the occurrence of a fact or phenomenon" [1]. As designers, we define all those conditions that allow us to evaluate different project alternatives. In engineering terms, this is equivalent to saying that mathematical equations that quantify the performance of a project are defined.

The parameter through which a given project is evaluated is the objective. It is clear that we can have more than one objective: for example, to carry out a project that maximizes safety while minimizing costs. In many cases, unfortunately, the objectives can contradict each other and for this reason it is often necessary to compromise to have a working project (MOO, Multi Objective Optimization).

The problem comes when there is no possibility of having infinite resources: not only issues like the cost of materials or production, but also processing and project limits. These limits, or constraints, allow us to define what is called constrained optimization: a solution that respects these constraints is called feasible, otherwise it is not.

As it is clear from the project described in this study, design is not always done from scratch. In fact, in many cases, we interact with an existing project and look for a way to improve it in the best possible way. This implies less freedom and more constraints, imposed by an already defined structure. Starting from scratch, of course, we have more freedom in defining objectives and constraints.

Another problem is that, in most cases, the optimized part will have to be assembled into a larger and more complex assembly. So a design space must be defined within which the various changes can be implemented. Finally, the presence of not editable characteristics must be considered. All editable features are called design variables.

Summarizing, the definition of the optimization problem of a given project consists in defining:

- design space
- constraints
- design variables
- objectives

1.3.2 The Objective of the Optimization Process

Modern optimization software integrates calculation programs (finite element analyzes) and improves the design based on these calculations. Furthermore, they mainly aim at the following objectives [5]:

1. Reduce the weight of a load-bearing structure to a minimum;
2. Maximize the first natural frequency.

In general, the objective of a structural optimization is to improve the behavior of components with respect to specific requirements. Defining these requirements is the first step in structural optimization. So, the questions we need to ask ourselves are:

- What is the ultimate goal of optimization?
- Can we define further constraints/restrictions within the model?

The second step is, instead, the definition of the design variable. In the figure below a simple optimization process is outlined, where you can see the main phases that characterize its implementation.

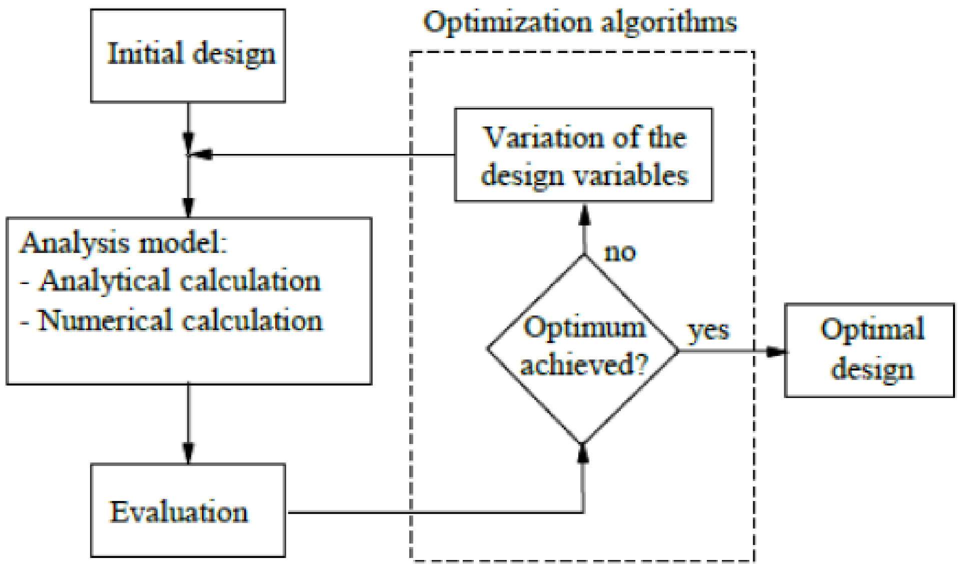

Figure 1.8: Optimization loop

With the design variable values from the initial project, the assignment is analyzed and evaluated. The optimization algorithm improves the component in a cyclic, iterative manner, until the optimum condition is reached.

The types of structural optimization are divided according to the type of project variables identified, since at a later stage the solution strategies used must also be selected:

- Dimensioning: wall thickness and cross section are the simplest design variables;
- Shape optimization: Design variables describe the shape of the component outline. The geometry of the building element can be changed;
- Topology optimization: project variables describe the layout of the structural elements;
- Choice of material behavior;
- Choice of construction method.

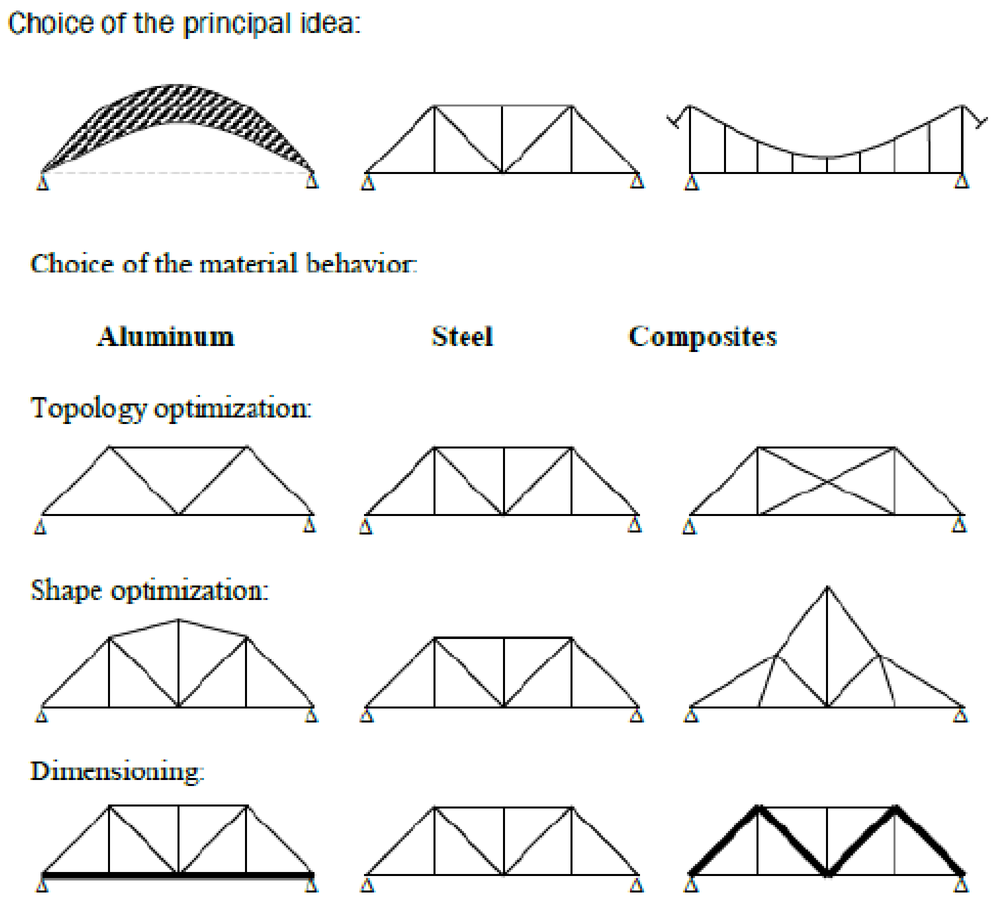

Figure 1.9: Classification of structural optimization task in the kind of design variables

The purpose of an optimization must be defined absolutely precisely. To do this, what is called the list of specifications is used: it should contain the different possibilities of variation of the structure (design variable), the requirements required of the component (objective and restriction functions) and the load cases to be taken into consideration. The analysis model, from which the optimization process starts, generally contains a finite element model.

In addition, material behavior and loading conditions must be determined before proceeding further. All requirements that a product must meet must also be considered in the optimization process. In the simplest case, an objective or constraint function corresponds directly to a certain parameter in the simulation program output file. However, this is quite rare. Generally, the output must be processed with additional routines.

1.3.3 The Algorithm Behind the Optimization Process

In optimization processes, by convention, we usually look for the minimum of the objective function. We should not see this as a limitation, as maximizing an objective is the same to minimizing its reciprocal [2].

A function that has only one minimum within the optimization domain is called a convex function. Let us remember that in the calculation, a minimum (as well as any other "turning point") of a curve is characterized by a slope (first derivative) equal to zero. If the objective function is a quadratic function, then the presence of a global minimum is certain, as a second order curve has only one turning point.

A higher order curve can have multiple turning points within its domain. If so, we might have multiple minima: the turning point where the objective function has the absolute minimum is the global minimum, while the other minima are called local minima. Depending on the chosen objective function, the optimizer may have to search for the minimum of a non-convex function. So how does the optimization software arrive at an optimal solution in a reasonable time? As can be easily understood, it will be an iterative solution.

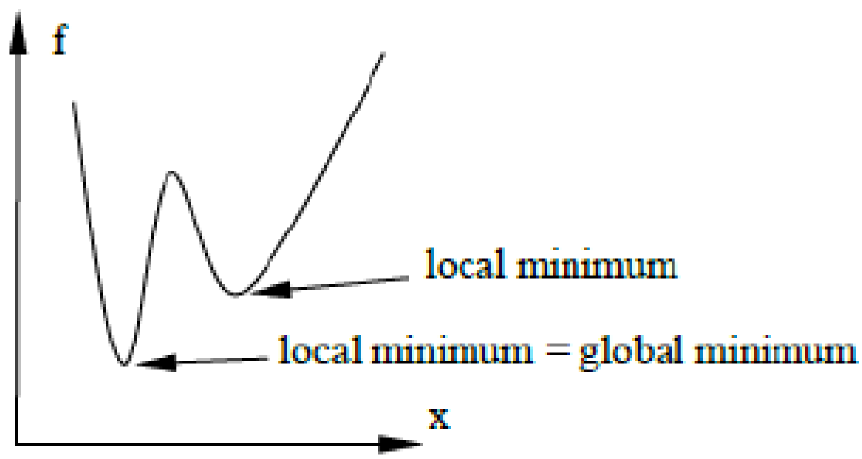

Figure 1.10: Function with several local minima

Resuming, to define an optimization process it is necessary to define the design space, the project variables, the constraints and the objectives. The corresponding mathematical statement is:

$$f(x) = f(x_1,\, x_2,\, x_3,\, ...,\, x_n) \tag{1.5}$$

Subject to:

$$
\begin{aligned}
&g_j(x) \leq 0, \qquad j = 1,\ ...,\ m \\
&x_i^L \ < \ x_i \ < \ x_i^U, \qquad i = 1,\ ...,\ n
\end{aligned}
\tag{1.6}
$$

where $f(x)$ is the objective function, $g(x)$ are the constraint functions, and x is a vector of design variables.

Evaluating the sensitivity of responses to changes in design variables is, of course, a key part of the optimization process. Some design problems have more constraints than design variables, while others have more design variables than constraints. Different algorithms are used by OptiStruct for each case in order to efficiently arrive at the optimal solution.

As we all know, the optimization process is iterative, but asking the analysis package to evaluate the responses every time a variable is changed can be very expensive in terms of computation time. Fortunately, OptiStruct takes a different approach: the optimizer builds a rough model and does most of its work within it, returning to the analysis software only when it is essential. This makes optimization much faster. But since the optimization model is an approximation of the analysis model, which in turn is an approximation of the physics of the structure, the result of the optimization needs further verification analysis.

As discussed above, a convex optimization problem has only a minimum (or maximum). This minimum is the global minimum. In the case of non-convex problems solved using gradient-based techniques, so the optimized result obtained depends on the starting point of the design. This makes these types of algorithms even more susceptible to finding the local optimal point.

With the release of Optistruct's Multiple Starting Point Optimization, we can do a thorough search of the design space for multiple starting points, in order to improve our chances of finding a more global optimum. This implies that n-different starting points of the project could potentially lead to n-different optimal solutions. But it is also very likely that different design starting points can lead to the same optimal solution. However, this does not mean that the optimal solution found is the global optimal one.

From the designer's point of view, it is essential to understand that the search for the best is an iterative procedure. First, we can define the search time to the optimizer, setting a maximum number of iterations. In addition, the precision of the search (i.e. the travel limit) can be imposed. If the difference between two successive iterations is less than a certain convergence tolerance, it can be concluded that this is acceptable for the purposes of our design.

In OptiStruct, basically, two convergence tests are used and the satisfaction of only one of the two is required:

1. Regular convergence (feasible design): the convergence criteria are met for two consecutive iterations, i.e. the change in the objective function is less than the objective tolerance and the constraint violations are less than 1%.

2. Soft convergence: there is little or no change in the design variables for two consecutive iterations. For this type of convergence it is not necessary to evaluate the objective (or constraints) for the final design point, as the model is unchanged from the previous iteration. Therefore, soft convergence requires one less iteration than regular convergence.

Since we mentioned gradient-based techniques earlier, let's remember what we mean. Most engineers are familiar with Newton's method of calculating the roots of a polynomial: as shown in the figure, this method uses the slope of the function to determine in which direction the initial estimate should be adjusted - to increase or decrease it.

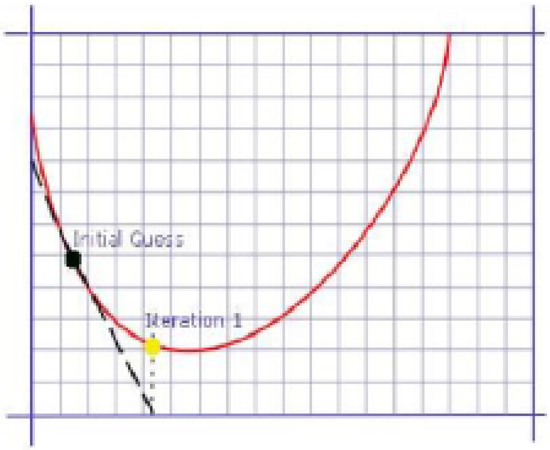

Figure 1.11: Representation of the Newton gradient method

Practically, the gradient is often calculated using a finite difference method. However the gradient search method is one of the many methods used by the optimizer to go from the initial configuration to the final solution.

Let's go to explain the logical procedure in a simple way. It all starts with an estimate of the optimal design. By iterating, convergence is achieved when the gradient of the objective function is 0. This optimization algorithm can be called the Gradient Descent Method, or simply the Gradient Method. It can be summarized as:

1. Start from point x_0:

2. Evaluate the function $F(x_i)$ and the gradient of the function $\widetilde{N}F(x_i)$ at the x_i;

3. Determine the next point using the direction of the negative gradient: $x_i + 1 = x_i - g\widetilde{N}F(x_i)$;

4. Repeat steps 2 to 3 until the function converges to a minimum.

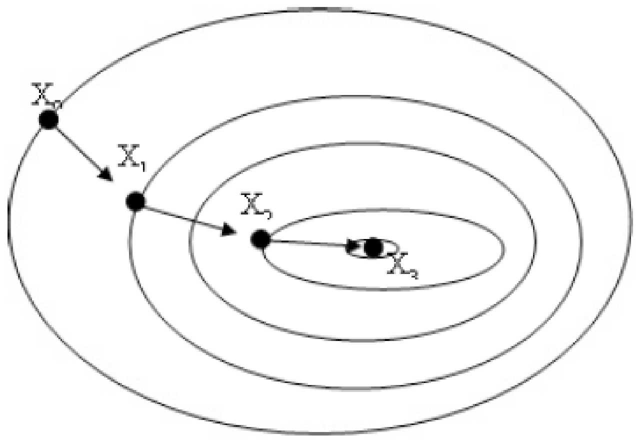

Figure 1.12: Gradient Descent Method

The gradient-based method depends primarily on the sensitivity of the system's responses to changes in design variables, with the aim of understanding the effect of design changes and optimizing the system accordingly.

To speed up the optimization process, the optimization model uses the following techniques:

- Constraint Screening, to identify which constraints are critical for the current iteration;

- Constraint Linking, to reduce the number of constraints that must be considered using factors such as symmetry;

- Constraint Deletion, to eliminate a constraint deemed not important for the iteration as it was not violated during optimization.

1.3.4 Types of Structural Optimization

Let's now see what the various structural optimization processes are available in OptiStruct. Optimization techniques fall into two categories: Concept Design and Design Fine-Tuning. The first, perform an optimization in the first phase of the design process to work with the best possible design (topology or topography optimization). The second allows you to modify the structure in detail to meet the design criteria without changing the overall topology (size and free size optimization, shape and free shape optimization). So the different types of available optimizations in Optistruct are [6]:

- Topology Optimization: it is about material distribution and how parts of a structure are connected. It considers the "equivalent density" of each element as a design variable. The solver calculates an equivalent density for each element, where 1 is equivalent to 100% material, while 0 is equivalent to no material. Thus with topology optimization a lower equivalent density is assigned to elements that have a low stress value. In this way the optimal design tends to 1 and all other elements tends to 0. As designers, for example, we may decide to omit material from all (finite) elements whose density is less than 0.3 (or 30%);

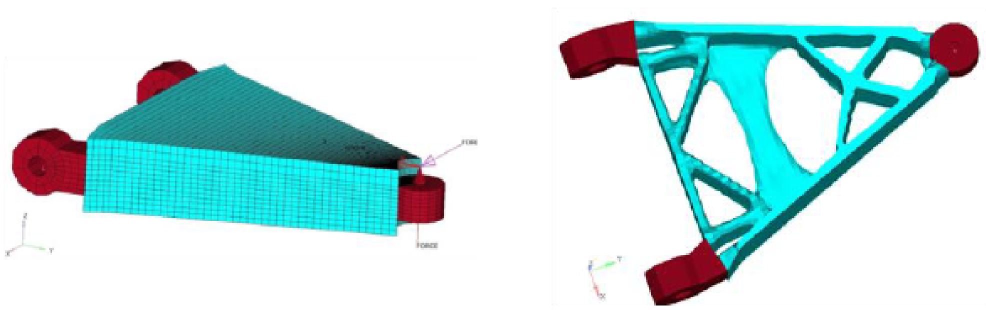

Figure 1.13: Topology Optimization example

- Topography Optimization: it is usually applied to shells and thin-walled structures with the aim of reinforcing them. Topography optimization is an advanced form of shape optimization in which a design region is defined for a given part and a shape variable base stiffener pattern is generated within that region using OptiStruct. The approach is very similar to the approach seen in topology optimization, except that shape variables are used instead of density variables;

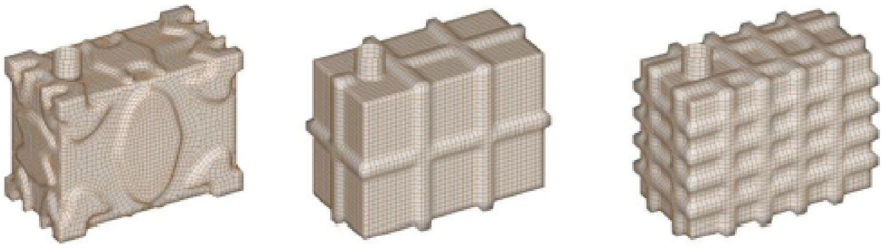

Figure 1.14: Topography Optimization example

- Size Optimization: it interact with the properties of structural elements such as shell thickness, cross-sectional properties, spring stiffness and mass. Since the optimization takes place on the property, it is not possible to change the thicknesses of the individual elements. Then there is Free Size Optimization, where the thickness value is altered on the element rather than on the property. The thickness of the element can vary continuously, giving a result similar to topology optimization;

Figure 1.15: Size Optimization example

- Shape Optimization: the shape of a structure is defined by the nodal coordinate vector. The solver then changes the positions of the nodes by resizing the shapes within the design space. One of the main problems is the need to define the shape perturbations in advance. Free shape Optimization avoids this by having the solver automatically move the boundary nodes within a certain specified distance;

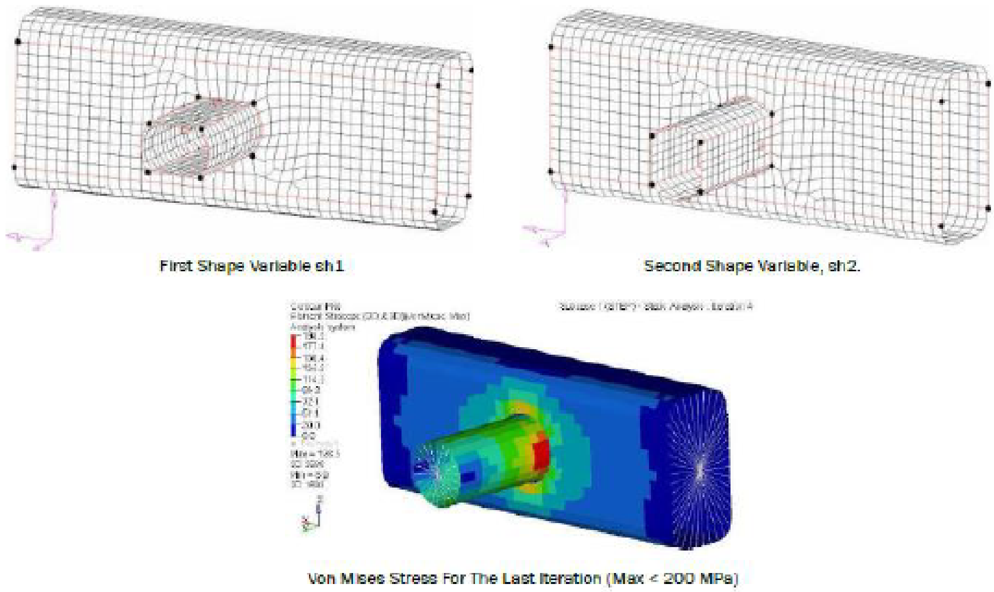

Figure 1.16: Shape Optimization example

- Lattice Optimization: lattice structures are currently the most accurate solution for representing elements with intermediate densities. Since topology optimization results (without manufacturing constraints) usually generate shapes suitable only for additive manufacturing, it is therefore appropriate to apply lattice optimization on topology optimization results in order to have better accuracy and performance.

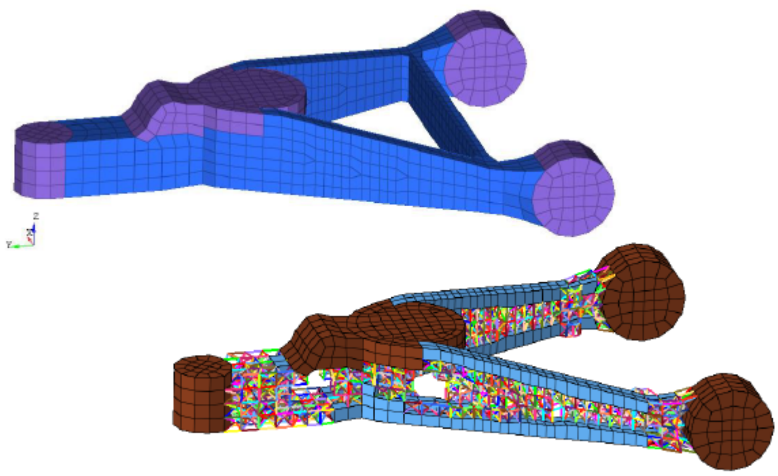

Figure 1.17: Lattice Optimization example

- Multi Model Optimization (MMO): it allows for simultaneous optimization of multiple structures with common design variables. In other words, MMO is useful when we have to consider different model confugurations or just parts of different assemblies. Although different load steps can be included in a single optimization problem, a different mesh size can also be imposed when MMO is applied.

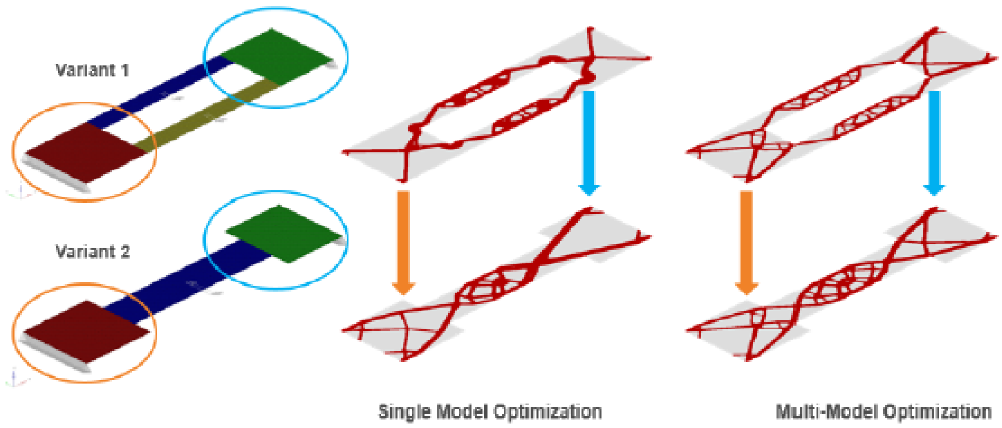

Figure 1.18: Multi Model Optimization example

1.4 PLT-2 TIR Mission Definition

The space segment of PLT-2 TIR mission is composed by a single satellite placed into a repeating ground track Sun-Synchronous Orbit at an altitude of 393.8 km: it assures a refresh time of 52 days (that is the repeat cycle of the ground tracks of the satellite, which completes 15+29/52 orbits per day).

The objective is to generate TIR (Thermal Infrared Radiation) images of the desired AoI (Area of Interest) with GSD = 40 m, swath = 40 km and strip length = 170 km.

In detail, the mission is aimed at providing thermal infrared (TIR) imaging products of Italy and the Mediterranean basin as principal Area of Interest with a fixed refresh interval and with a fixed images resolution with the possibility of acquisition of other areas like poles, deserts and major urban areas without revisit time and resolution constrains.

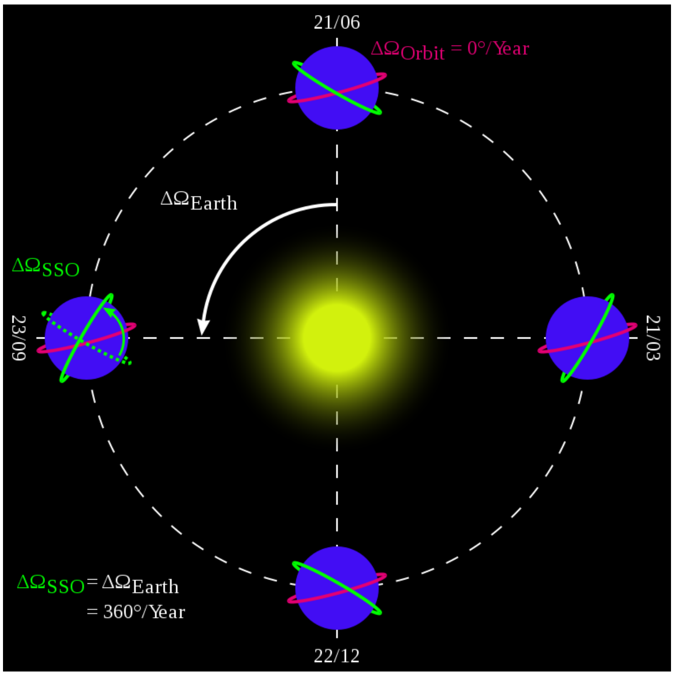

Figure 1.19: Sun (green) and non-Sun Synchronous (magenta) Orbit [7]

Aside from the players involved in the demonstration and in-orbit validation of the platform, the end-users for the TIR mission are public or privately-owned entities interested in Earth-Observation applications in the thermal infrared spectrum (and thus to phenomena linked to surface temperature). We have a very performing spatial resolution, such as land and sea surface temperature, precision farming, forestry and water resources monitoring, water stress, irrigation, biogeochemical cycles/carbon budgets, pollution and urban areas energy monitoring.

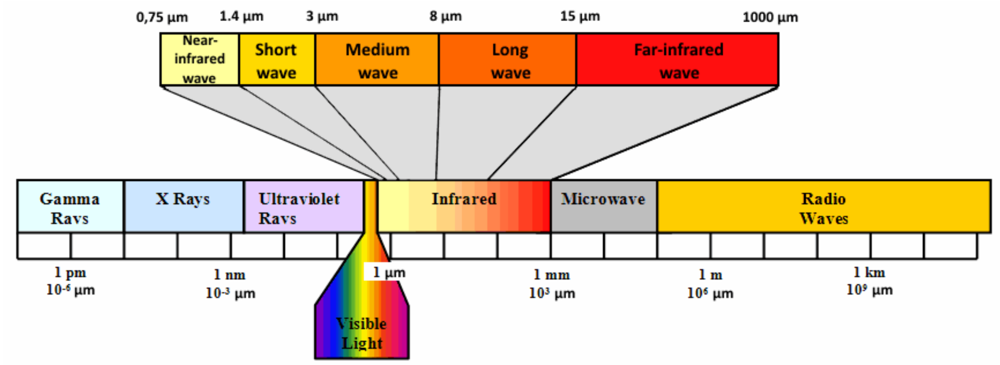

Figure 1.20: Thermal Infrared Radiation (TIR) [8]

Then also urban heat island (UHI), anthropogenic fluxes, heat waves, urban and peri-urban hydrology, thermal pollution in coastal waters, air-sea fluxes, sub-mesoscale activity in coastal and open ocean, estuaries, deltas, biological activity and productivity, post eruptive study, eruption cloud and etc.

In more details, TIR data is fundamental to retrieve Land Surface Temperature and to monitor the energy exchange between Earth surface and atmosphere. For agricultural applications, PLT-2 TIR mission will provide important data useful to estimate Evapotranspiration (ET) and to monitor water deficit of vegetation. In combination with VNIR data (used to derive Normalized Difference Vegetation Index and the fractional vegetation cover) and soil moisture data, PLT-2 TIR mission high resolution data will be fundamental to retrieve soil moisture at an agricultural parcel scale by means of disaggregation algorithms.

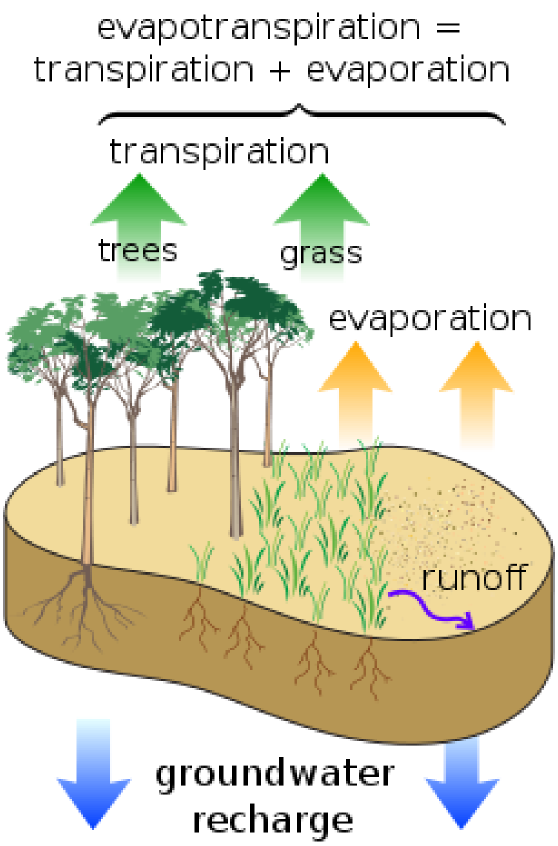

Figure 1.21: Evapotranspiration (ET): transpiration and evaporation [7]

The estimation of soil moisture data at a crop field scale will be useful to study water stress conditions of vegetation and to derive root zone soil moisture estimates with important implications in precision farming and hydrology. Furthermore, ET is important to study the water transfer within soil-plant-atmosphere continuum and biogeochemical cycles. In forestry, the knowledge of water stress conditions is useful to estimate the fire risk and tree growth with implications in wood production.

Due to the important role played by ET in governing the water cycle and energy exchanges between hydrosphere, biosphere and atmosphere, PLT-2 TIR data will be useful to predict regional-scale surface runoff and underground water flows, which interact with large-scale atmospheric circulation and global climate change.

Moreover, TIR data is used to derive surface water temperature of lakes, which has been defined as an essential climate variable by the Global Climate Observing System (GCOS). PLT-2 TIR data will be also useful in monitoring pollutant discharge from rivers into coastal waters and water quality and in detecting fresh water resurgences and algae blooms. In coastal areas, Sea Surface Temperature (SST) data at high resolution will be useful to monitor gradients of SST and air-sea fluxes and winds.

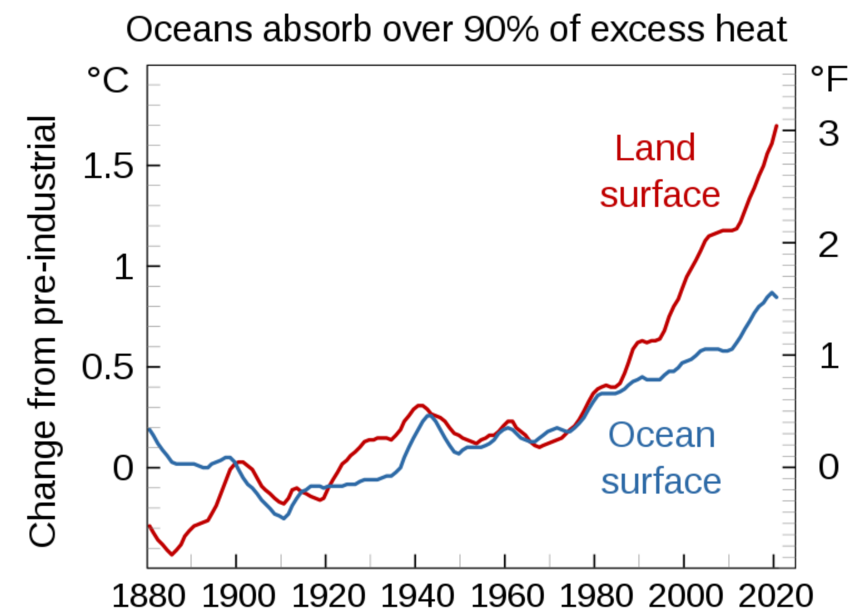

Figure 1.22: Land and Sea Surface Temperature variation in forty years [7]

SST at the ocean–atmosphere interface represents a key variable for monitoring and predicting fluxes of heat and oceanic dynamics at large scale. If used in meteorological models, SST data will be useful to study cyclical phenomena such as El Niño-Southern Oscillation (ENSO) with its opposite phases called El Niño and La Niña.

In urban environments, the knowledge of Land Surface Temperature and Evapotranspiration is fundamental to provide useful information about urban climatology and vegetation. Urban vegetation plays an important role in urban climatology and, due to Evapotranspiration, influences air quality and pollution. PLT-2 TIR mission will provide useful data to monitor Urban Heat Islands (UHI), which caused a lot of casualties among the elderly in last years in South Europe.

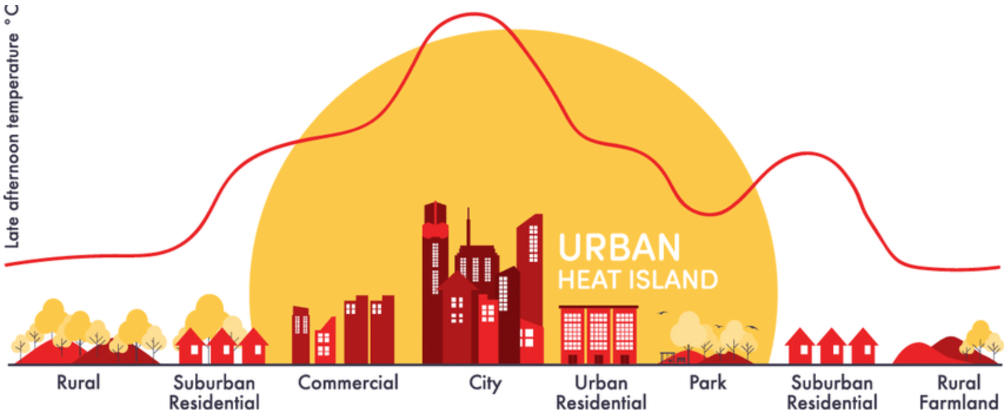

Figure 1.23: Urban Heat Islands (UHI) definition [9]

PLT-2 mission will provide useful information for other applications such as the estimation of area covered by water in flooding events, monitoring of burnt areas and, in volcanology, the volcanic activity and thermal anomalies, which often reveal to be precursor signals about eruptions. TIR data is also useful to detect volcanic ashes and for post eruptive study.

A future constellation of small satellites with the PLT-2 TIR payload will increase the temporal resolution, will provide a more frequent data and will allow having a better understanding of dynamics of applications described above.

A technological demonstration of a TIR payload such as the one foreseen for PLT-2 can be considered attractive in the space borne observation marketplace and represents an appealing scenario to employ as a benchmark for a commercial, multi-mission platform.

Chapter 2

Preliminary FEM Analysis

The main objective of this first part of the study is to carry out a preliminary finite element analysis, starting from a previously defined geometry to which simplifications are applied. This analysis allows us to evaluate the first resonant frequencies, the total mass involved and the forces acting on the system. We start from a pre-existing CAD model, where the geometry of the object is defined, then we import it into a calculation environment in order to be simplified and analysed. The working environment is Hyperworks 2020 X, provided by Altair.

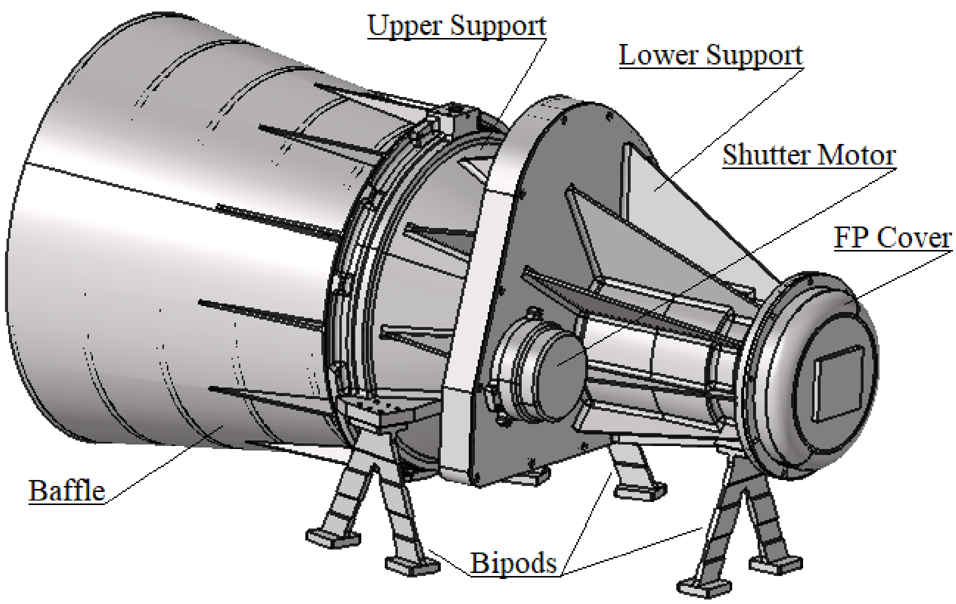

Figure 2.1: PLT-2 TIR initial geometry

The last figure shows the initial geometry containing all the components considered in the study: there are two conical supports (upper and lower) with ribs, a baffle, three bipods, the shutter motor and the focal plane cover. Inside the conical supports, there are five circular lenses and a filter located between the lower support and the focal plane cover.

2.1 Geometry Simplification

The first thing to do consist in making the structure as suitable as possible for FEM analysis and to do this we simplify the geometry through various commands contained in the "Geometry > Defeature" panel.

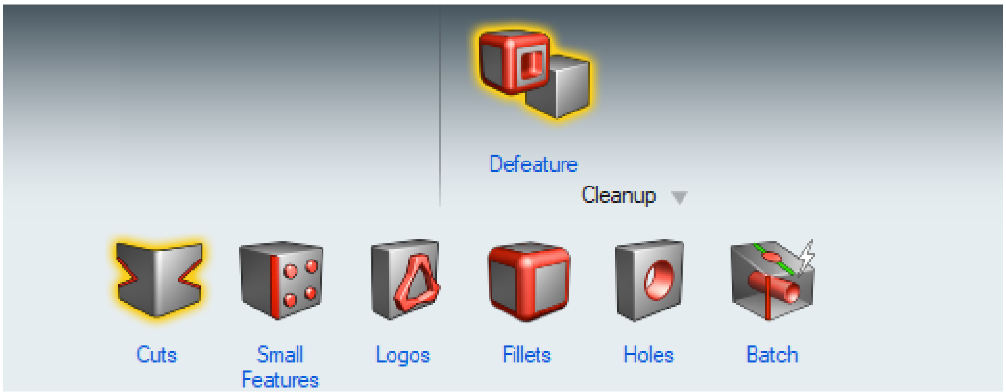

Figure 2.2: Defeature panel

First of all, through the "Holes" command, we can fill all the holes that has a not relevant behaviour for the purposes of the structural analysis. So we remove:

1. Interface holes between the telescope and the outside;

2. Connection holes between the components excluded from the analysis (only those between the two supports, between the upper support and the baffle and between the supports and the bipods are considered).

Then, through the “Fillets” function, most of the fillets are eliminated, in order to have the most edgy solids possible. These simplifications, at a geometric level, are carried out by considering each component of the structure individually. In the following images, you can see some of the changes made to the geometry.

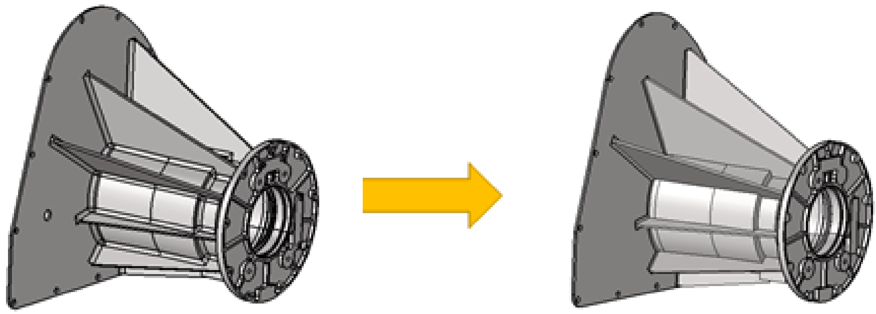

Figure 2.3: Lower support: all fillets and some interface holes with the focal plane cover have been removed

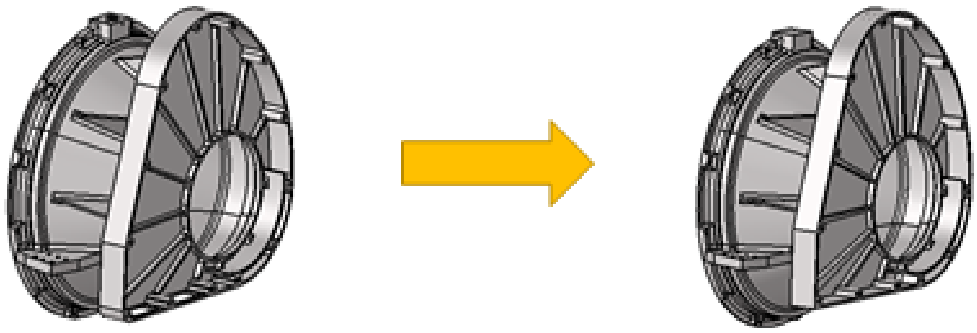

Figure 2.4: Upper support: some fillets and interface holes with components not considered have been removed

A further simplification is made for other components such as the focal plane cover, the shutter motor and the lenses: we can approximate all of them with concentrated masses in their centres of gravity, always respecting the structure.

2.2 Mesh Creation

Then, when the entire geometry is sufficiently simplified, we can proceed to create the mesh of the components. The meshes used in this study are of two types: a three-dimensional HEXA mesh and a two-dimensional MIXED mesh.

The three-dimensional mesh is applied only to the three bipods, as they have a geometry simple enough to be divided into small cubes. The use of a HEXA mesh requires, however, that the meshed component is defined "mappable". This means that we can identify simpler sub-volumes, geometrically speaking, in order to have a more accurate analysis. In our case, the three bipods are divided into different sub-volumes, cutting them through parallel planes placed along the height, obtaining the result in the following figure.

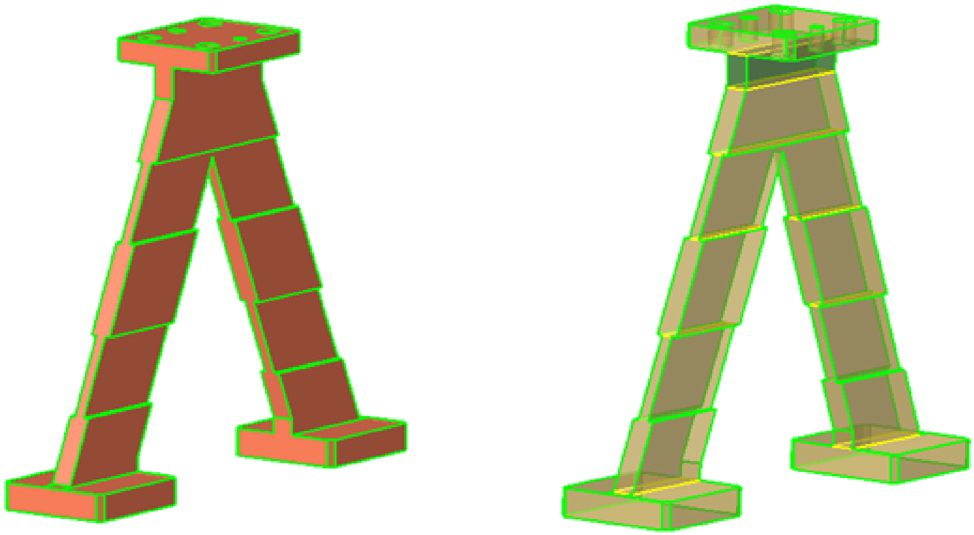

Figure 2.5: Difference from unmappable (left) and mappable (right)

In the first image, the solid is considered "unmappable", so not yet suitable for the application of a three-dimensional HEXA mesh. In the second case, however, all possible simplifications have been applied and the fact that it is transparent indicates that it can be considered "mappable".

The colours of the lines are not random, in fact the yellow lines in the figure indicate the division between the various sub-volumes into which the solid has been divided, but the continuity of the solid is still guaranteed. Otherwise, when the dividing lines between the sub-volumes are red, there is no volume continuity of the solid. The green lines, instead, indicate the external boundaries of the entire volume.

Once the solid is simplified and made "mappable", it is possible to apply the mesh and, as already mentioned before, in this case a three-dimensional mesh of the HEXA type is used. The mesh is defined for the single sub-volumes, with a size grain average of 2 mm. After full volume application, we obtain the result shown in the figure below.

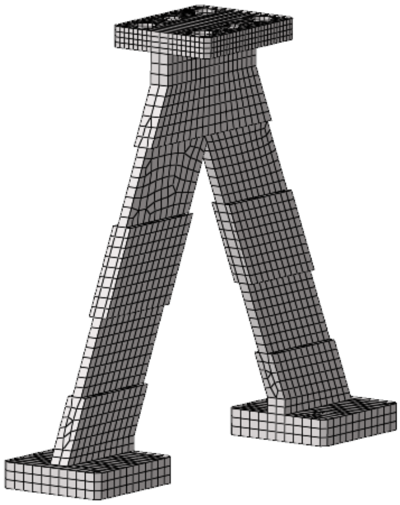

Figure 2.6: Bipod three-dimensional HEXA mesh

What has been said so far can be applied equally to all three bipods, as they have the same geometry. Regarding all the other parts, two-dimensional MIXED-type mesh is used, i.e. the solids were approximated with thin mid surfaces, characterized by a single parameter: the thickness defined in function of the single part geometry.

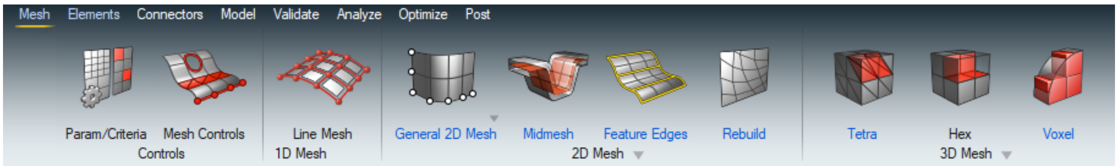

Figure 2.7: Mesh panel

Through the "Midmesh" command in the "2D Mesh" panel, it is possible to extract both the mid-surface of the solid and the mesh itself in a single step. This surface, however, may be incomplete, poorly defined or lacking some parts due to common errors in extracting a mesh from a complex geometry such as the one considered. Some adjustments were therefore necessary, as in the three-dimensional case, working only on the surface for the moment.

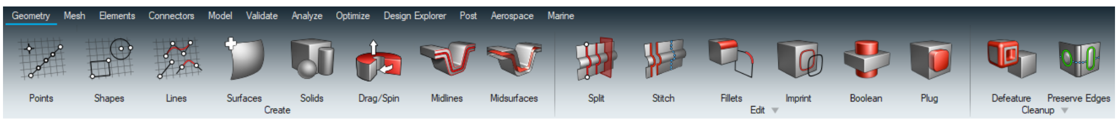

Figure 2.8: Geometry panel

To extract only the mid-surface and then manually apply the two-dimensional mesh, the "Midsurfaces" function in the "Geometry" panel can be used. Once we extract the surface and the mesh is applied, after some geometrical adjustment, we obtain what is shown in the figures below.

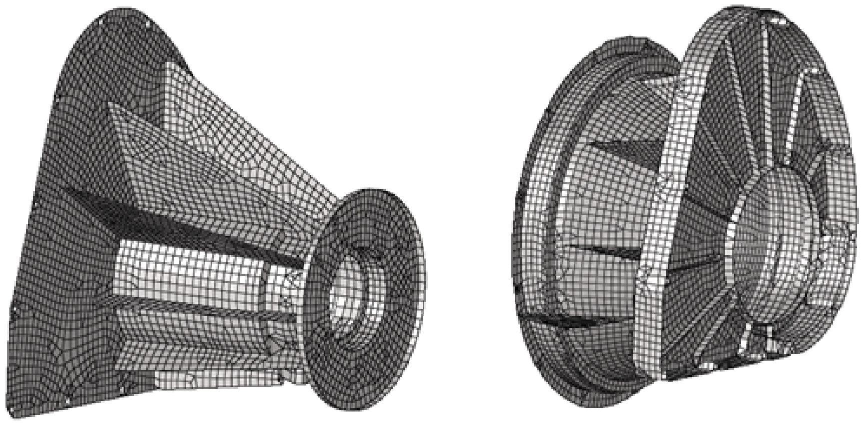

Figure 2.9: Lower (left) and upper (right) support two-dimensional mesh

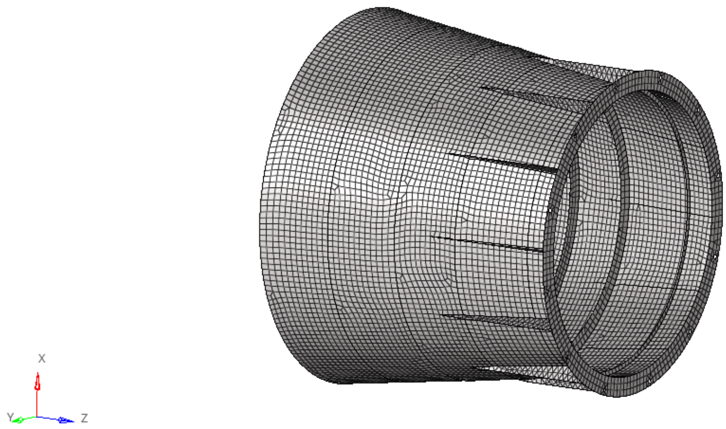

Figure 2.10: Baffle two-dimensional mesh

In this case, the size of the elements is set between 3 mm and 5 mm. In the first two images we can see the mesh applied to the two conical supports (including ribs and holes), while below it is applied to the baffle.

2.3 Materials and properties definition

Once the mesh is applied to the entire structure and once all the elements are appropriately modified in order to reach an optimal quality, it is then necessary to define the materials involved and the properties related to the individual components. The materials used in this study are two:

1. Titanium (Ti);
2. Aluminium (Al).

Material	Young Module $[Mpa]$	Density $[t/mm^3]$	Poisson Coeff
Titanium	114000	$4.50e^-9$	0.34
Aluminium	73000	$2.8e^-9$	0.33

Table 2.1: Materials mechanical characteristics

As we can see from the table above, Young module is assigned in MPa and the density in t/mm3. This is due to the fact that Hyperworks 2020 X uses millimetres as the measurement unit for length. So we can act in two ways: either we can change all the measurement units (as is done in this case) or we can scale the whole system to have everything defined in meters (to use the International System).

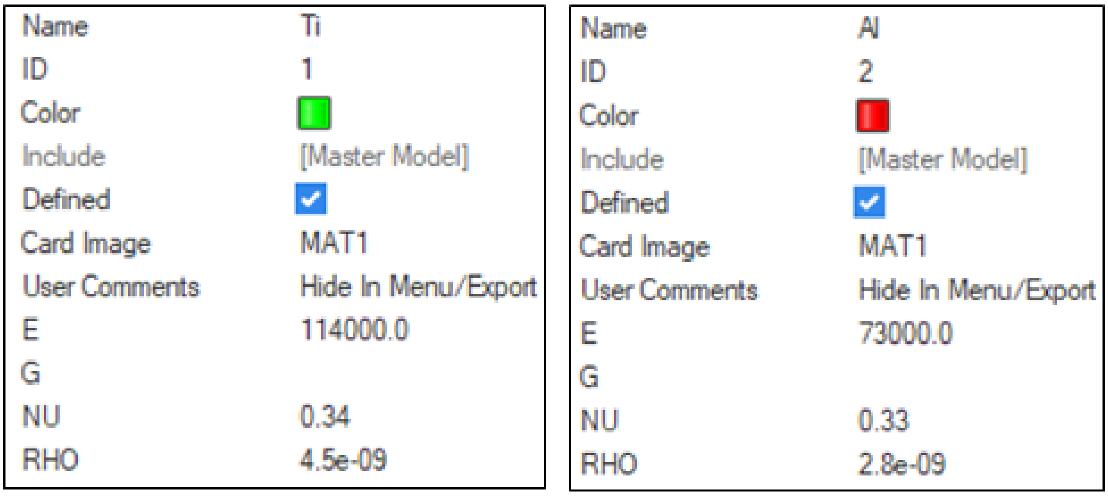

Figure 2.11: Material definition

Once we define the two different materials, we can create properties to connect the single parts to materials and define their thickness (T) (this parameter can be defined only for SHELL elements, not for three-dimensional ones as they already have their own thickness).

Both materials and properties are defined manually by acting on the command bar in the "Model" window. In total, six properties are created:

1. One for the bipods (Ti_solid): solid elements in titanium;

2. Three for the two conical supports (Ti_shell_t1.5, Ti_shell_t2, Ti_shell_t8): surface elements in titanium (T = 1.5 mm, T = 2 mm and T = 8 mm);

3. Two for the baffle (Al_shell_t1.5, Al_shell_t2): surface aluminium elements (T = 1.5 mm and T = 2 mm).

In the following two images, we can see the entire system divided by material (Figure 2.12) and properties (Figure 2.13) used.

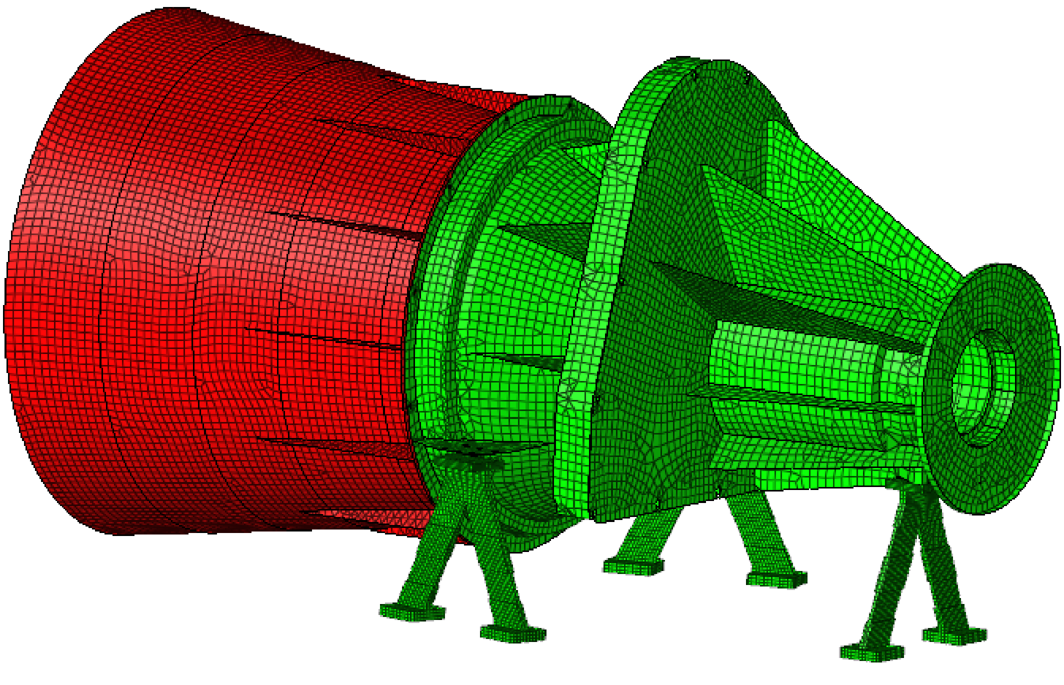

Figure 2.12: Material distribution: aluminium (red) and titanium (green)

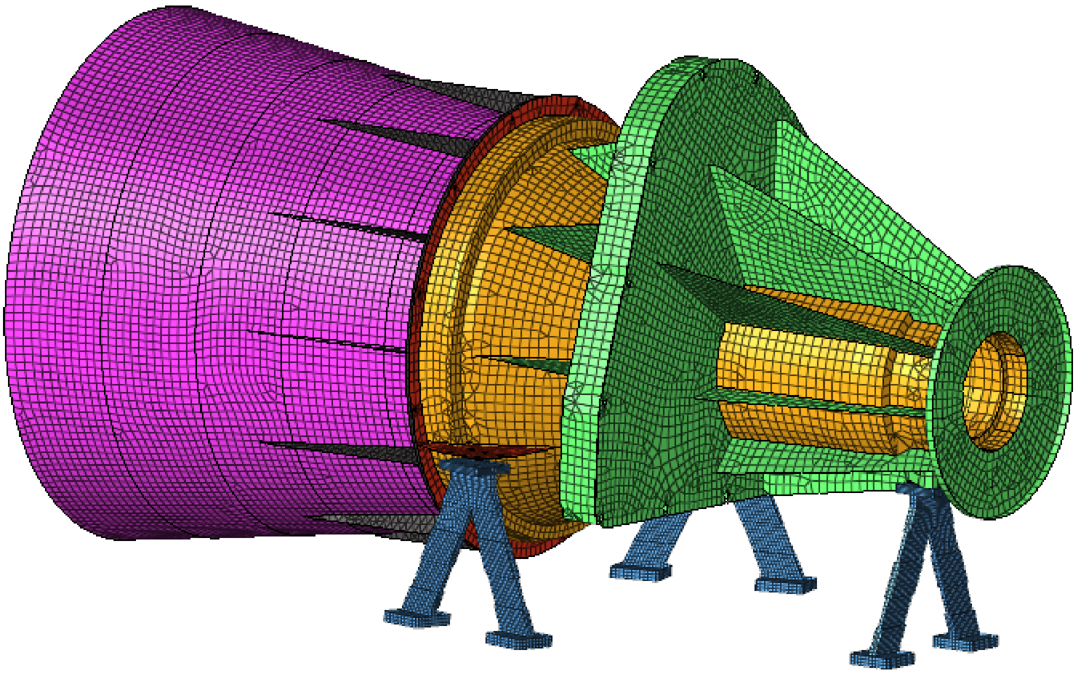

Figure 2.13: Properties distribution

In the following image there is a legend containing the various properties and their respective colors, so that we can better understand how the thicknesses are distributed in the structure.

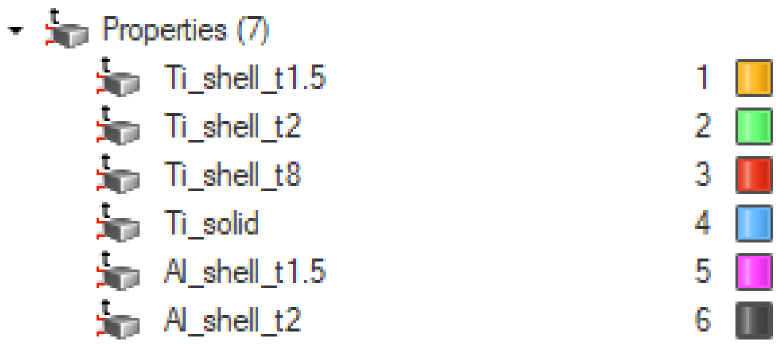

Figure 2.14: Properties definition

2.4 Boundary conditions, constraints and mass of the system

Once the mesh, the materials and the properties have been applied and the quality of the elements have been improved as much as possible, before carrying out the various analyses, we have to define the boundary conditions, the connections between the various components and the loads.

Among the boundary conditions, we must first consider that the bipods and the baffle mesh will remain the same, even after having done the topological optimization with lattice. So we must be sure that we have made a mesh as correct as possible (we can verify this through modal analysis and static analysis).

The other boundary condition, fundamental to obtain a result as truthful as possible, concerns the constraints applied to the structure: this is free to translate and rotate, except at the interface (bibods) with the rest of the satellite on which it is mounted. So they are connected together through a rigid spider (RB2), which generates a central node on which a generic SPC (Single Point Constraint) load of general module 123456 N is then applied.

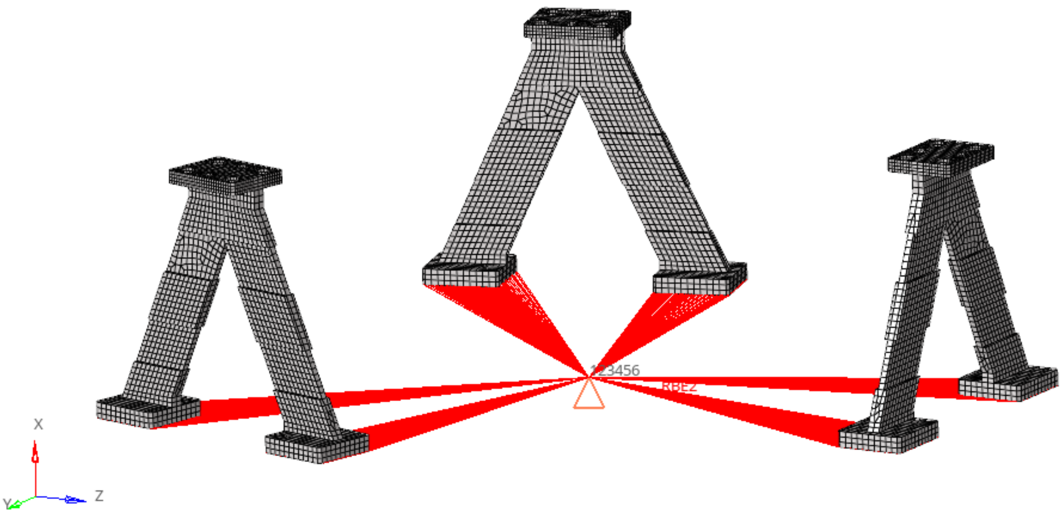

Figure 2.15: RB2 (lines) and SPC load (triangle) representation on the bipods

To connect the various parts to each other, on the other hand, we act on the interfaces, simulating the presence of screws in the various holes. This is done using SPRING elements: we define a CBUSH element, with a certain stiffness of translation (10e7 N/mm) and rotation (10e5 N/mm) in the three directions, between two rigid spiders calculated on the nodes of the connected holes.

The choice to use CBUSH elements rather than CBEAM stand in the simplicity and convenience of this solution: it is sufficient, in fact, to define a single PBUSH property to describe all the CBUSH elements. Instead, we should indicate different properties for each CBEAM element that has different dimensions and applied moments.

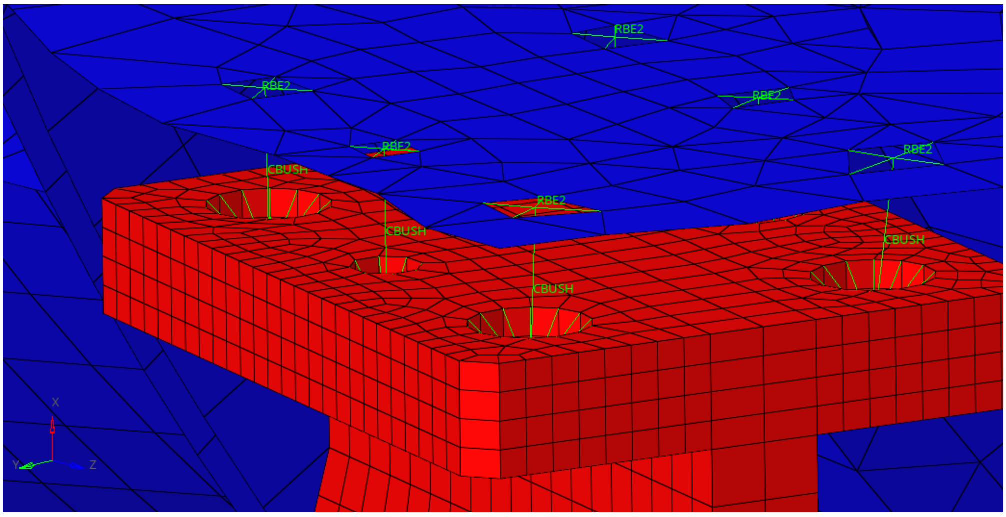

Figure 2.16: CBUSH elements representation on some holes of the structure

Then, we can add this last property for the connection elements to the previously defined list.

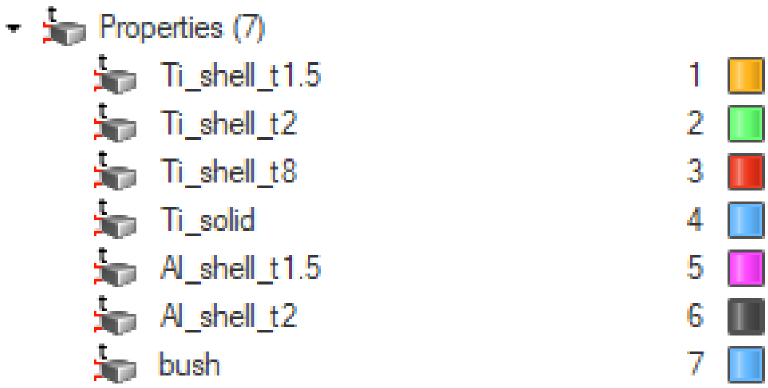

Figure 2.17: Properties definition (with PBUSH)

Finally, to ensure that the analysis is as complete as possible, we must define the concentrated masses of those elements present in the system, but not modelled. And so we have:

1. The mass of the five lenses (calculated from their volume measured in the CAD file, considering a generic density of 5.4e-9 t/mm3), including rings;
2. The mass of the support and the focal plane cover (with the filter inside it);
3. The mass of the shutter motor.

These masses are manually inserted in the nodes corresponding to the centroids of the corresponding components. Once this is done, it is possible to have an initial mass budget for the entire structure.

Component Name	**Mass** [kg]
Lens #1 + Ring	2.5789
Lens #2 + Ring	1.0489
Lens #3 + Ring	0.2779
Lens #4 + Ring	0.2376
Lens #5 + Ring	0.1309
Lens Total Mass	**4.2742**
Bipods (x3)	0.2196
Upper Support	1.2680
Lower Support	0.8545
Baffle	0.9414
Focal Plane Cover	0.1500
Focal Plane Support + Filter	0.1500
Shutter Motor	0.5000
Structure Total Mass	**4.0835**
Lens + Structure Mass	**8.3577**

Table 2.2: Mass Budget

2.5 Modal Analysis

At this point, all the inputs necessary to carry out the finite element analysis of the structure are present. First of all, we proceed with the modal analysis, which outputs a series of resonant frequencies and the modal participation of the individual masses involved. This last parameter allows us to identify the main frequencies, that is, those that involve a large part of the structure and not just a single component. To start the analysis, we must define the number of modes to consider: in this case we choose the first twenty modes.

#	Frequency [Hz]	X_T	Y_T	Z_T
1	**1,277000E+02**	0,01%	**70,99%**	4,65%
2	**1,895000E+02**	3,71%	**6,36%**	**41,14%**
3	2,534000E+02	0,03%	**5,21%**	3,68%
4	**3,591000E+02**	**25,70%**	0,00%	**13,29%**
5	3,770000E+02	1,85%	0,02%	**6,65%**
6	4,226000E+02	**40,85%**	0,06%	**18,72%**
7	4,883000E+02	2,14%	**6,74%**	0,75%
8	5,910000E+02	0,01%	0,26%	**5,77%**
9	6,260000E+02	0,00%	0,00%	0,00%
10	6,263000E+02	0,00%	0,00%	0,00%
11	7,079000E+02	0,47%	**6,48%**	0,08%
12	8,505000E+02	0,17%	0,13%	0,00%
13	9,500000E+02	0,06%	0,14%	0,81%
14	1,122000E+03	**14,90%**	0,00%	0,27%
15	1,183000E+03	0,02%	0,01%	0,00%
16	1,193000E+03	0,03%	0,03%	0,00%
17	1,218000E+03	1,62%	0,00%	0,13%
18	1,275000E+03	2,96%	0,00%	0,09%
19	1,287000E+03	0,64%	0,03%	0,01%
20	1,328000E+03	0,06%	0,00%	0,24%
Subcase Total		**95,24%**	**96,45%**	**96,28%**

Table 2.3: Modal participation of the first twenty frequencies

The mass modal participation is shown as a percentage for the translation along the three axis (the rotation is not considered). The percentages to be considered are highlighted in red, as they are higher than 5%. The last row ("Subcase Total") shows the percentage of total mass that is involved in that particular movement: this is equal to about 90% in all three DoF. It means that this first twenty resonant modes are sufficient to extinguish the entire mass of the structure.

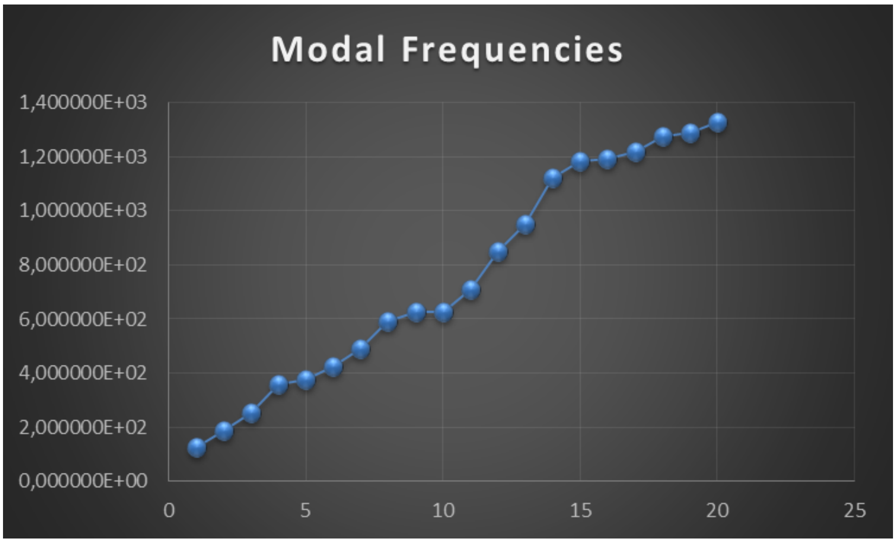

Figure 2.18: Resonant frequencies trend

Only ten of these twenty frequencies are relevant. This means that only ten frequencies show a high modal participation in at least one degree of freedom: frequencies number 1 to 8, 11 and 14.

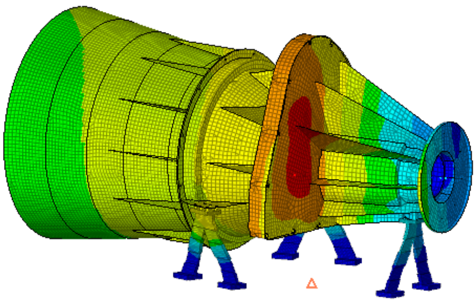

(a) *F1*

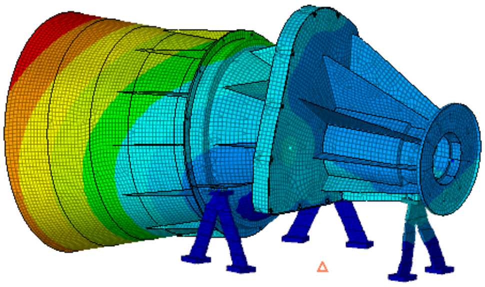

(b) *F2*

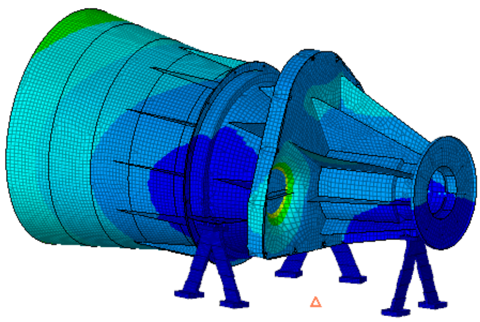

(c) *F3*

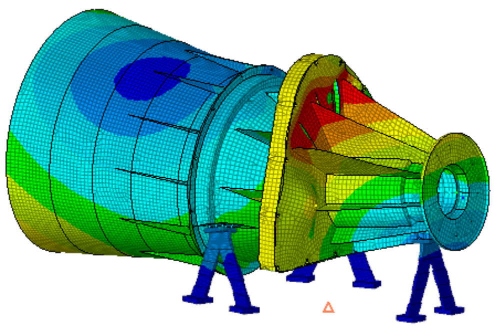

(d) *F4*

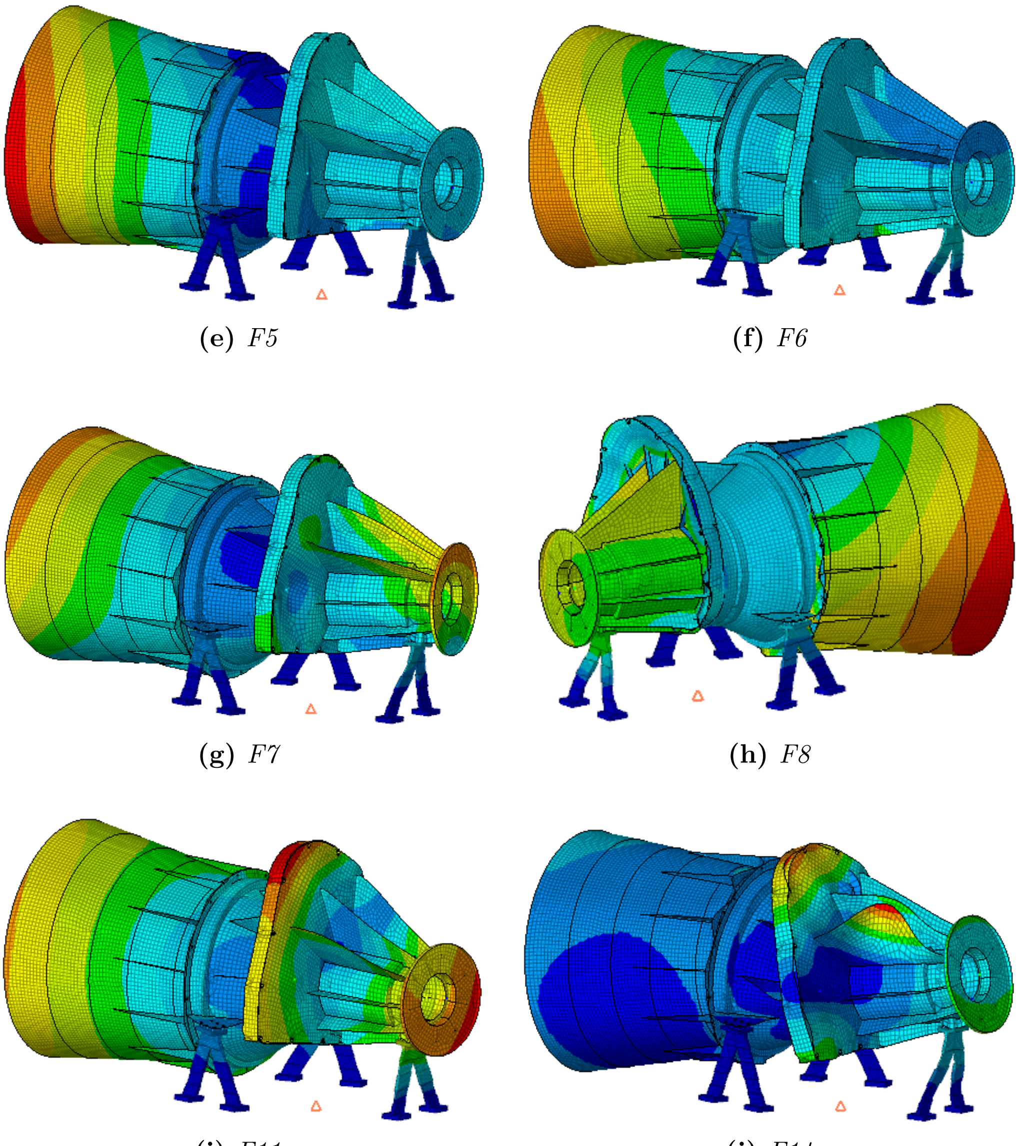

(e) *F5* **(f)** *F6*

(g) *F7* **(h)** *F8*

(i) *F11* **(j)** *F14*

Figure 2.19: Relevant resonant frequencies (high modal participation)

In the images above we can see the contouring of the structure subjected to relevant resonant frequencies and the parts most (highlighted in red) and less (highlighted in blue) involved, with a scale factor of 1.

In the two images below, instead, we can see what happen to the structure while frequencies 9 and 10 are applied: they show a completely no modal participation, in fact we notice localized load concentrations, to not be considered.

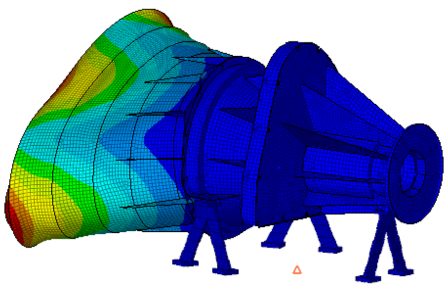

(a) *F9*

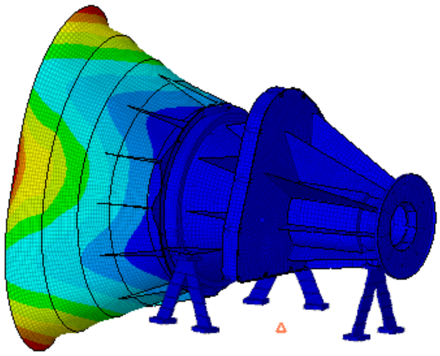

(b) *F10*

Figure 2.20: Not relevant resonant frequencies (no modal participation)

2.6 Static Analysis

Once we have done the modal analysis and all the relevant resonant frequencies have been collected for the study, it is possible to move on to the static analysis in order to establish other information regarding displacements, stresses to which the structure is subjected and deformations.

As for the modal analysis, in this case it is necessary to enter adequate inputs. We have to study the behaviour of the structure under a gravity load equal to 25G in the three main directions, taking the three cases individually (all the images that we can see below are obtained using a model units equal to 50, in order to better highlight the application of the load).

For each of the three cases, a load step is defined to carry out a linear static analysis, entering the gravitational load along the considered direction and the constraint conditions (SPC load). To define the gravitational load, we have just to write the module (25G = 245.25 m/s^2) and indicate the direction of application through a three-coordinate unit vector (N1, N2, N3). For example, for the case along the x axis, we consider the unit vector (1, 0, 0).

2.6.1 Static Analysis along the x-axis

We start by considering the case of 25G along the x-axis and in the image below we can see the displacement contouring: it is maximum on the baffle with a value of 0.122 mm.

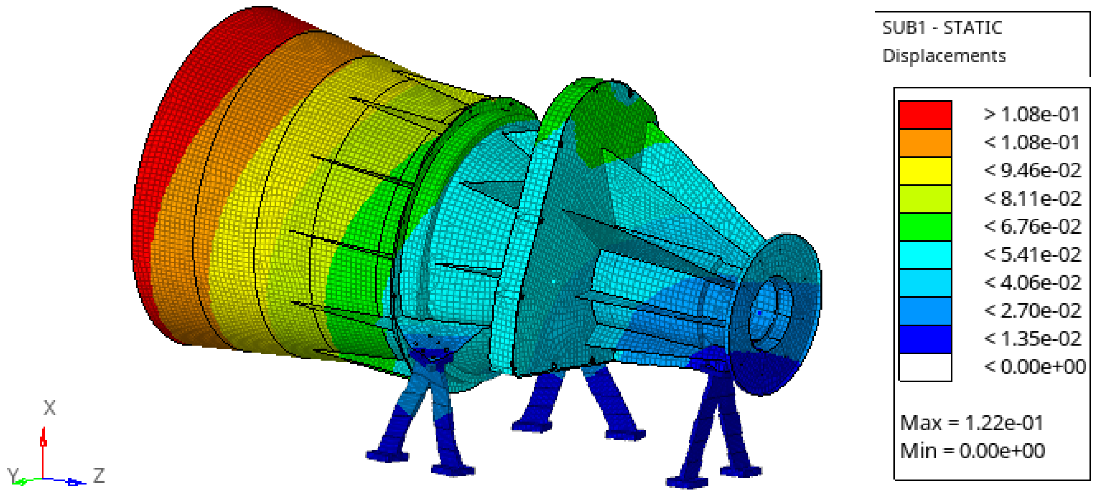

Figure 2.21: Displacement along x

This result is exactly what was expected since the baffle, not being fixed to the ground, is free to move along the x-axis, unlike the other components constrained by the three bipods interface.

Then we can take a look to the stress and deformation maps and how they modify the structure. We obtain what is shown in the following images:

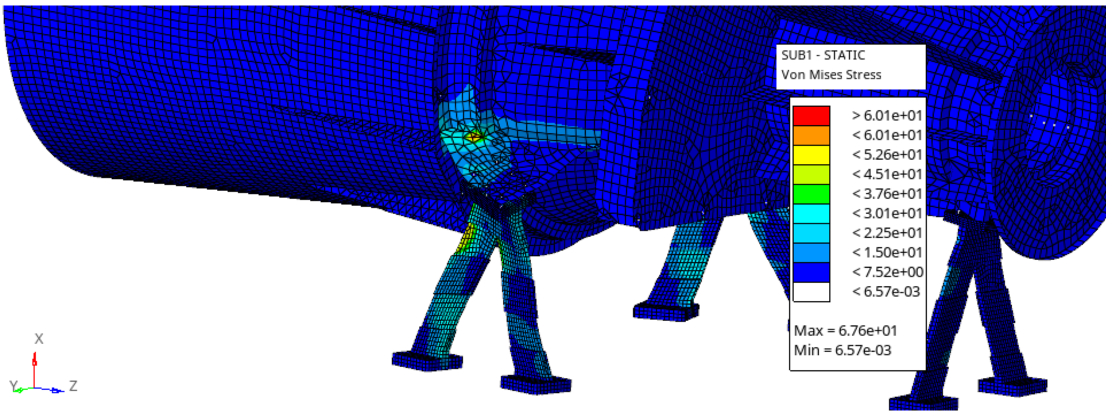

Figure 2.22: Von Mises Stress along x

As we could easily guess, the stress is concentrated on the two lateral bipods, with a maximum of 67.6 N/mm^2. The same can be said for the deformation, with a maximum at $4.23e^{-}4$ on the same area.

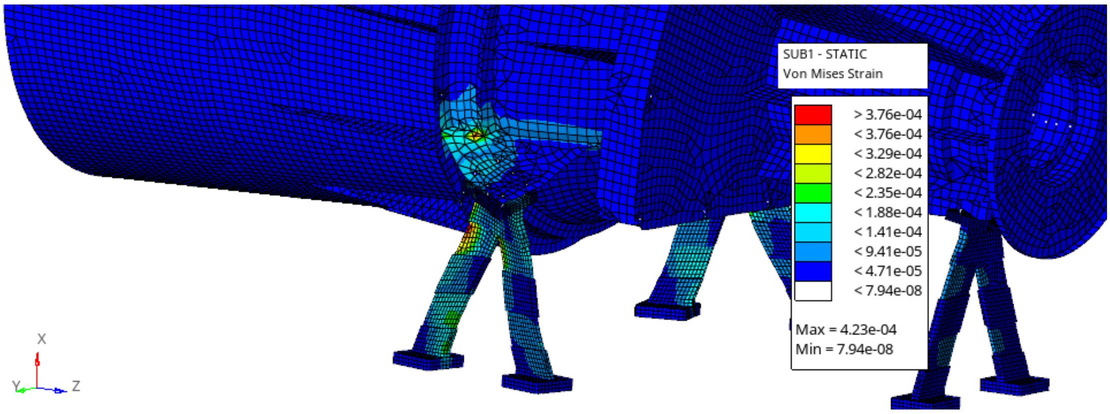

Figure 2.23: Von Mises Strain along x

If these results do not meet our expectations, a check that we could make consist in visualizing the SPCF (Single-Point Constraint Force) contouring. By displaying this we obtain a maximum force of $2.01e^3$ N which, divided by the acceleration of 25G, it must equal the mass of the entire structure, since $m \cdot a = F$:

$$m = \frac{F}{a} = \frac{2.01e^3}{25G} = \frac{2.01e^3}{245.175e^3} = 0.0081982t \approx 8.3577kg \tag{2.1}$$

Since we have got approximately the mass of the entire structure, the verification is done with success and the analysis is correct.

2.6.2 Static Analysis along the y-axis

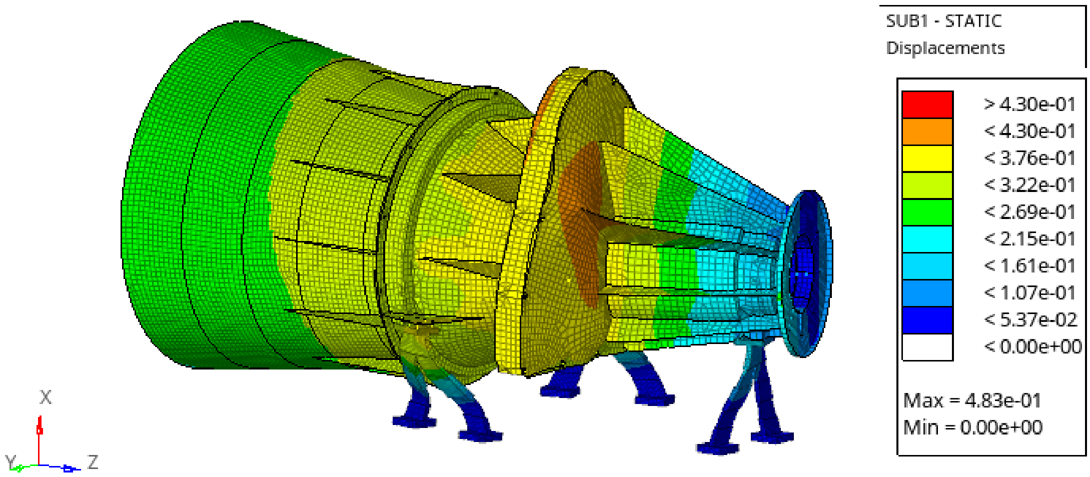

Figure 2.24: Displacement along y

Proceeding in the same way for the case of 25G along the y-axis, we obtain a maximum displacement of 0.483 mm, located near the shutter motor at the interface between the two conical supports. Regarding the stress and the deformation, we have a maximum of 151 N/mm^2 and $1.14e^{-}3$ respectively.

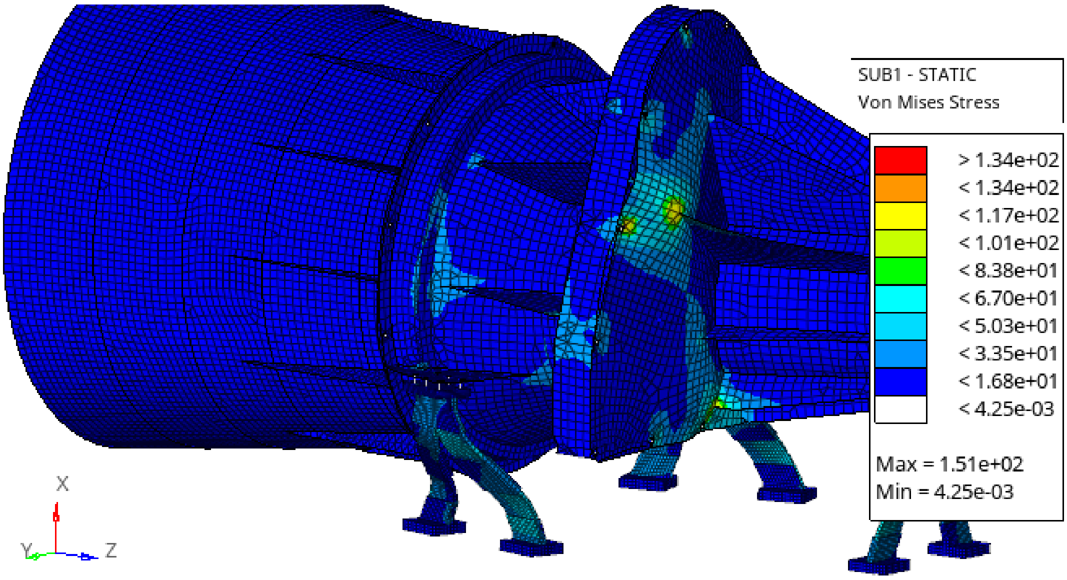

Figure 2.25: Von Mises Stress along y

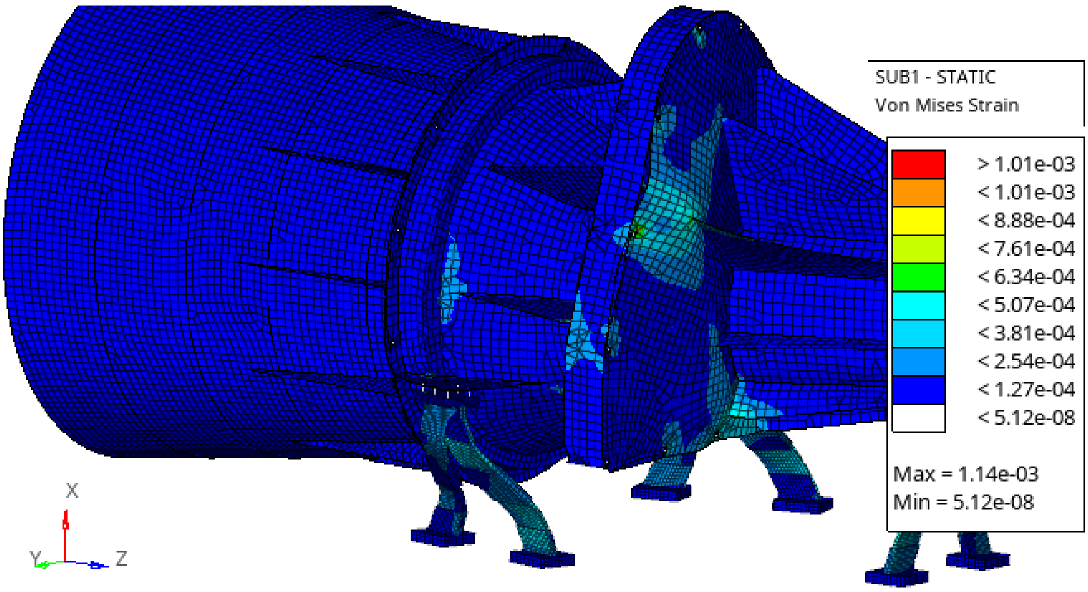

Figure 2.26: Von Mises Strain along y

In this case, the stress is concentrated at the interface between the two conical supports, considering the shutter motor mass and the structure shape.

2.6.3 Static Analysis along the z-axis

Finally, we have to see what happens in the case of 25G applied along the z-axis. We obtain a maximum displacement of 0.313 mm near the baffle, since the application of a force along z-axis (i.e. along the conical supports symmetry axis) and the constraint applied to the bipods, cause a displacement along the x-axis of the only unconstrained element, so the baffle.

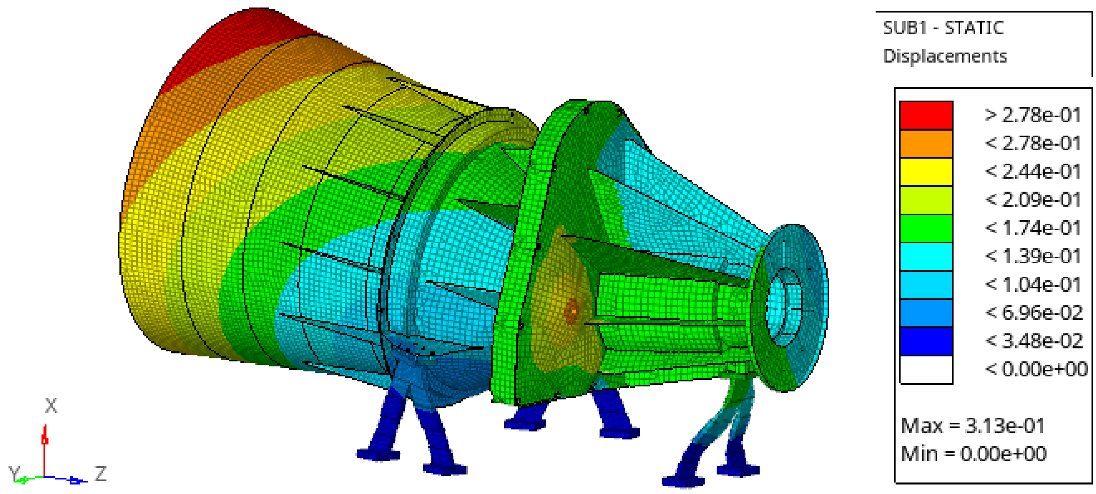

Figure 2.27: Displacement along z

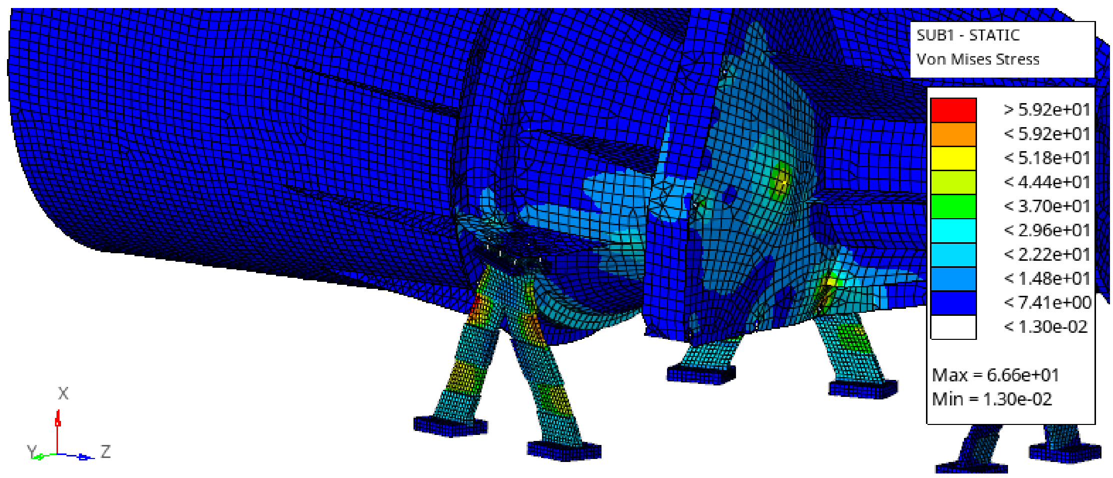

Figure 2.28: Von Mises Stress along z

Regarding the maximum stress along the z-axis we get 66.6 N/mm^2 and 5.21e^{-}4 for the maximum deformation.

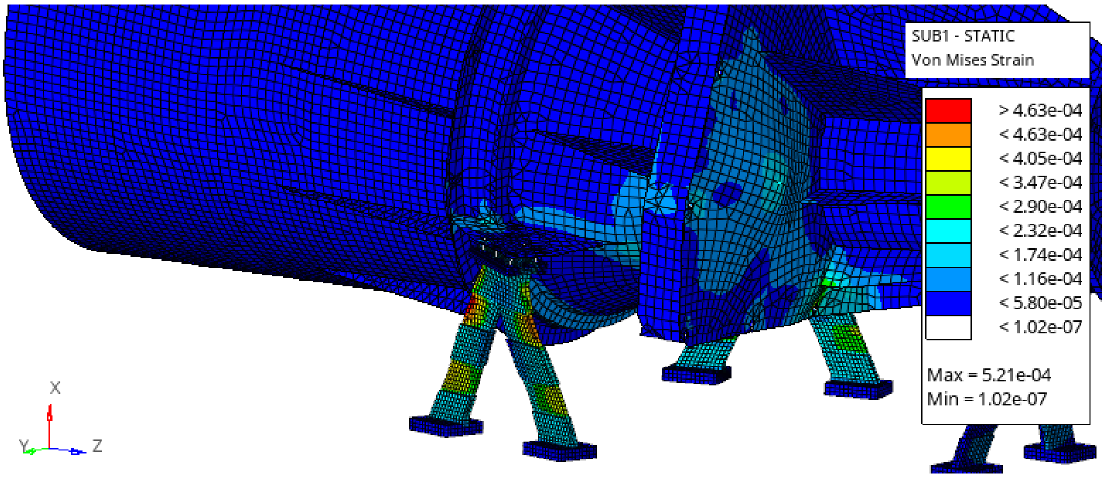

Figure 2.29: Von Mises Strain along z

In this case, the stress (and so the deformation) is maximum on the bipods and near the shutter motor, due to the concentrated masses displacement along z. The verification of the accuracy of the results through the SPCF contouring can be done for the load cases along y and z too, but in both situations we obtain values that allow the two static analyzes to be considered correct.

2.6.4 Static Analysis in the three directions

Now all that remains is to see what happens in the global case in which there is an acceleration of 25G along all three directions and then the three previously studied cases will be superimposed. The results obtained are:

1. Maximum displacement of 0.659 mm, located near the shutter motor

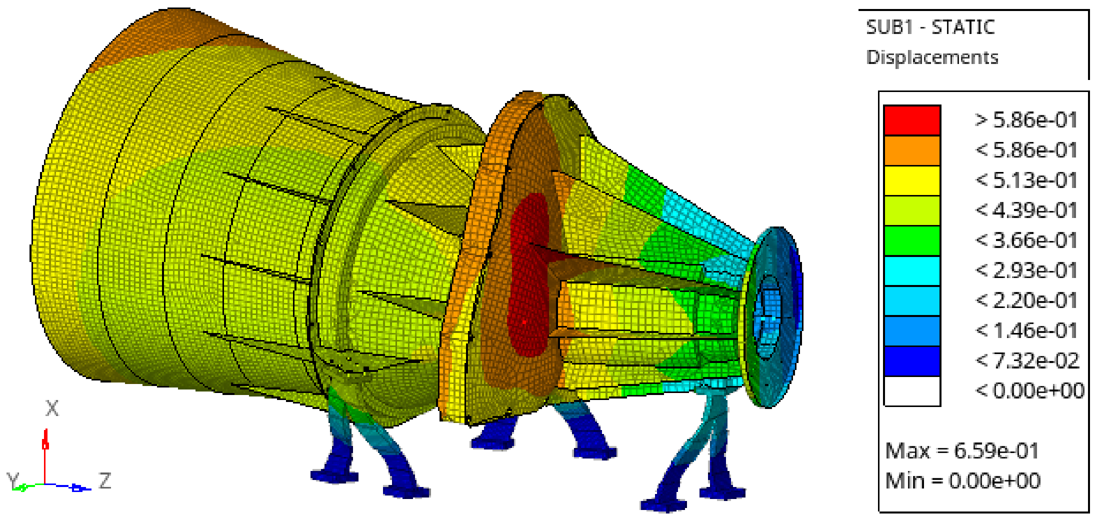

Figure 2.30: Total Displacement

2. Maximum stress and deformation at 176 N/mm^2 and $1.09e^{-}3$ on the lateral bipods and the interface between the two supports

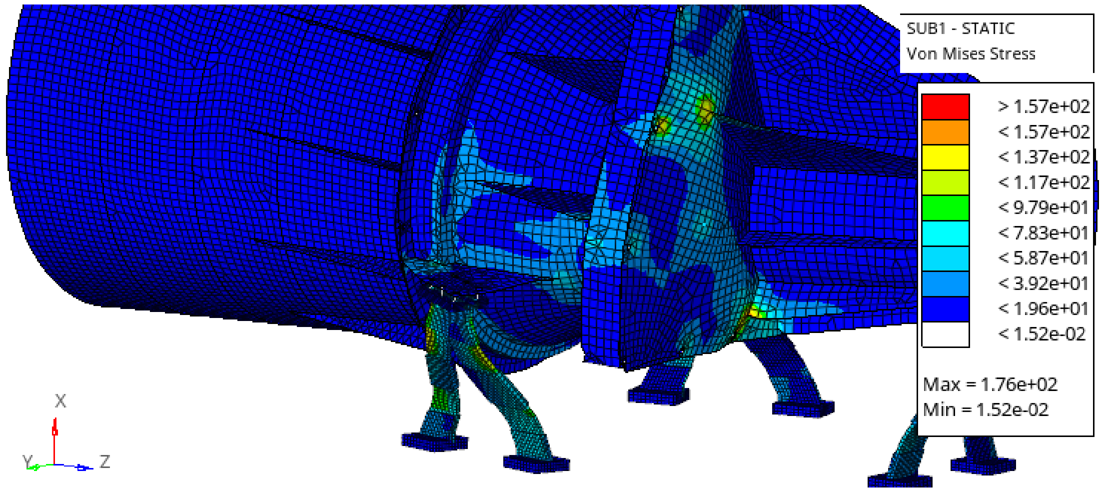

Figure 2.31: Total Von Mises Stress

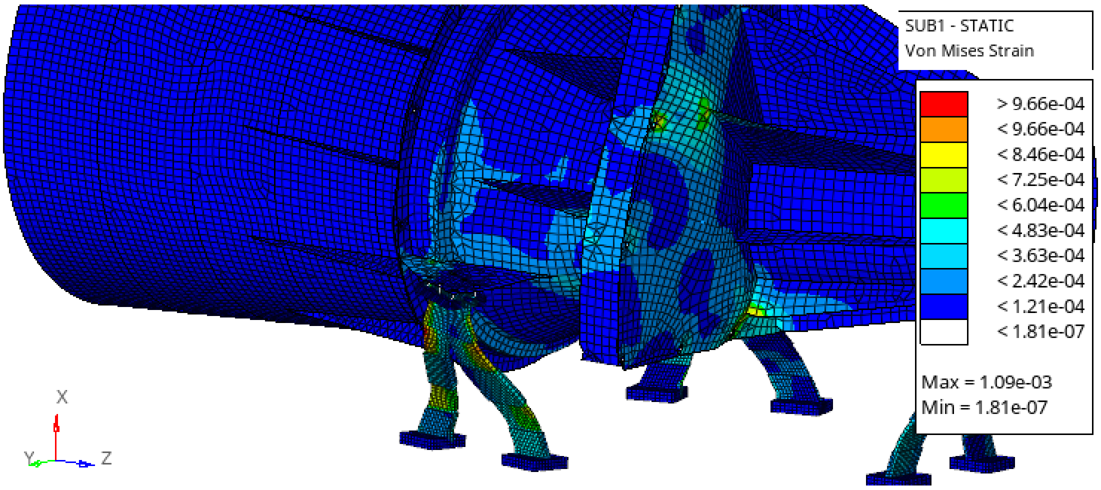

Figure 2.32: Total Von Mises Strain

Both for the three static analyzes carried out considering the load along each of the three main directions and for the one carried out considering the loads overlap, we mainly get two values from the output file: Compliance and Epsilon. We can see these values in the table below:

Axi	Compliance	Epsilon (residual strain energy ratio)
x	3.631576E+01	8.572569E-10
y	2.961576E+02	-7.154130E-09
z	1.122275E+02	1.539704E-09
Tot	5.537939E+02	-4.444291E-09

Table 2.4: Static Analysis results: Compliance and Epsilon

Epsilon (Residual Strain Energy Ratio) is a measure of the performed analysis error, which is the ratio between the work done by the non-equilibrium forces and the work done by the external force (so it is a ratio between residual and deformation energy). If this value is less than 1.0e-8 then it is acceptable, otherwise, the analysis is not correct. According to what has just been said, all the analyses are correct.

Compliance (reciprocal of stiffness) , on the other hand, represents the energy of deformation: in general, when a force is applied, a certain displacement results. It can be calculated as

$$C = FT \cdot U, \qquad with \begin{cases} FT = transposed\ force \\ U = displacement \end{cases} \tag{2.2}$$

This parameter is very useful if you want to analyse the structure individually under different loads. The total Compliance is calculated by adding the values of the individual cases, multiplied by a weighting factor chosen based on the importance given to that particular case. In our analysis, the total result is automatically calculated during the global static analysis.

Chapter 3

Preliminary Topological Optimization

In this second phase of the project, the focus shifts from the preliminary structural analysis to the search for a geometry that maintains the same performances as the previous case (or maximizes them), while decreasing the mass or maximize the stiffness. To do this, we set up a topological optimization of the structure.

For this second part of the study we use Inspire 2020, which is another software provided by Altair. First of all, we now consider the maximum overall volume of the two conical supports, that is the part of the structure involved in optimization. So a solid volume is created using CAD and then reduced through optimization.

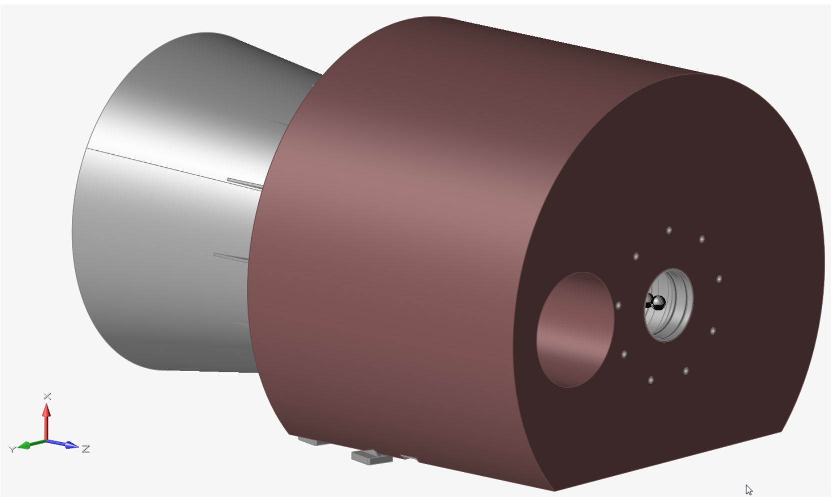

Figure 3.1: Maximum overall volume considered for the optimization

3.1 Design space and non-design space definition

Before the topological optimization we have to divide the design space from the non-design space, so we need to isolate the part of the structure that we want to optimize. In the last image, the design space is identified by the brown colour (in gray we have the non-design space).

First we need to understand what design space is and what it is for. The design space is constituted by that portion of volume that is changed as a result of a topology optimization. This design space allows us to define the area of interest and separate it from everything that must not change after all the simplifications obtained by the optimization.

Since our object is part of a larger assembly, it will then have to interface with other components. If we did not define the design space, after optimization, we could get a structure with a completely different geometry and arrangement, causing assembly difficulties.

Understanding the importance of the design space and its usefulness within the project, we can now identify which areas of the structure must remain the same and which must change after optimization. We start from the assumption that the optimization has to reduce, even if in small part, the mass and maximize the rigidity of the structure. Another constraint is the increase of the first resonant frequencies.

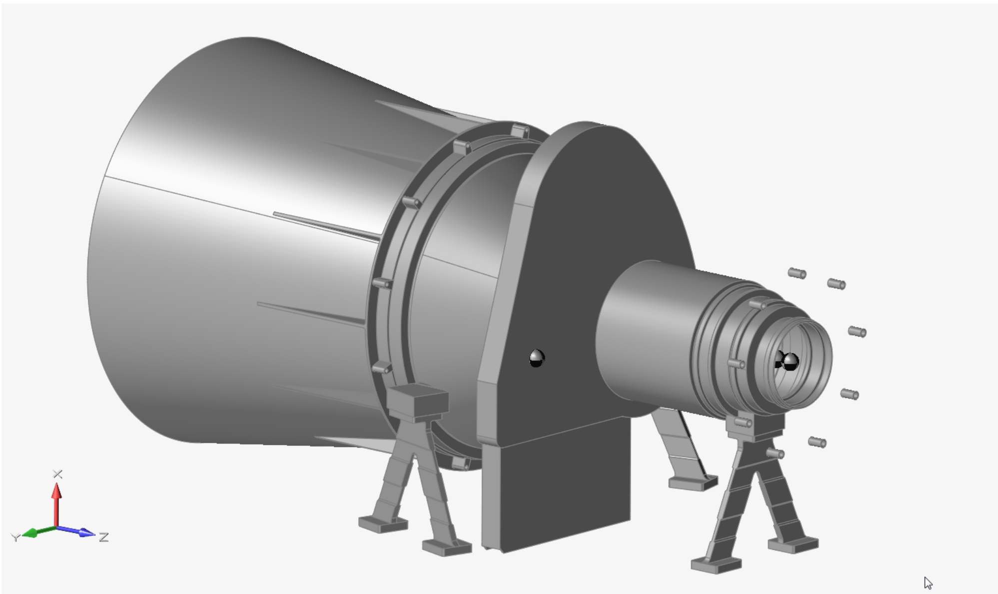

Figure 3.2: Non-design space

3.1.1 Non-design space definition

In the image above we can see all the different parts that define the non-design space. Some of them are connected through connectors (such as the baffle and the optical tube) or simple contact (the two supports), while others are completely separated from everything else (such as the interface holes between the conical support and the focal plane cover).

First we must ensure an interface between our telescope and the satellite, so the bipods must remain unchanged, both in shape and position. They also represent the main constraint of the structure under analysis. Further we must consider that the interface between the bipods and the supports must remain so as to be able to ensure their structural stability and the presence of connecting elements such as screws. For this reason, parallelepipeds containing the locations for the screws of the conical supports have also been inserted in the non-design.

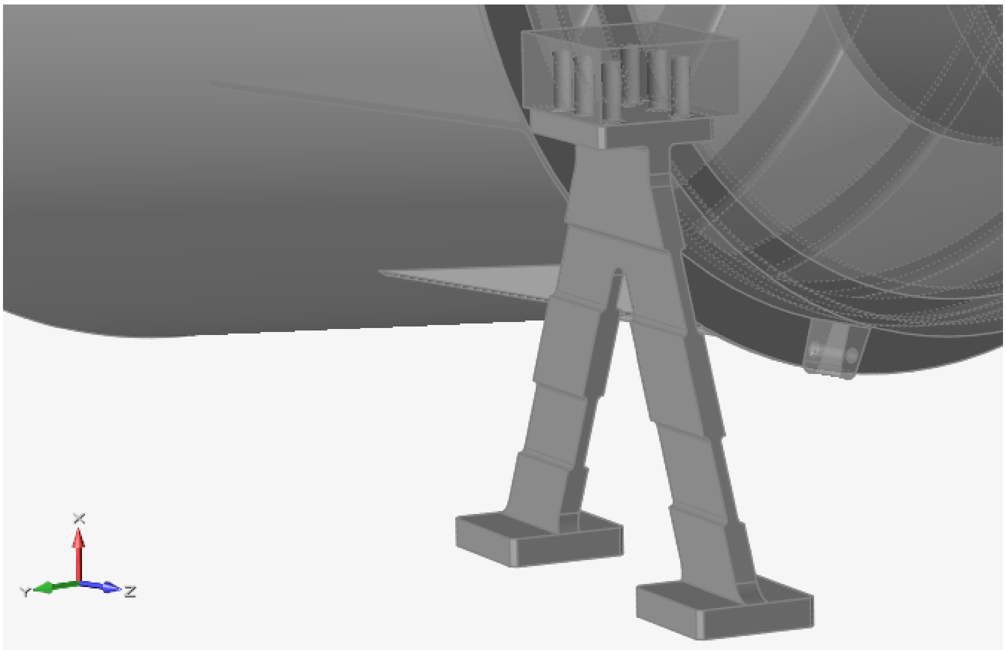

Figure 3.3: Detail on the bipod: locations for the screws

Another part of the structure that does not change in topological optimization is the baffle, which remains the same as seen in the previous chapter. Also for the optimization process we must proceed with necessary geometric simplifications, so we must remove all those details that we do not have to take in consideration, as they could cause problems during the calculation.

Surely, the most important part to include inside the non-design space is the optical tube, i.e. the part of the structure that hosts the lenses. This part must be the same as defined in the design phase, otherwise we risk not being able to allocate the lenses or change the diffusion of the optical beams.

To obtain this volume, we used the "Partition" function, present in the Geometry panel. Through this command, we can select the surfaces that we want to part from the design space and define their thickness. Then, through modifications to the structure and Boolean combinations (Geometry > Boolean > Combine), we arrived at the definition of the entire optical tube, which will then be further modified externally, as it has a too intricate geometry to create a precise mesh.

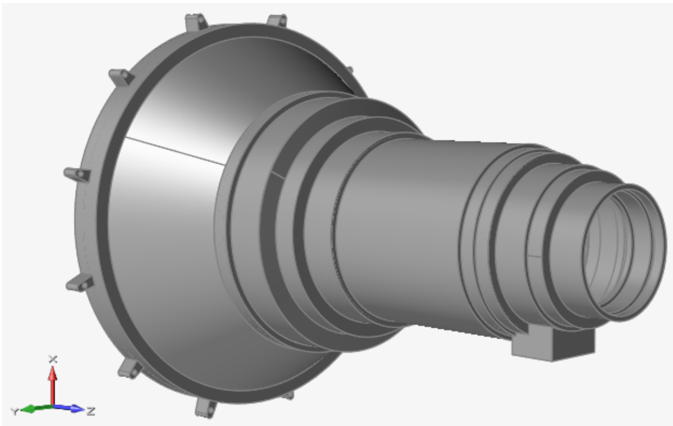

Figure 3.4: The optical tube (with geometrical simplifications)

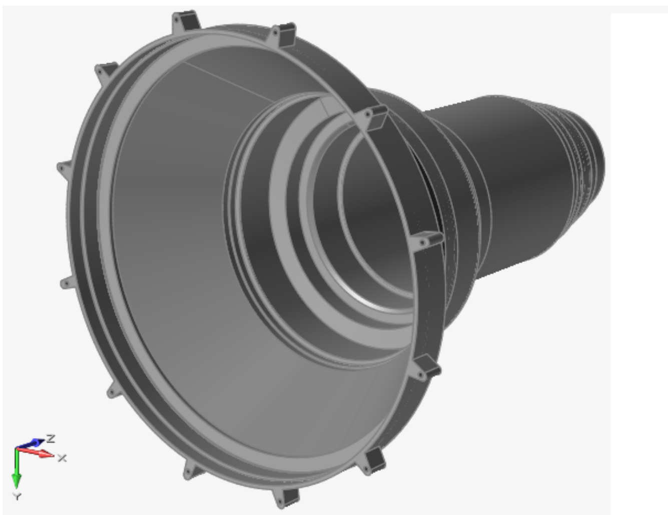

Figure 3.5: Detail on the optical tube: interface holes (with baffle)

An important change is the upgrade from two conical supports to a one-piece support. A further modification to the geometry consists, as in the previous case, in the modeling of comfortable holes for the insertion of screws, which connect the support to the baffle. This modification was done using the Boolean commands in the Geometry panel (combine, subtract and intersect).

The last two elements that are part of the non-design space are:

1. the space needed to insert the shutter rosette;
2. the interface holes between the conical support and the focal plane cover.

For the first one, as we can see in the image below, the original geometry, where the rosette can be inserted once the entire component has been produced, was maintained . For the holes, we create allocations thick enough to prevent a break due to high stresses at the interface points.

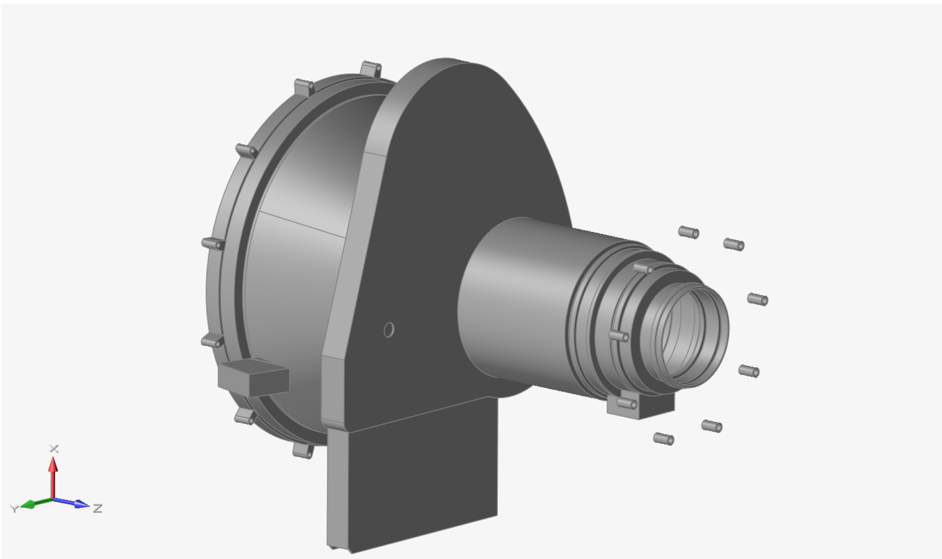

Figure 3.6: Detail on the shutter's rosette allocation and interface holes (with focal plane cover)

3.1.2 Design space definition

Now that the non-design space has been identified, defining the design space becomes very simple. Considering the maximum volume that can be occupied by the two conical supports, the non-design volume is subtracted to it, so we obtain a design space as precise as possible. This is done, again, through the Boolean functions in the geometric edit panel.

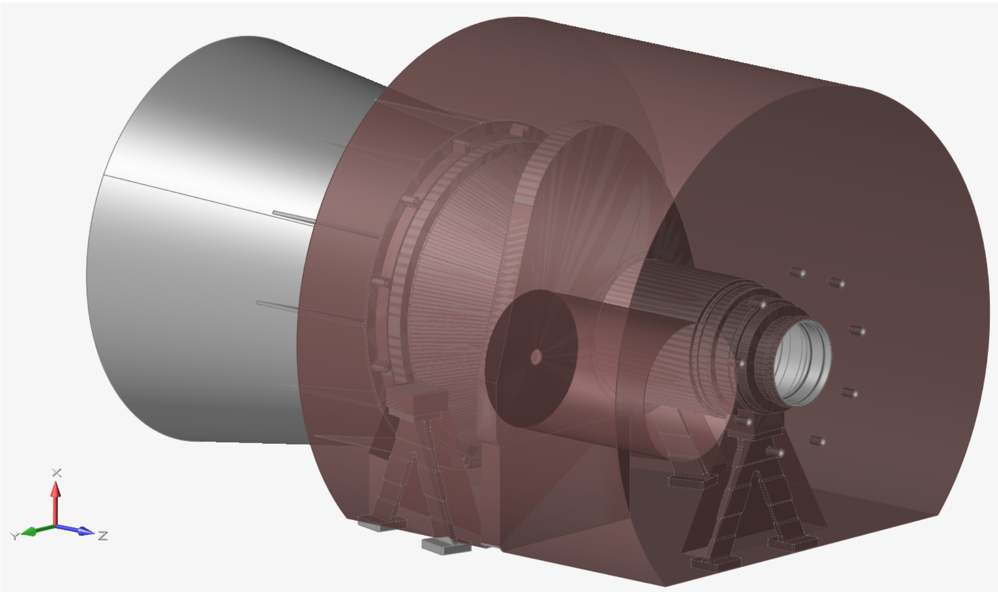

Figure 3.7: Design space definition

As we can see in the figure, in the design space, the space necessary to host the shutter motor and to connect the three bipods is already available.

3.2 Application of constraints, connections and forces

Once we have defined the design space, before starting the topological optimization, we need to verify that the structure works well under applied loads. So it is necessary to start a static analysis to evaluate its behavior.

To run a static analysis of the structure, however, we need to define constraints, connections and applied forces:

1. The constraints are positioned on the three bipods, as in the case of the preliminary FEM analysis seen in the previous chapter. This is done because our structure is connected to the satellite through these three bipods, in which we expect maximum stress.

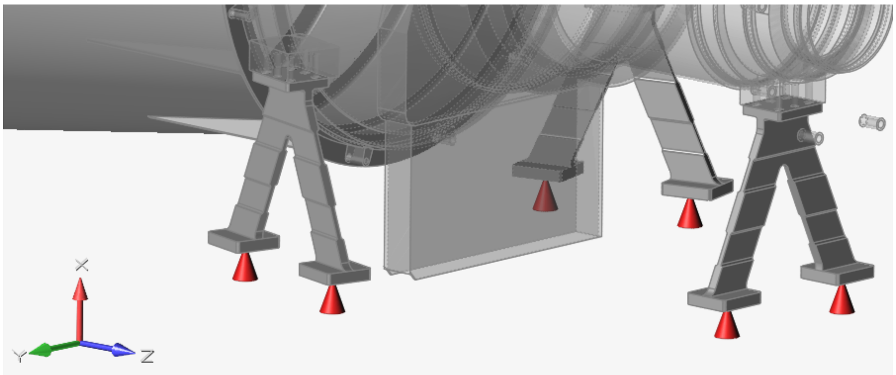

Figure 3.8: Constraints

2. To check the connections between the various components of the telescope there is a command in Insire 2020 called "Contacts" in the Structure panel. This verification allows us to see which surfaces are bonded to each other, coupled or between which there is any type of contact.

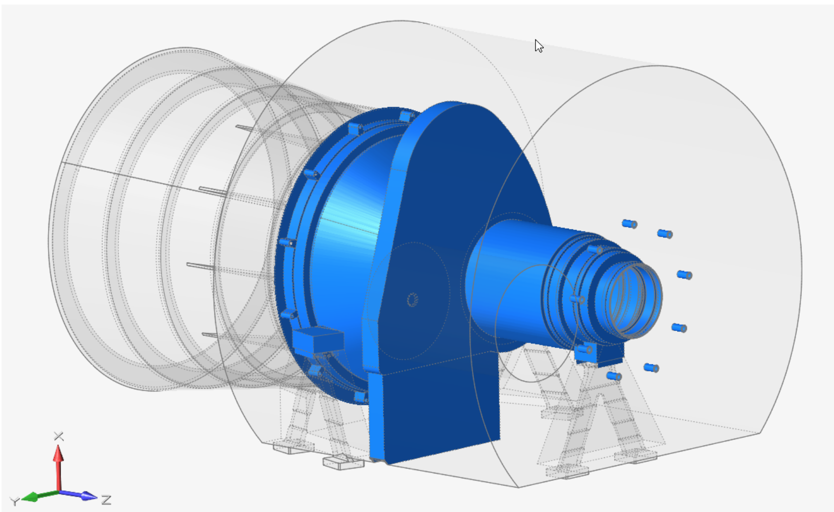

Figure 3.9: Bonded surfaces (blue)

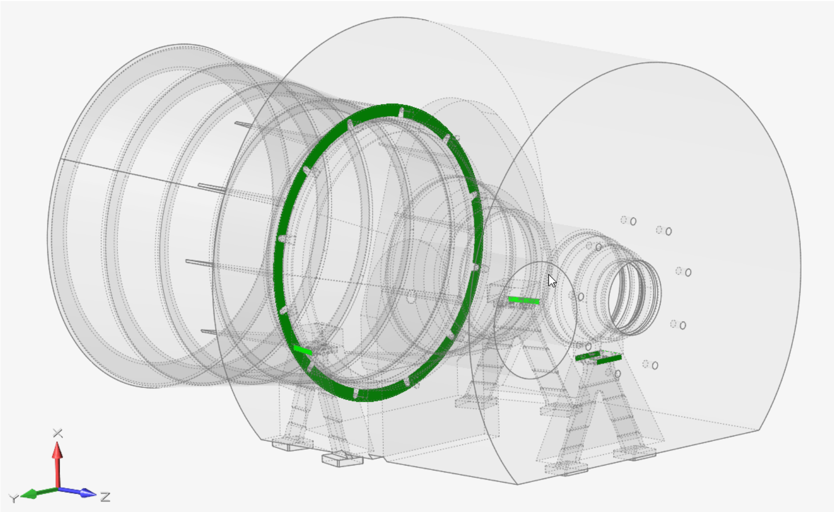

Figure 3.10: Contacting surfaces (green)

As we can see in the two previous images, the bonded surfaces are mainly those of contact between the design and non-design space. While, as regards the connection surfaces, we have those that represent the interface between two parts that have been fixed together with screws.

3. Finally, we just have to define the masses and loads acting on the structure.

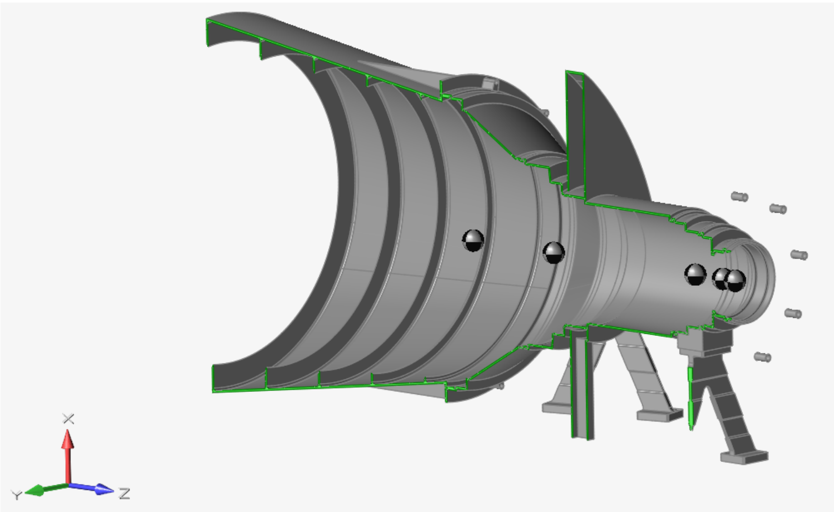

Figure 3.11: Lenses approximation with concentrated masses

In addition to the mass of the structure itself, already considered as the materials are applied, we must take into account the masses of the lenses, the shutter's motor and the focal plane cover.

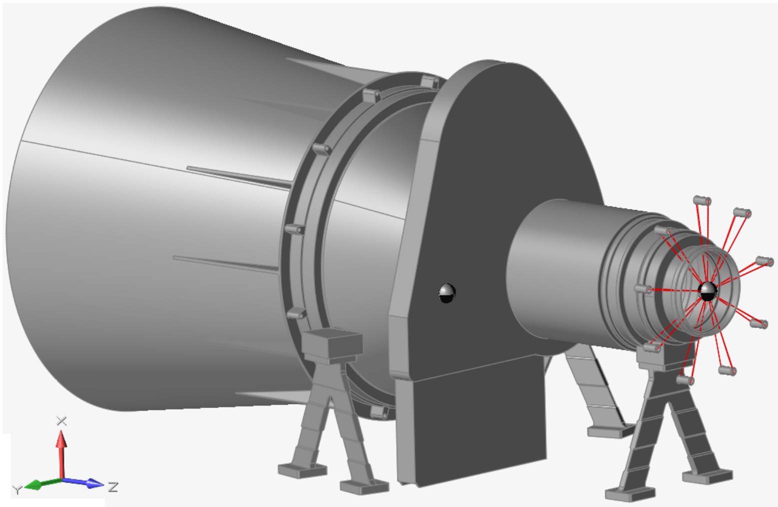

Figure 3.12: SM and FP cover approximation with concentrated masses

At this point we can enter the inertial load acting on the structure. In our case we have an overlap of three gravitational loads along the three axes (x, y and z), which for simplicity are positioned on the baffle (they could be positioned at any point in the non-design space, as they are applied to the entire structure).

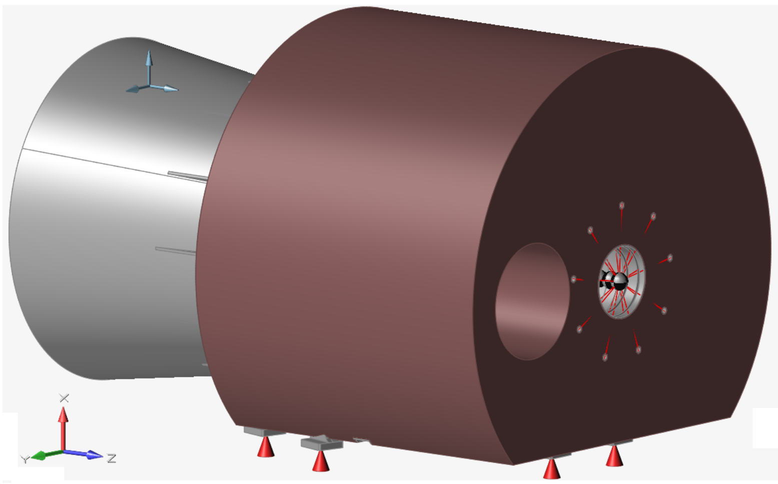

Figure 3.13: Inertial load of 25g along the three directions

3.3 Topological optimization with Inspire 2020

Now that we have all the necessary details defined, we can run the static analysis from "Structure > Analyze":

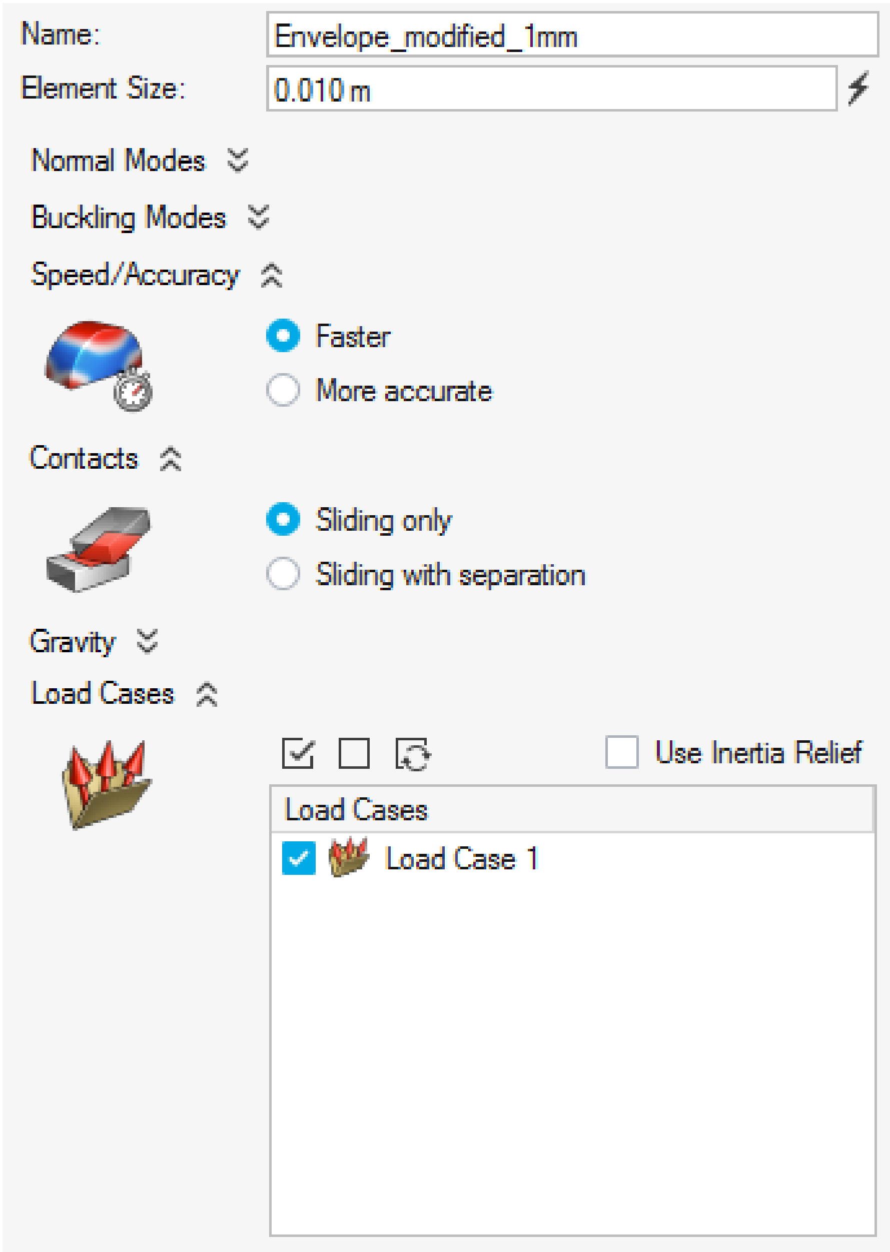

Figure 3.14: Static Analysis Run Options

Unlike Hyperworks X, Inspire automatically applies a mesh to the structure, entering only the size of the elements as input (in this case a size equal to 10mm was used, so coarser than last time).

As can be seen in the following images, the static analysis give us the expected results, as there is a maximum stress in the three bipods. While as regards the displacement, it is maximum in the baffle.

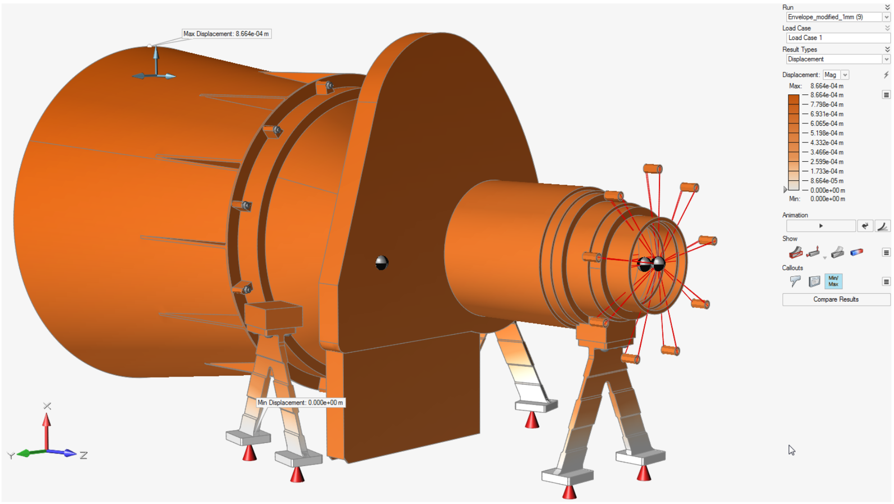

Figure 3.15: Static Analysis Displacement

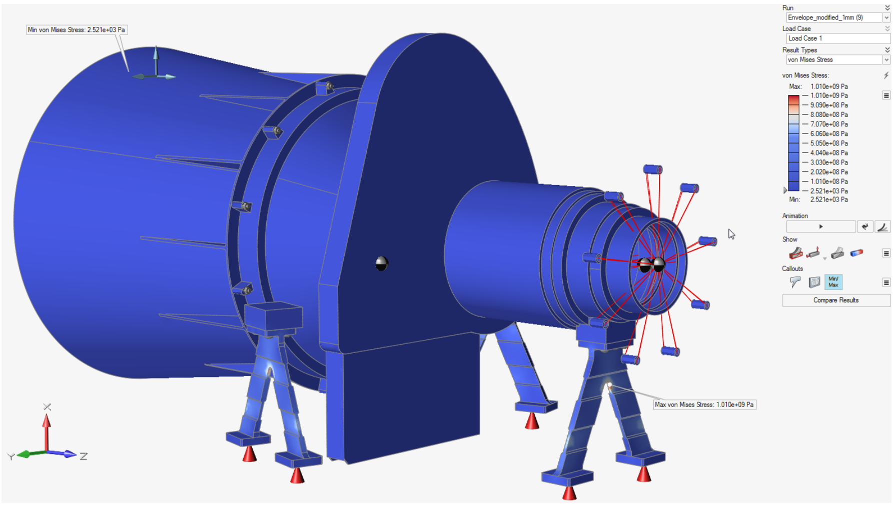

Figure 3.16: Static Analysis Von Mises Stress

Obviously the results are different from those obtained in the preliminary FEM analysis carried out in the previous chapter: this is due to the fact that in this case we consider the maximum overall volume of the conical supports and so we have more mass and so a more resistant structure, with greater volume through which the load can develop.

Once the static analysis has been performed and having verified that everything works, we can proceed with a first topological optimization, to create an idea of what the structure could be once optimized.

To do this, go to the "Structure > Optimize" panel and set the run options, as we can see below.

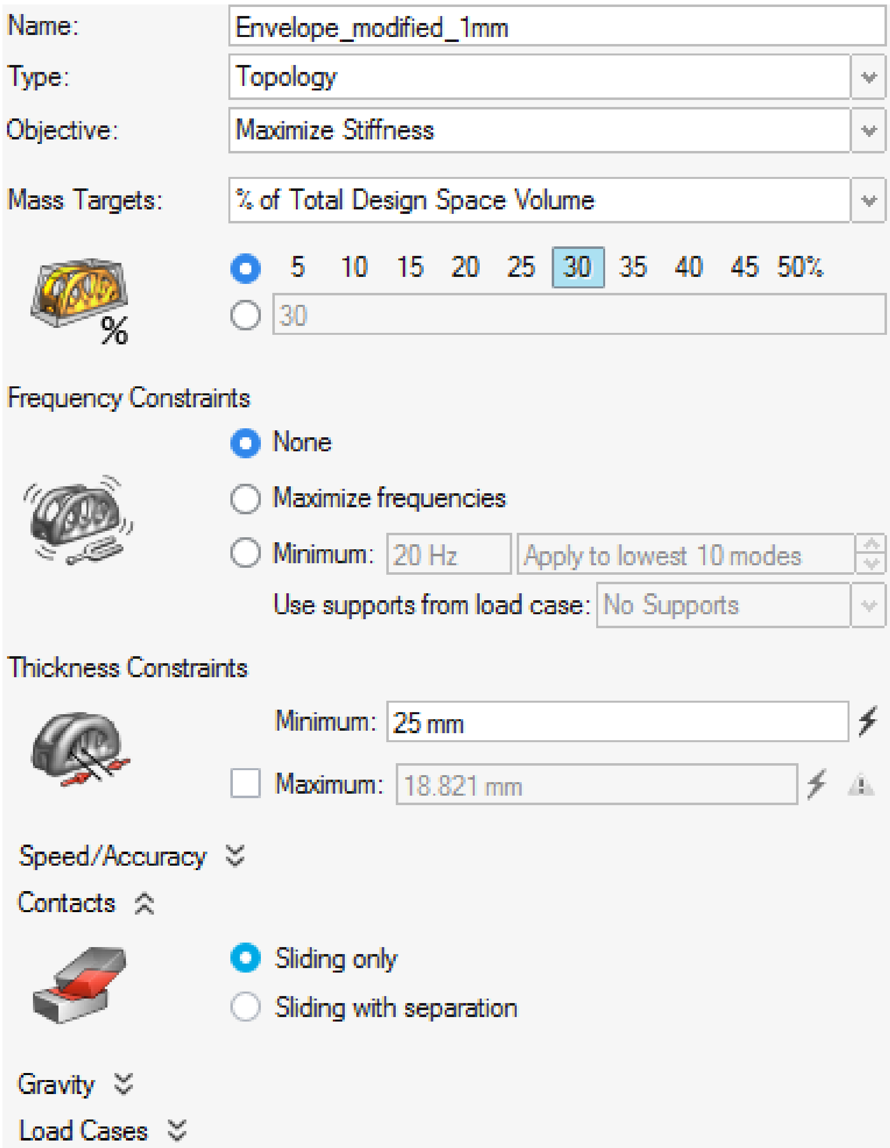

Figure 3.17: Topological Optimization Run Options

As it is higlighted in the previous image, the main goal consists in maximizing stiffness, with a mass target of 30%. No frequency constraints are placed, but a minimum thickness constraint is defined. As in the case of the static analysis, gravity is not considered, but we take into account the current load case, that is the one constituted by the constraints to the bipods and the inertial load of 25g along the three directions.

Now that we have defined all the various parameters, we just have to run the topological optimization and wait for the result (see figure 3.18).

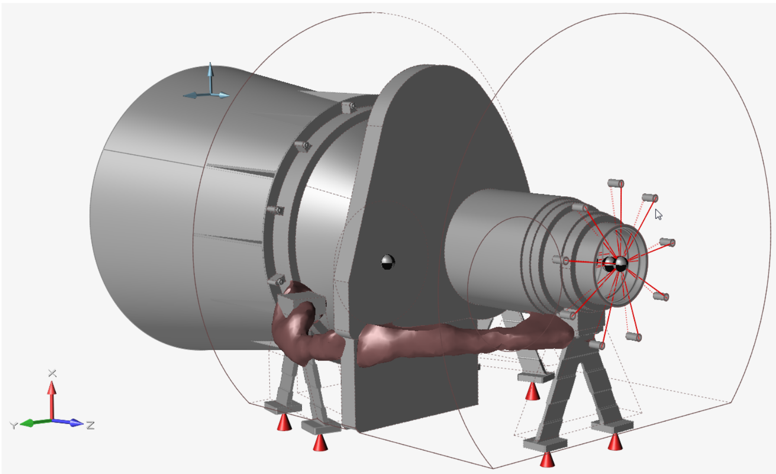

(a) *Detail #1*

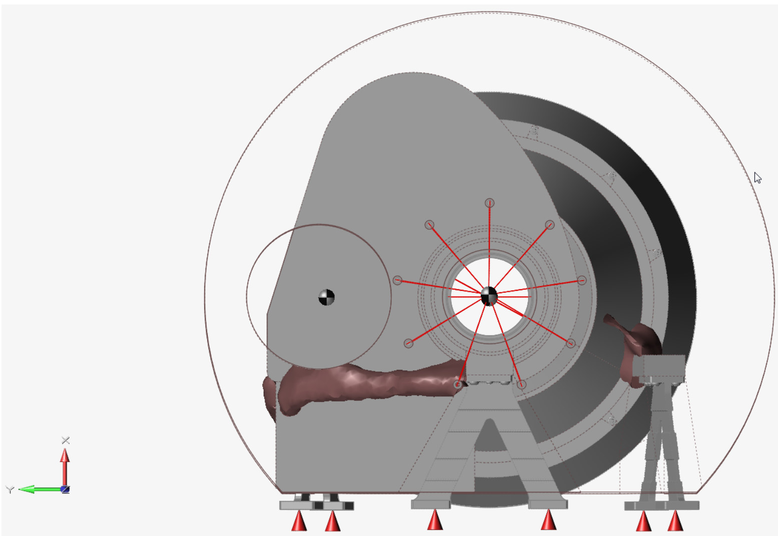

(b) *Detail #2*

Figure 3.18: Topological Optimization Results

These images represent the topologically optimized structure: practically the design space is reduced to the minimum necessary, maintaining a maximum weight of 30% compared to the original, to ensure the stability of the structure and load bearing.

In fact, as we can well see, there are some arms that connect the various parts of the structure, precisely in the areas along which the loads are spread. To verify the feasibility of the optimization it was necessary to carry out a second static analysis on the new optimized structure and below we can see the results.

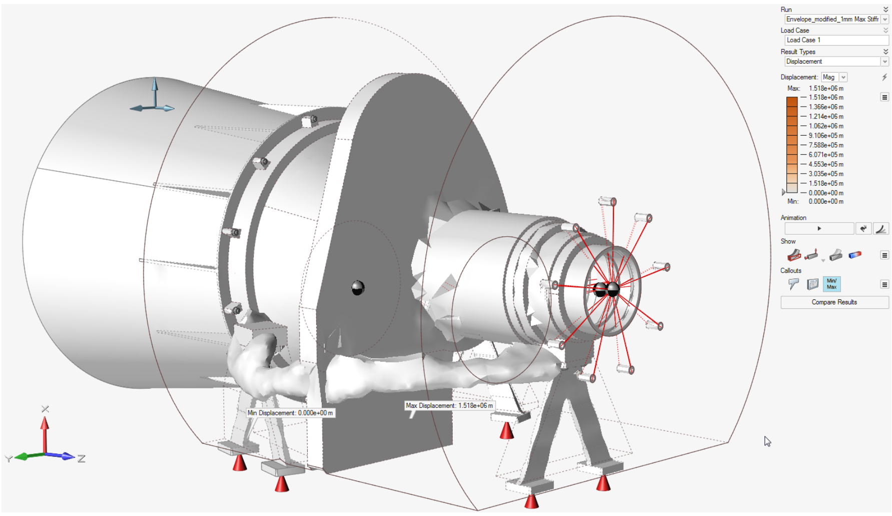

Figure 3.19: Optimized Structure: Static Analysis Displacement

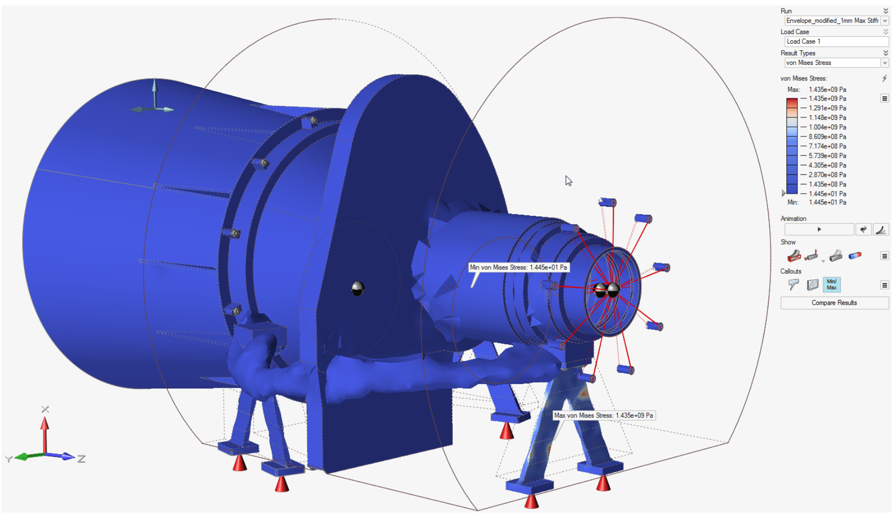

Figure 3.20: Optimized Structure: Static Analysis Von Mises Stress

As we can see in these images, the results are very different from the previous case, as the structure is completely different: we certainly have less mass and therefore less volume and the shape is completely changed. This means that even displacements and stresses have a different behavior and more specifically we can note that:

1. the displacement is practically null in this case;
2. the stress, consequently, is greater on the bipods and especially on the two lateral ones.

Remembering that these analyzes and optimizations are used as a method of verification of the structure to determine its correct functioning and correct design, we must now move on to the HyperWorks X working environment. This is because we must be able to evaluate the mesh that is automatically applied from Inspire 2020 and, in case of good results, proceed with different topological optimizations (trade-off) of the structure to find the best for lattice application.

3.4 Preliminary setup of topology optimization in HyperWorks 2020 X

By importing the FEM file obtained in output from the topological optimization carried out in Inspire into HyperWorks X, we can view both the mesh that has been automatically calculated by the software and all the connections, constraints and loads.

As we can immediately notice in some areas (for example in the conical support) there are some missing elements and so the mesh is not applied in a completely correct way. This is most likely due to the maximum size assigned to the mesh during the static analysis run options definition. In fact, to save processing time, we use an element size of 10 mm, which obviously turns out to be too large for our structure, considering the presence of many curvilinear parts too.

So to solve this problem there are two ways:

1. the first is to go and work on this piece, trying to solve as much as possible the errors in the mesh;
2. the second and certainly the less laborious is to redefine the starting parameters for the static analysis in Inspire, reducing the size of the elements and importing the structure again inside HyperWorks X.

To design a mesh as accurate as possible, we decided to follow the second option and launch a second static analysis on Inspire, reducing the size of the mesh elements from 10 mm to 4 mm. In this way we got a finer mesh (see figure 3.21), but the computation time increased dramatically: we went from a few minutes to about an hour of processing.

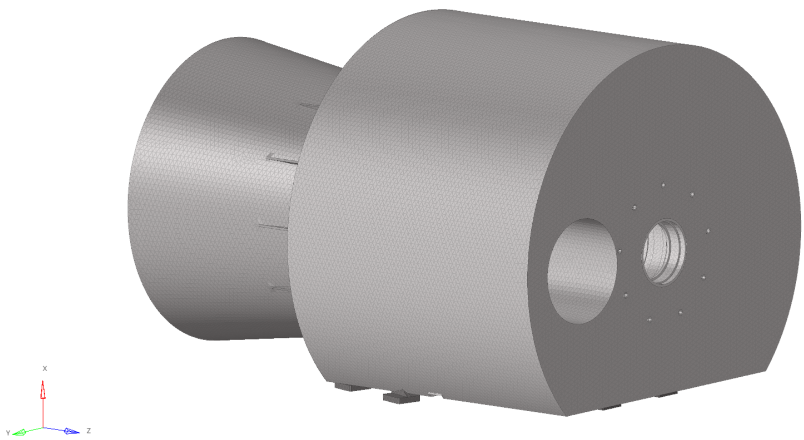

(a) *Mesh with Design Space*

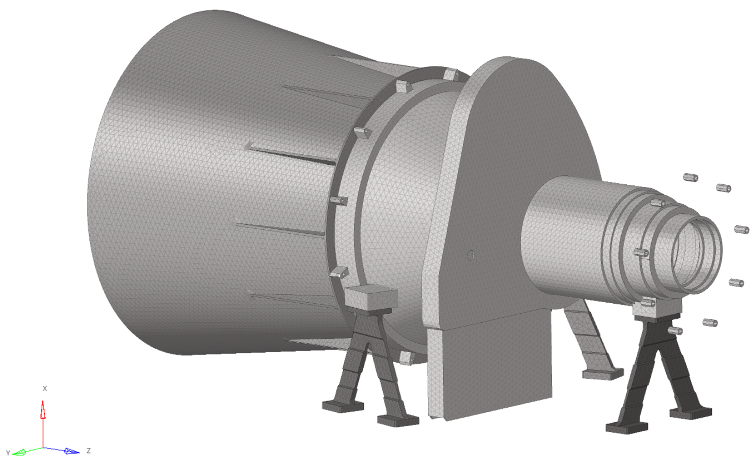

(b) *Mesh without Design Space*

Figure 3.21: Imported structure with finer mesh applied

As we can see, reducing the size of the elements, inside the new mesh there are no discrepancies or errors. At this point, it is necessary to proceed with the observation of the constraints, connections and loads and verify that these correspond to those used in the preliminary FEM analysis, carried out in the previous chapter. After that, further static analysis and topological optimization must be carried out before we can proceed with the lattice optimization. But let's take it one step at a time.

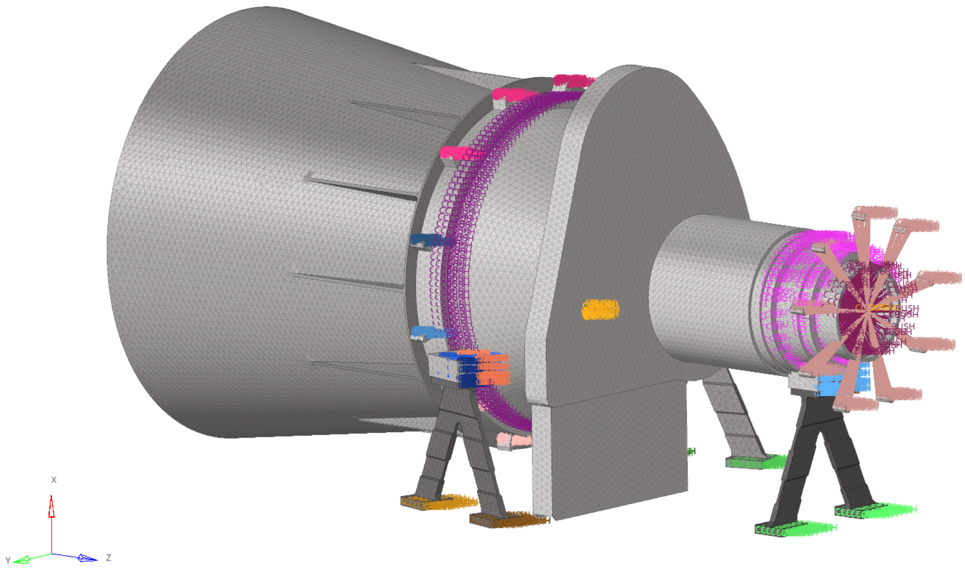

Figure 3.22: Imported structure with constraints, connections and loads

To better understand the difference between the several components of the assembly, in this part, each part is identified with various colors. As we say, we must verify the correspondence between the old and the new constraints, connections and loads. Unfortunately, due to the import of the FEM file into the HyperWorks environment and the simplifications done by Inspire, all these objects have to be redone from the beginning in the most precise way possible.

First of all, we must review the ground constraints, as they are applied individually on each pin of the three bipods. For simplicity, as we do in the previous chapter, we now consider a single constraint (SPC) that connects all the three bipods to the ground, through a rigid spider (element RB2).

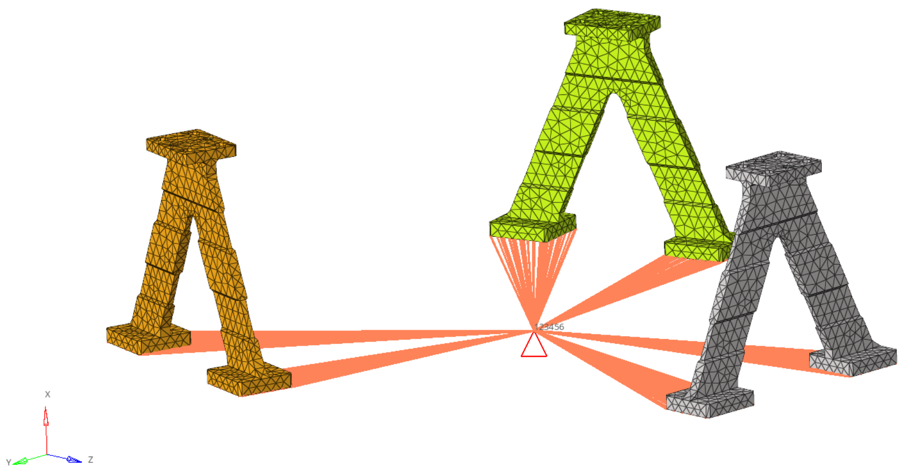

Figure 3.23: RB2 element and SPC load

Another very important check consist in verifying the connections between the various parts of the assembly. Unfortunately, when we import the file from Inspire, the connecting elements are replaced by CBAR elements placed between two CBUSH spider webs. This solution is difficult to manage and unnecessarily complex, since in order to have a sufficiently stable connection, a very high stiffness must be defined for the CBUSH elements. At this point, the use of rigid RB2 spiders is more immediate, as we have already seen in the previous chapter. Then we use CBUSH elements to connect the various pairs of RB2 elements.

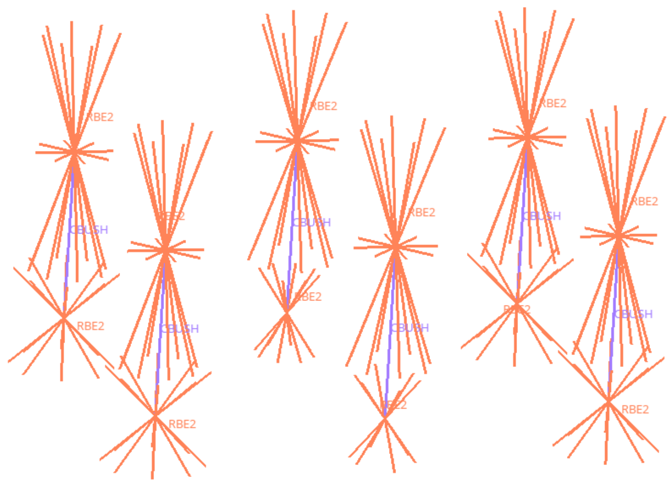

Figure 3.24: Example of CBUSH connection between two RB2 elements

Like the connections between the various components, those between the structure and the concentrated masses must also be verified. Since in Inspire the masses are connected to surfaces through rigid connectors, during the transfer in HyperWorks, these rigid elements are applied to point CBUSH elements and not to specific component nodes. To have a direct connection between the concentrated masses and the structure, it is necessary to eliminate the point-like CBUSH elements and carry out what is called 'equivalence'.

To do this you need to go to the panel "Validate > Fix Elements > Free Edges" and select the rigid elements and components to which the masses must be connected to, imposing a tolerance that determines the space where the various nodes can be found. This command generates the connection between the RB2 elements and the corresponding nodes of the structure. The masses will then be applied in the center of the various rigid spiders.

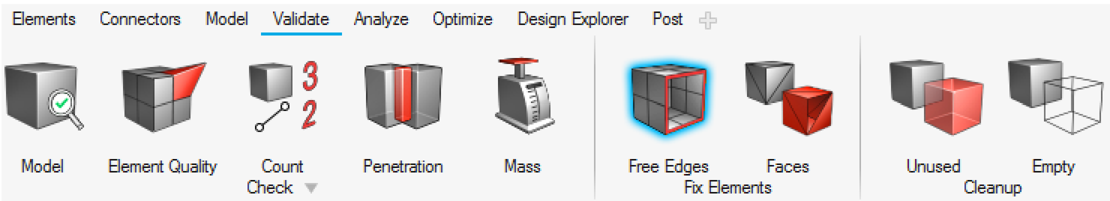

(a)

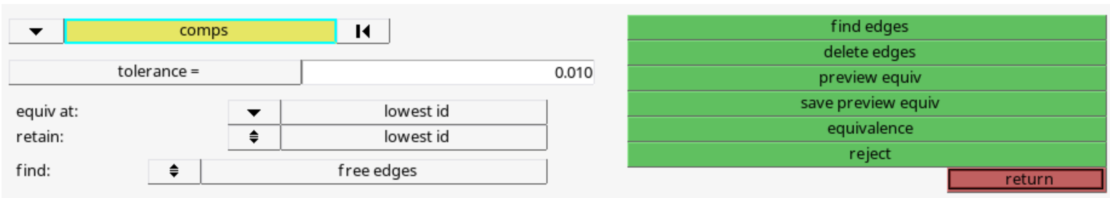

(b)

Figure 3.25: Equivalence command path

Finally, before starting a static analysis to verify that the structure works well even with the latest changes, we just have to define the load to apply. Since our load is distributed along the three directions, we use an overlap of three single gravitational loads (gX, gY, gZ) equal to 245.25 m/s^2 along the three principal axes to define it. This is achieved through a LOADADD type load.

Chapter 4

Topological Optimization Trade-off

Now that all the variables necessary for the optimization are verified and modified, in order to allow the software to work after importing the structure from Inspire to HyperWorks X, we just have to launch a static analysis on it.

As we can see in the images below, the results reflect our expectations and that is what we have already seen in the previous chapters: maximum displacement on the baffle and maximum stress/deformation on the three bipods.

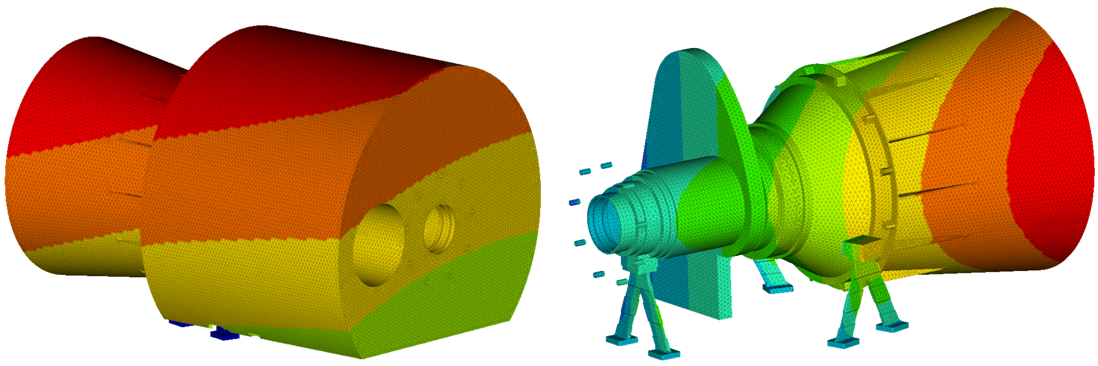

(a) *Total displacement* **(b)** *Displacement along x-axis*

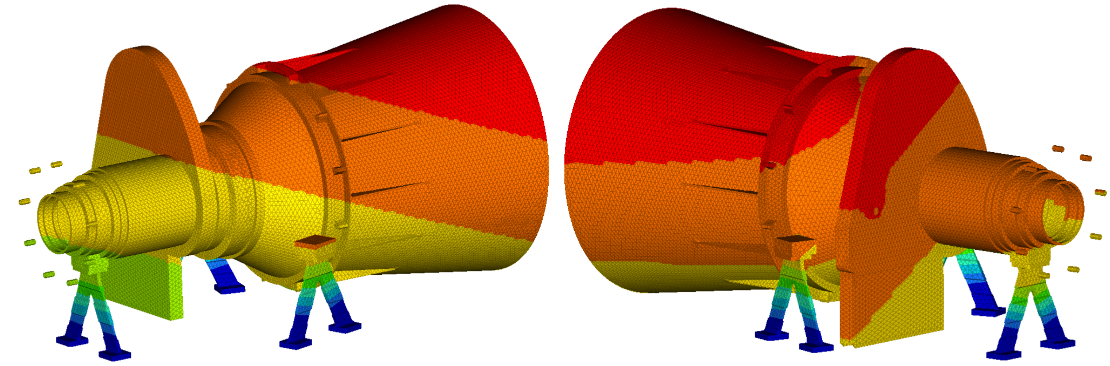

(c) *Displacement along y-axis* **(d)** *Displacement along z-axis*

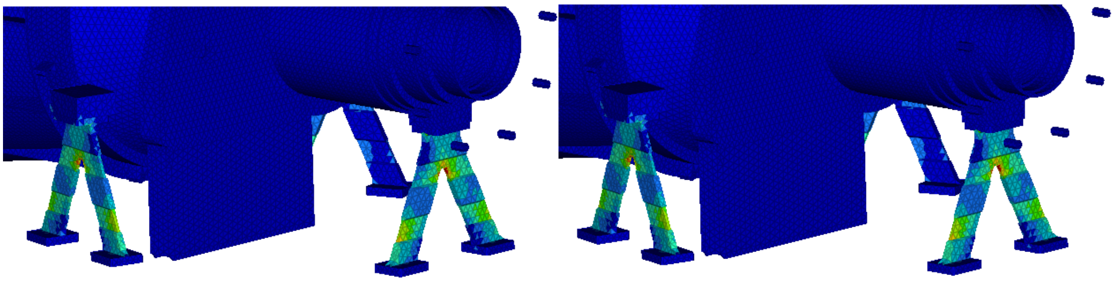

(e) *Total von Mises stress* **(f)** *Total von Mises strain*

Figure 4.1: Static analysis results

4.1 First Trade-Off

After realizing that the geometry is correct just like the solid mesh and that the static analysis give us appropriate results, we can proceed with the various topological optimizations. As we can understand from the title of this chapter, different manufacturing constraints will be considered in order to start different optimizations and find the one that best reflects our needs.

There are two main set-ups for topological optimization: maximizing stiffness, acting on the volume (and so on the mass) or minimizing the mass, acting on the applied static stress. For each optimization, manufacturing constraints can be defined to indicate to the software how the components will then be produced. There are several types of these constraints, but here we will consider only four possibilities: no constraints (free optimization), draw direction, extrusion and overhang angle (additive manufacturing constraint).

Let's consider them one by one.

1. Free (no manufacturing constraints): upper bound at 30% applied to the maximum overall volume;

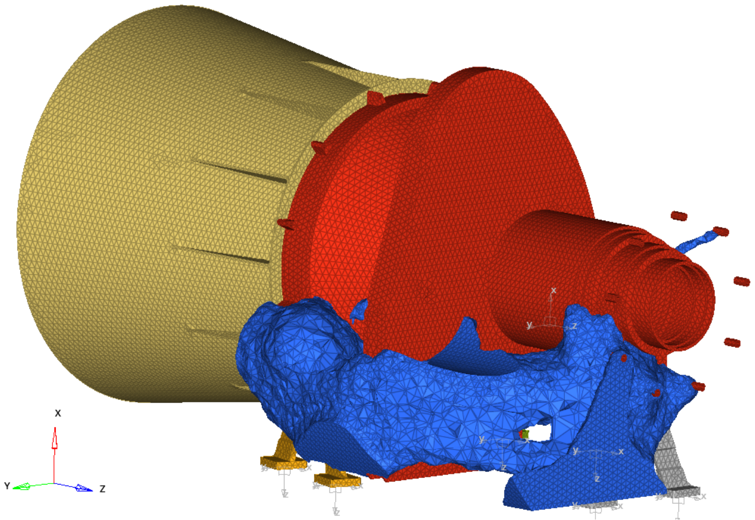

Figure 4.2: Trade-off #1: maximize stiffness with 30% of volume

2. Free (no manufacturing constraints): upper bound at 3% applied to the maximum overall volume;

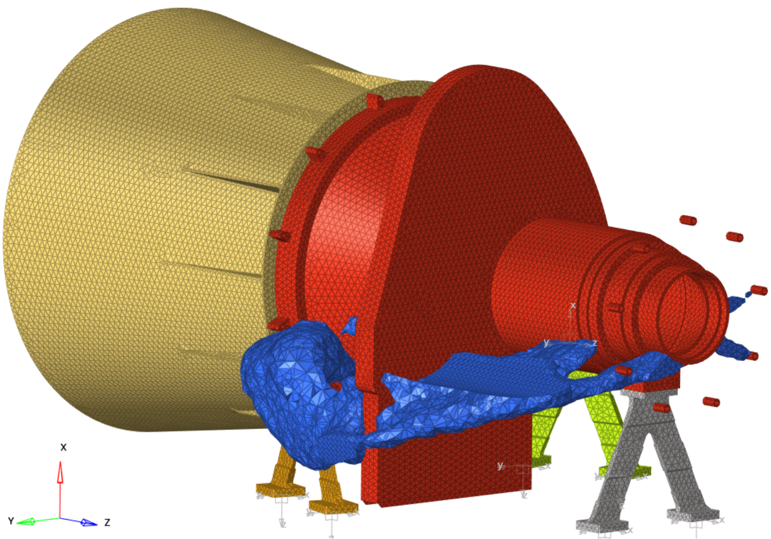

Figure 4.3: Trade-off #1: maximize stiffness with 3% of volume

3. Draw Direction (indicates that casting constraints are being applied): single draw, so a single mold will be used, withdrawn in the given draw direction, along the three directions:

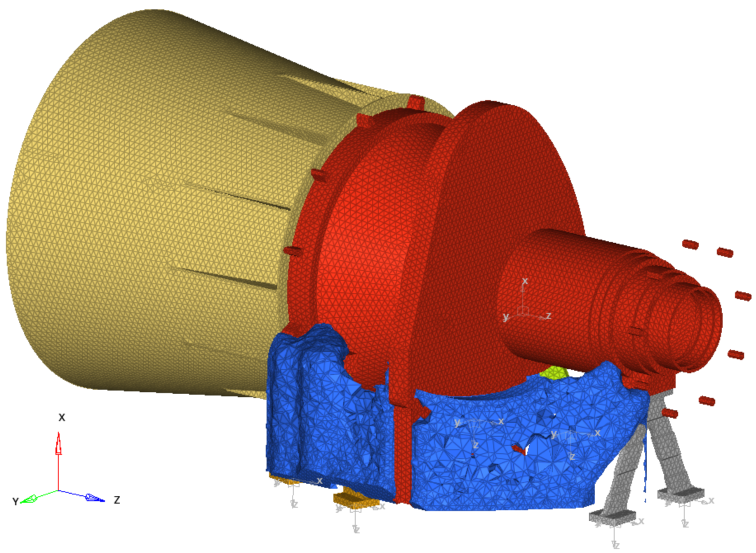

Figure 4.4: Trade-off #1: maximize stiffness with draw direction along x

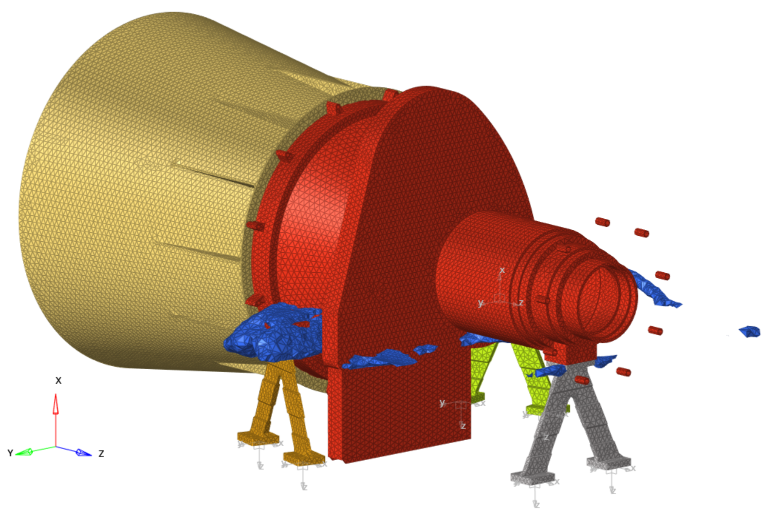

Figure 4.5: Trade-off #1: maximize stiffness with draw direction along y

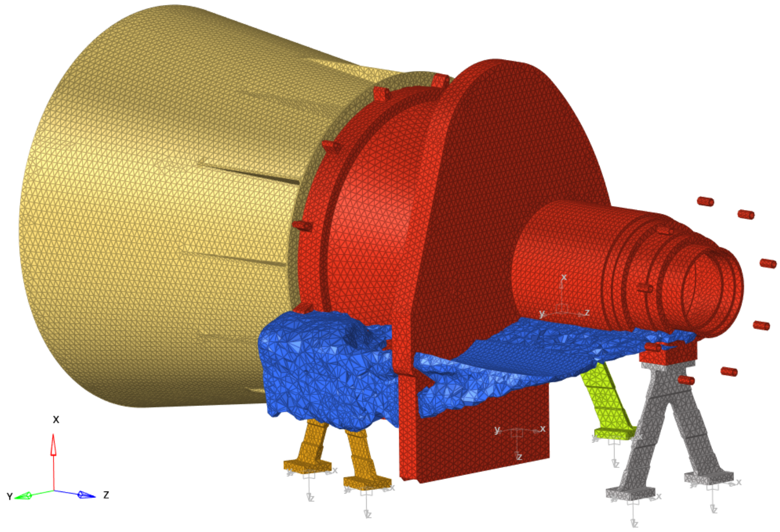

Figure 4.6: Trade-off #1: maximize stiffness with draw direction along z

4. Extrusion (indicates that extrusion constraints are being applied): no twist extrusion, so the cross-section cannot twist about the neutral axis, along the best draw direction (x-axis):

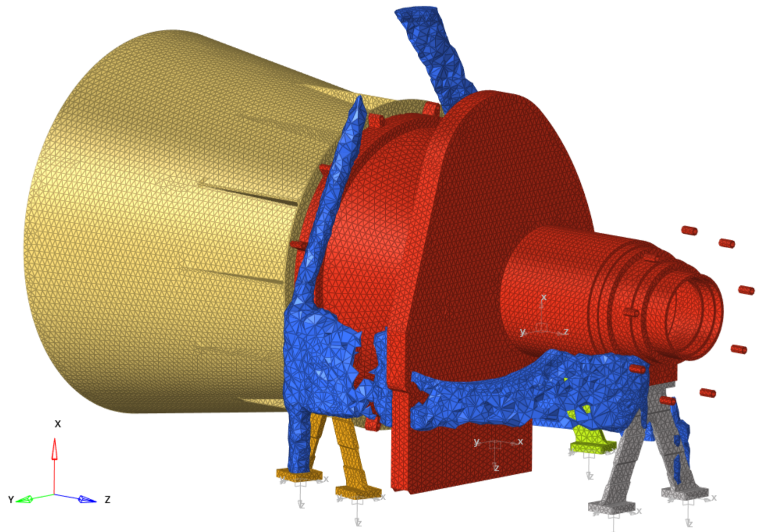

Figure 4.7: Trade-off #1: maximize stiffness with extrusion along x

5. Overhang Angle (additive manufacturing constraint).

In the optimization with the extrusion constraint, the x-axis was defined as the best direction along we can carry it out, as from the three previous cases it is emerged that, with the same design mass and applied forces, the compliance of that case is the lowest (i.e. maximum stiffness). All this can be seen better in the table below:

Manufacturing Constraints	Design Mass [kg]	Compliance
Free (upper bound at 30%)	12.156(15%)	0.2332
Free (upper bound at 3%)	9.424(11%)	0.1708
Draw Direction x-axis	**9.424(11%)**	**0.1725**
Draw Direction y-axis	9.424(11%)	0.1994
Draw Direction z-axis	9.424(11%)	0.1750
Extrusion x-axis	9.424(11%)	0.2116

Table 4.1: Trade-off #1: topological optimization results

It must be specified that the values contained inside the table are approximations, as they do not take into account the defined mesh, so the masses, above all, can oscillate between higher and lower values. For all the optimizations seen so far, a minimum thickness value of 15 mm is imposed. The last type of topological optimization is not carried out, since during the work we realize that, as can be seen from the previous images, most of the mass of the design is concentrated in the lower area of the structure. At this point it must be checked if this depends on purely structural reasons or on the presence of the non-design space.

To do this we are going to modify the geometry in Inspire and repeat the various verification steps (mesh creation, constraint definitions and static analysis), and then perform new topological optimizations. These continuous changes to the geometry are necessary in this phase of the design, as the final shape of the structure is defined through these optimizations.

A very important thing that must be considered in the optimization phase is the meaning of the results: the optimized part (the blue areas in the previous images) does not define how the mass must be positioned, but simply indicates where it must be inserted.

4.2 Final Geometry Adjustment

The only geometric changes that must be implemented concern the design and the non-design space, as bipods and baffles do not make a significant contribution in the optimization phase. As we just see, in fact, the non-design space strongly affects where the mass is positioned: much of it is positioned in the lower part of the structure, intersecting the pocket left free for the insertion of the shutter blades. Our goal now is to verify if this mass is placed in that area despite the absence of the pocket.

A further modification must be made to the non-design space before proceeding: the nine connection holes to the focal plane cover must be connected with the entire structure. To do this, a circular plate is created on the front, so that, once the cover is mounted, there will be no passage of light inside the optical duct.

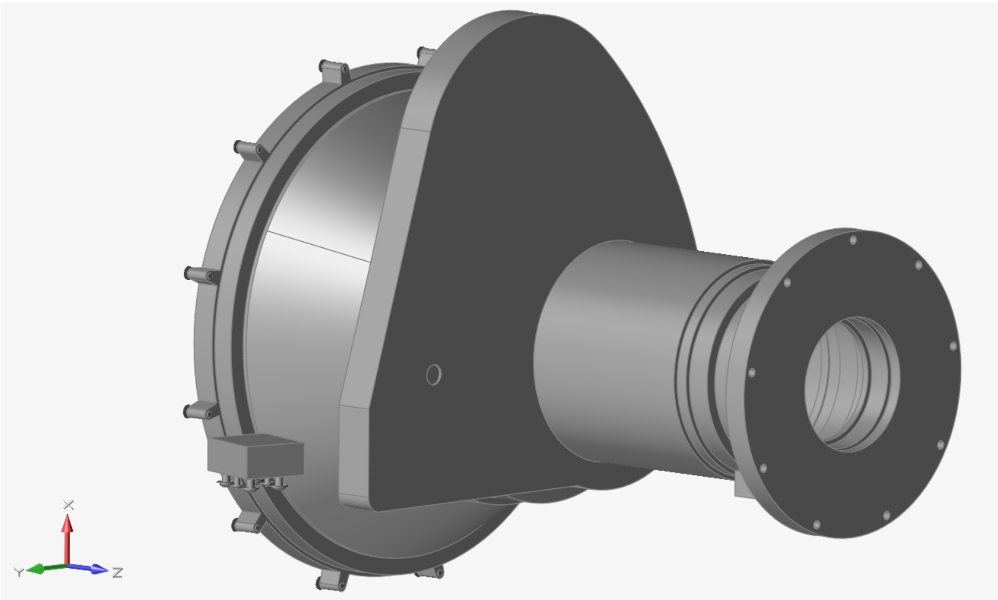

Figure 4.8: Non-design space geometry changes

The change to be made to the design space is not due to structural reasons or production needs, but rather to calculation reasons. In fact we decide to reduce the maximum overall volume in order to minimize the amount of mesh elements, with a consequent reduction of optimization calculation times. Obviously, this change considers the previous optimization results, so those parts that have been eliminated in the optimization will not be considered.

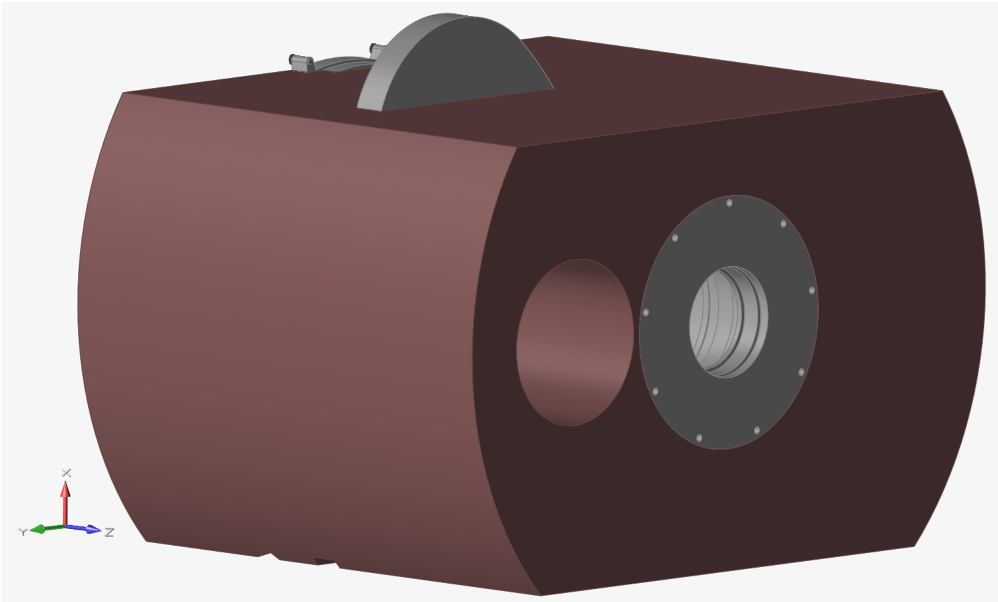

Figure 4.9: Design space geometry cuts

As soon as the changes are done and we are sure that we reach the final shape, we can import again the geometry into HyperWorks X and proceed with the creation of the mesh, which in this case is done on each single component in order to have more control during the analysis and optimization phases. For each component, first of all, a two-dimensional TRIA-type mesh is made and subsequently this is filled with a three-dimensional TETRAhedral mesh.

At this point, as in the previous cases, properties and materials are assigned, taking into account that in this case we have only solid elements and no more 2D skins. Then the constraints to the ground on the bipods and the rigid spiders inside the interface holes between components are created, in order to be able to insert CBUSH connecting elements, with such a stiffness that they can be considered rigid.

Finally, all that remains to do is to set up the concentrated masses of the lenses, the shutter motor and the focal plane cover. In order to prevent problems in the analysis phase, due to the presence of non-coincident meshes between components, a contact surface is created between the design and the non-design.

We can now launch a static analysis, considering the resultant of 25g on the three main directions as the global gravitational load and verify if the results match what we aspect. As can be seen in the images below, we obtain a maximum displacement of 1 mm on the baffle, a stress of 1153 N/mm^2 and a deformation of $9e-3$ on the bibods.

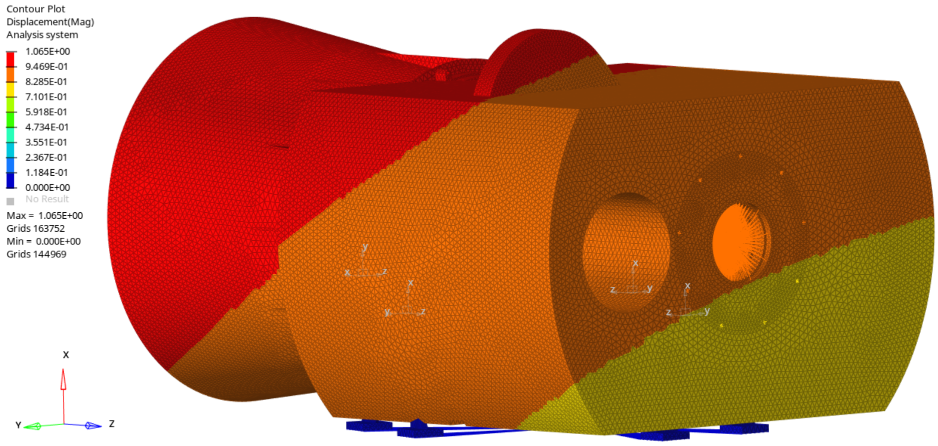

(a) *Displacement*

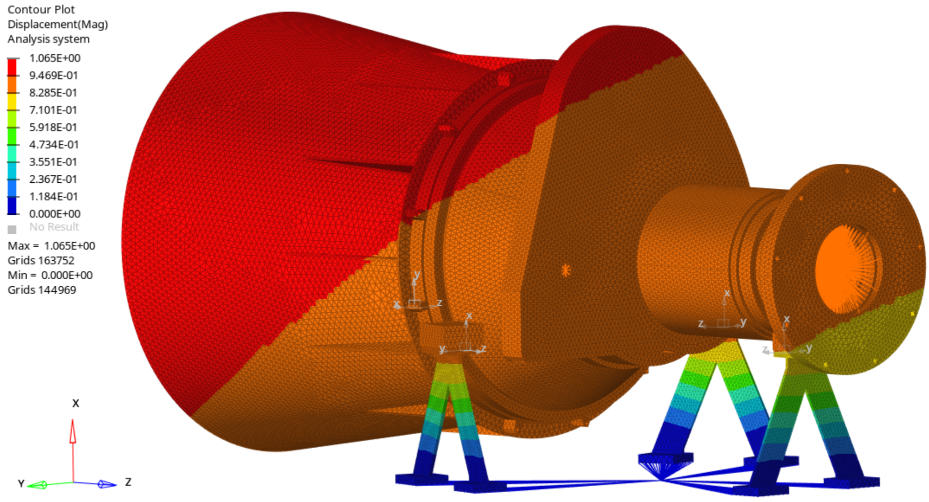

(b) *Displacement (hiding design space)*

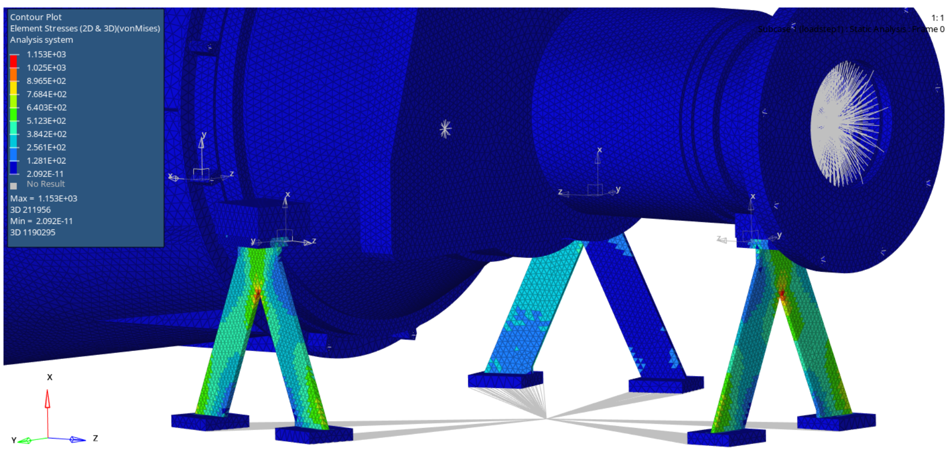

(c) *Von Mises stress*

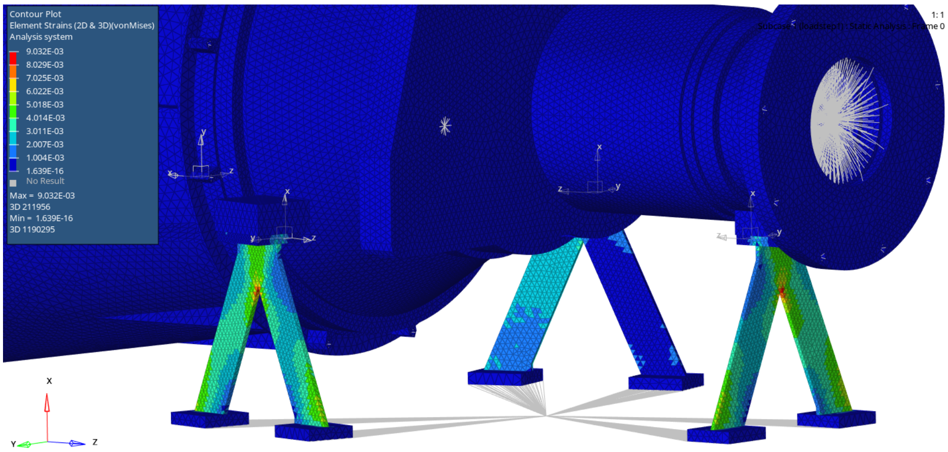

(d) *Von Mises strain*

Figure 4.10: New model static analysis results

Now that the new geometry is verified and the static analysis give us good results, we just have to go on with a second topological optimizations trade-off, following the same guidelines seen previously.

4.3 Second Trade-Off

The first topological optimization that is launched is a classic optimization without manufacturing constraints, with the aim of minimizing compliance (i.e. maximizing stiffness), imposing an upper bound constraint on the volume fraction up to 0.30 (corresponding to 30%) and a minimum thickness value of 0.015.

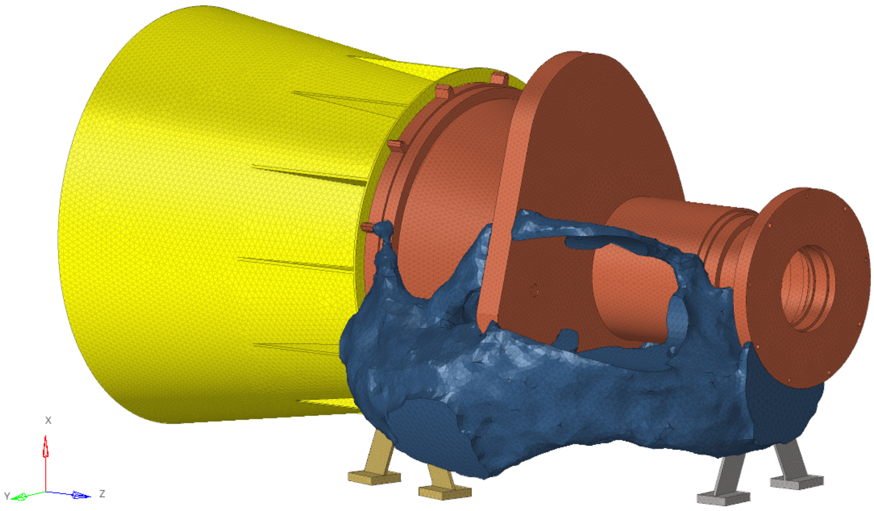

(a)

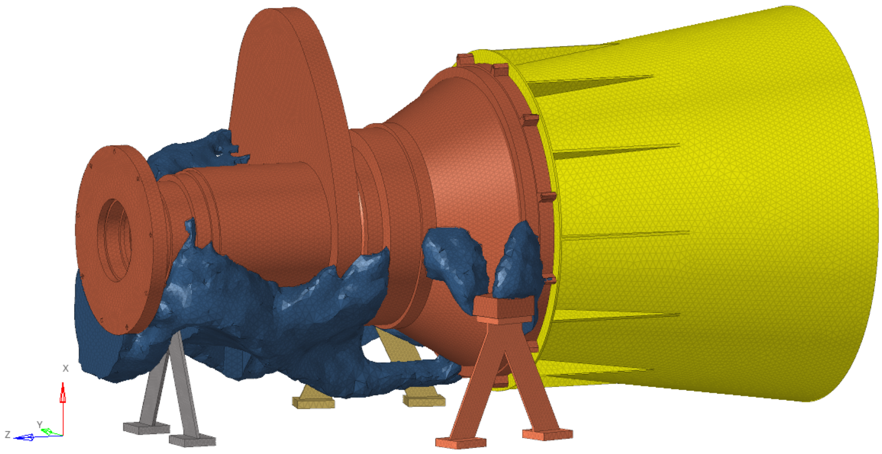

(b)

Figure 4.11: Trade-off #2: maximize stiffness with 30% of volume

The result obtained from this first optimization is good, as can be seen in the previous images. We obtained a reduced design space mass equal to 5.925 kg, that is 9% of the original, with a compliance of 443.617 Nmm. This result allows us to proceed with further optimizations, starting with another one without manufacturing constraints, but by imposing an upper bound constraint on the volume fraction smaller than that in the previous case: a bound of 0.03 is imposed (corresponding to 3%), with the same minimum thickness value.

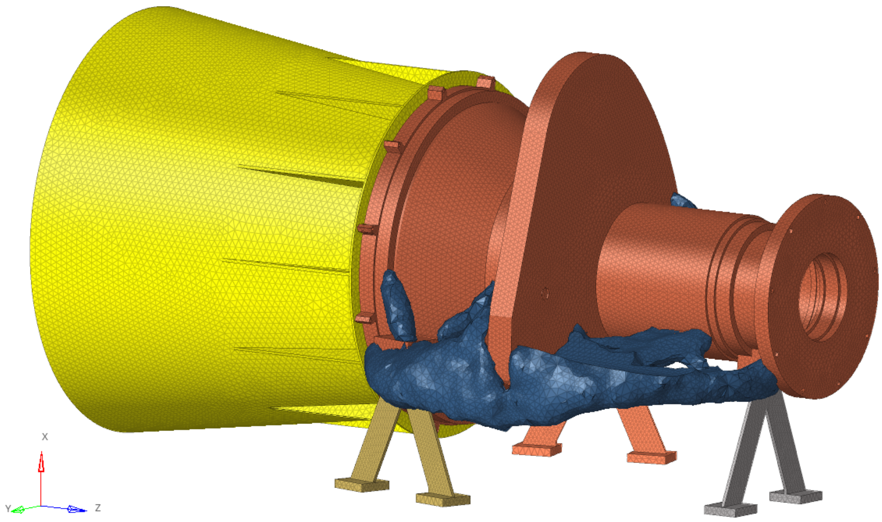

(a)

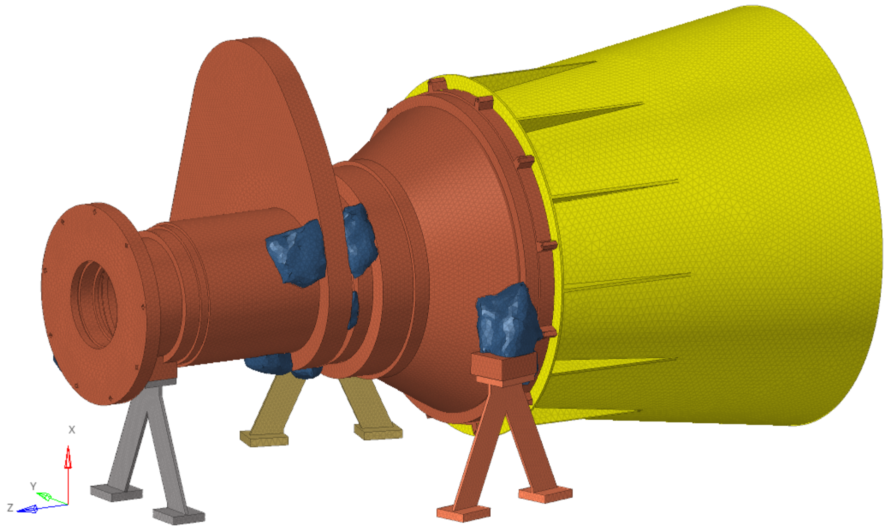

(b)

Figure 4.12: Trade-off #2: maximize stiffness with 3% of volume

As we can see from the previous images, the result obtained from this second optimization highlights a lower use of material and therefore a mass reduction no longer to 9% but to 2%, for a total design space mass of 1.169 kg, with an equal compliance at 224.696 Nmm. We have an important reduction in compliance, which means a large increase in resistance.

At this point, understanding that the best results are obtained by considering a value of 0.03 for the volume fraction, we proceed with other topological optimizations by considering the various manufacturing constraints. Since in the previous trade-off, we see that the x-axis represents the best direction along which an optimization can be carried out, we no longer consider the cases along the y and z axes.

So let's proceed in order and let's consider:

1. Draw Direction (indicates that casting constraints are being applied): single draw, so a single mold will be used, withdrawn in the given draw direction, along the x-axis:

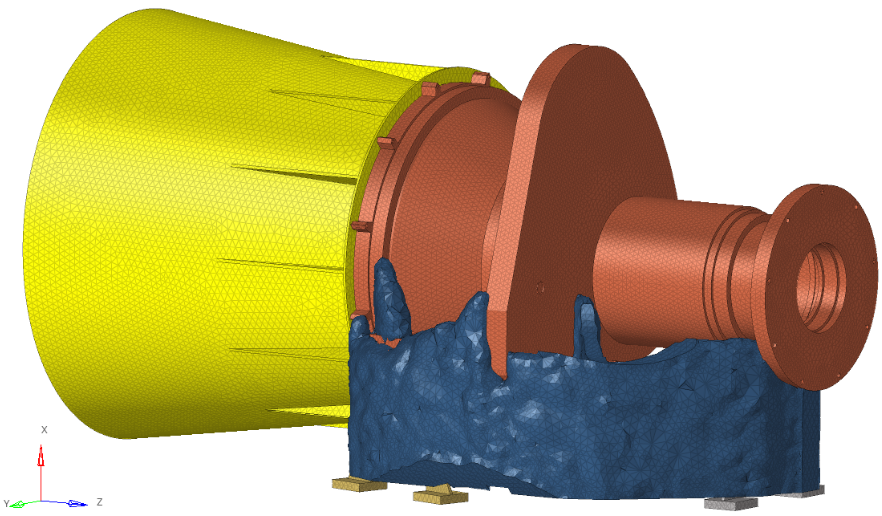

(a)

These result makes us notice a very important thing that is already evident in the last trade-off: the need to insert material between the two bipods under the SM is highlighted, regardless of the presence or absence of the pocket where we insert the shutter blades (which is removed from the non-design space during the last geometric modifications). This means that in order to have maximum stiffness, material must be placed in the lower part of the structure.

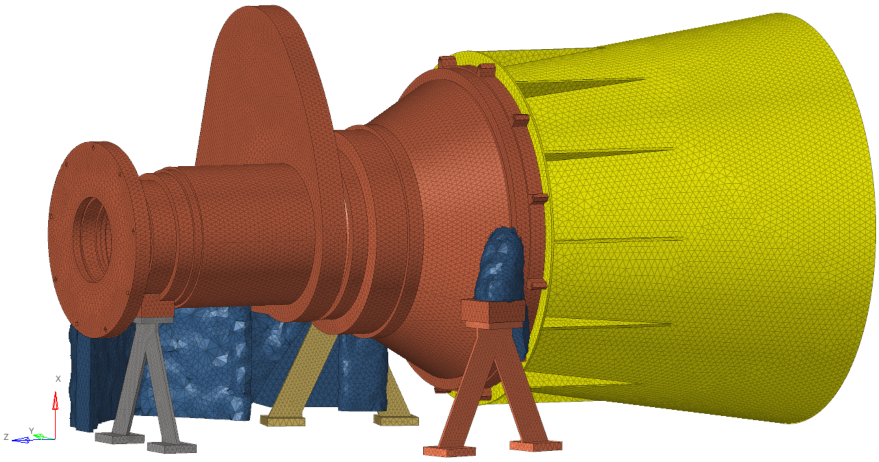

(b)

Figure 4.13: Trade-off #2: maximize stiffness with draw direction along x-axis

2. Extrusion (indicates that extrusion constraints are being applied): no twist extrusion, so the cross-section cannot twist about the neutral axis, along the x-axis:

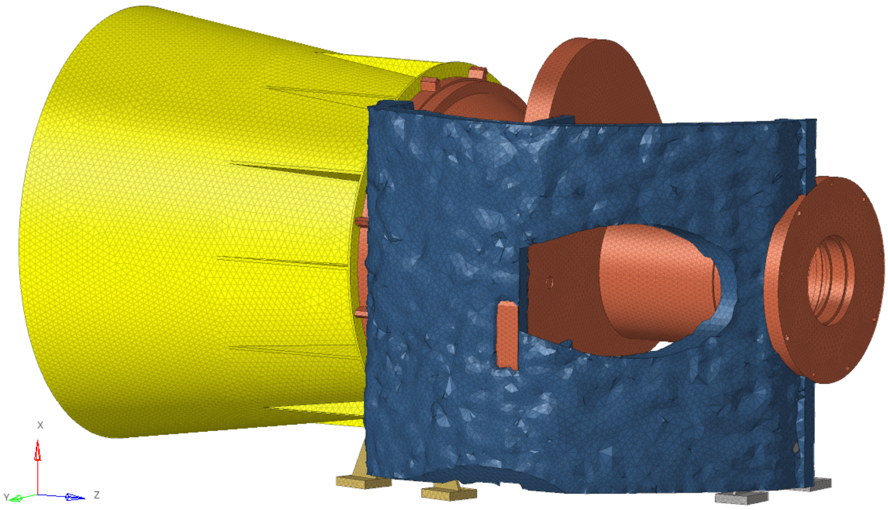

(a)

A sort of curved shield comes out. Through this optimization, the usefulness of placing mass on the shutter side to have maximum stiffness is confirmed. Compared to the previous case, however, the presence of mass is also indicated in the upper part and so, certainly, this solution will have a higher weight.

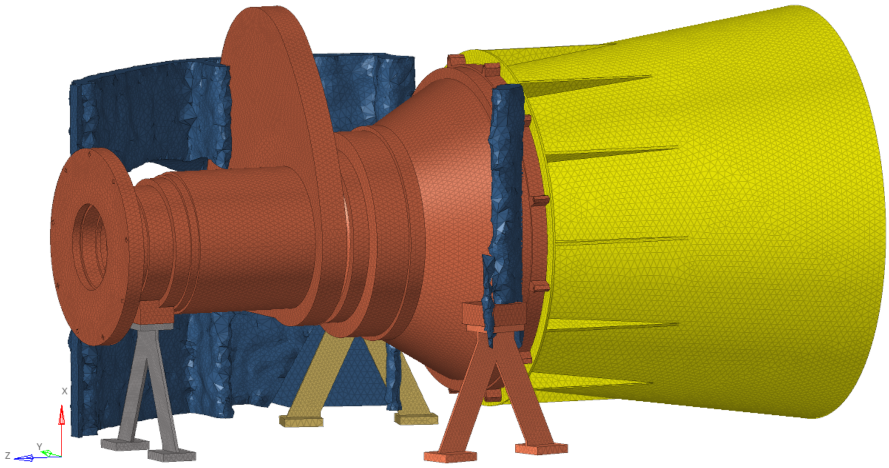

(b)

Figure 4.14: Trade-off #2: maximize stiffness with extrusion along x-axis

3. Overhang Angle (additive manufacturing constraint), with an angle of 45°, along the x-axis. A 3D printing overhang is any part of a print that extends outward, beyond the previous layer, without any direct support. The angle of the overhang should not exceed 45°. This is to make sure that each successive layer has enough support on it:

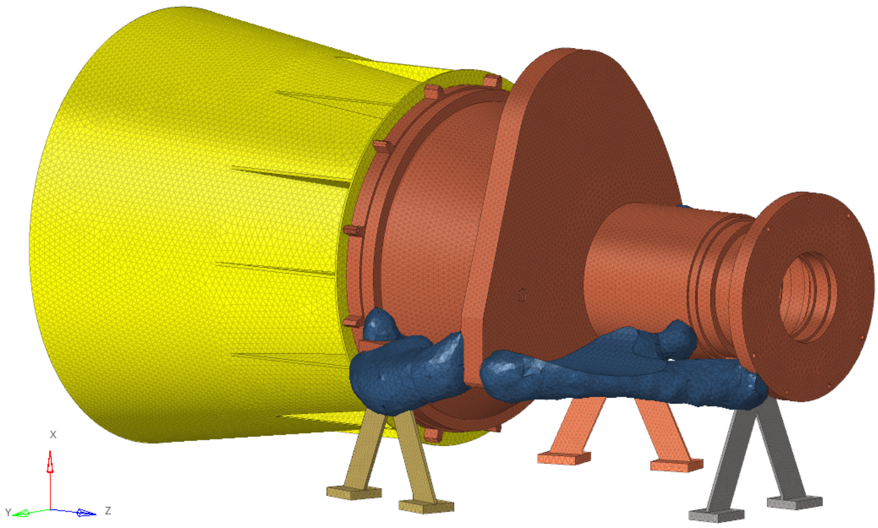

(a)

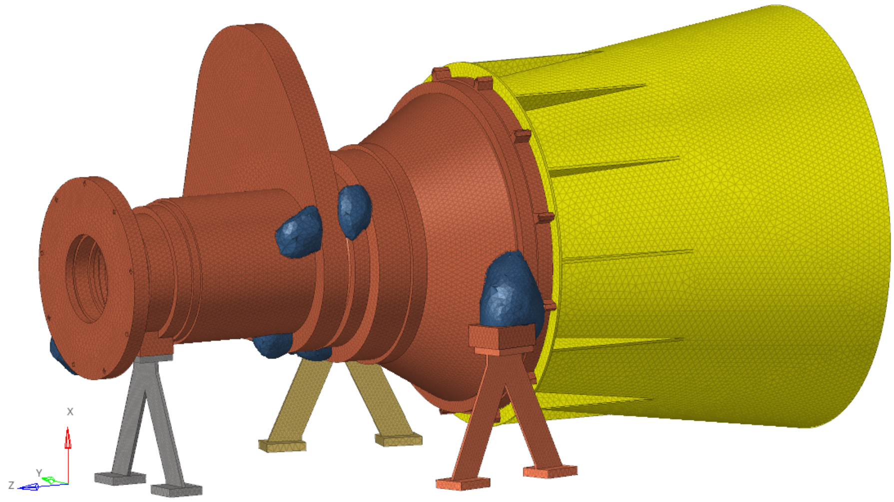

(b)

Figure 4.15: Trade-off #2: maximize stiffness with overhang angle of 45° along x-axis

> We obtain a result similar to that seen in the free case, but now the branches have a tapered and rounded shape. This optimization presents a good compromise between design mass (1,152 kg) and compliance (232,256 MPa).

We must remember that the compliance values are approximations, as they do not take into account the defined mesh. In order to have more precise values, a static analysis must be carried out for each case, so as to define the stress and displacement parameters to be compared with the original values of the ribbed structure (see Chapter 2). Before the static analysis, however, all meshes must be converted from first to second order to have more accurate results:

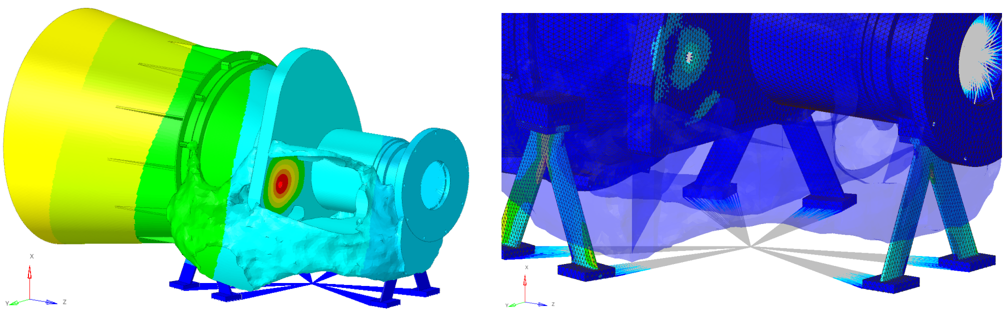

(a) *D = 0.48 mm* **(b)** *S = 243 N/mm2*

Figure 4.16: Trade-off #2 results: free optimization (volfrac upper bound at 30%)

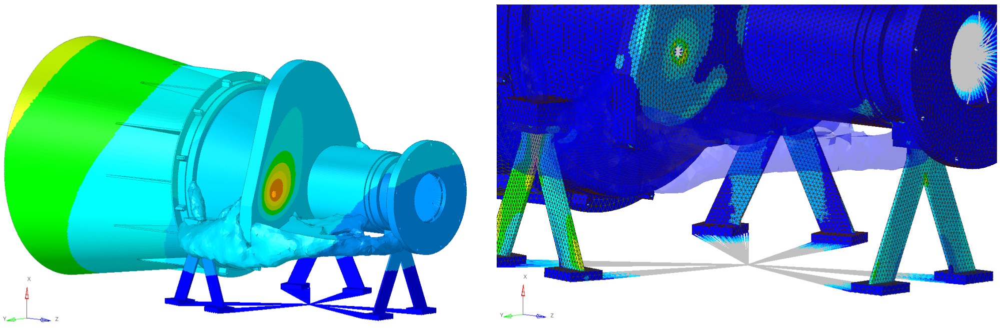

(a) *D = 0.491 mm* **(b)** *S = 146 N/mm2*

Figure 4.17: Trade-off #2 results: free optimization (volfrac upper bound at 3%)

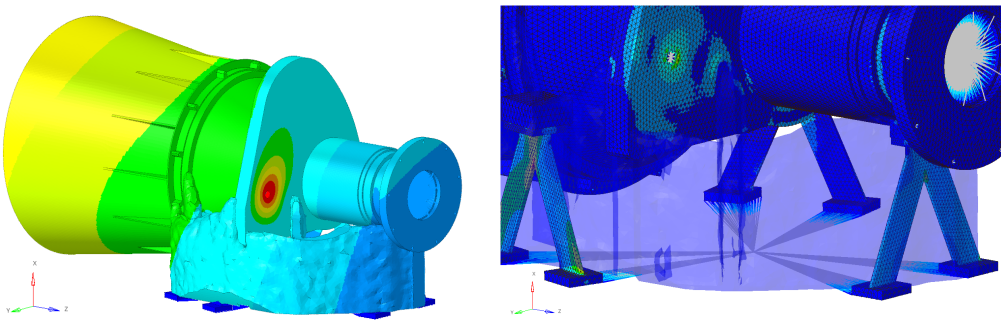

(a) *D = 0.479 mm* **(b)** *S = 172 N/mm2*

Figure 4.18: Trade-off #2 results: draw Direction along x-axis

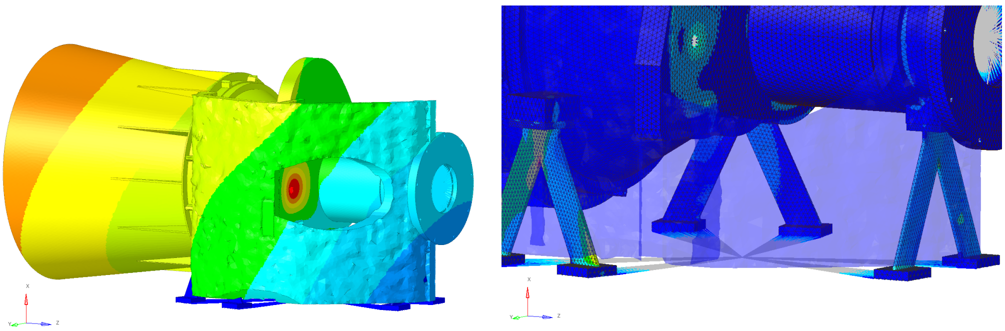

(a) *D = 0.469 mm* **(b)** *S = 198 N/mm2*

Figure 4.19: Trade-off #2 results: extrusion along x-axis

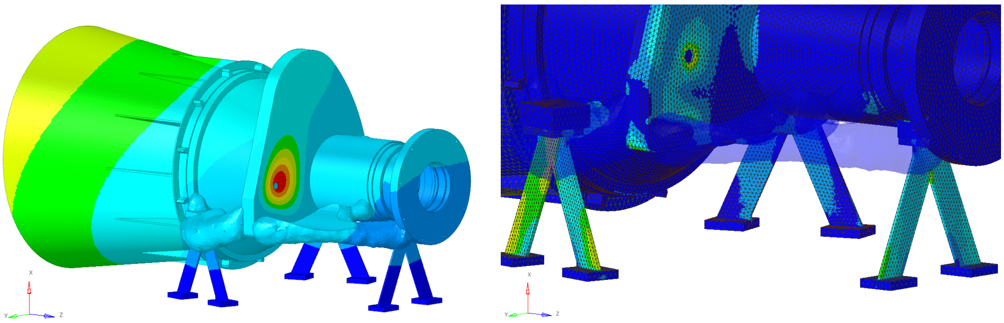

(a) *D = 0.544 mm* **(b)** *S = 137 N/mm2*

Figure 4.20: Trade-off #2 results: overhang angle 45° along x-axis

In all the displacement images, there is a maximum in the point where the concentrated mass of the shutter motor is applied. However, this is not a realistic result, as that mass, in reality, is not concentrated but distributed and so it pushes against the structure. For this reason, the only shift that interests us is the one on the baffle. The same is for the stress graphs: we are only interested in stresses located on the bipods.

Although at this stage static stresses and masses are not so important, since we use titanium (which has a high yield stress, about 800 MPa) and the mass will then be reduced with the introduction of a lattice structure, the solutions which show good mass and stress values as well as high stiffness are the free optimization and the one obtained by imposing a constraint on the overhang angle (both in the case of a volume fraction less than 0.03). We can see what has just been said in the tables below:

Manufacturing Constraints	Design Mass [kg]	Compliance [MPa]
Original Values	1.291	553.794
Free (upper bound at 30%)	5.925	456.835
Free (upper bound at 3%)	**1.169**	**245.623**
Draw Direction x-axis	2.317	312.649
Extrusion x-axis	3.865	432.511
Overhang Angle 45° x-axis	**1.152**	**257.667**

Table 4.2: Trade-off #2: design mass and compliance

Once the various static analyzes are done, we proceed with the modal analyzes, to really evaluate which of the various cases provides an improvement in terms of resonant frequencies (see Chapter 2). Take, for example, the case in which the overhang angle constraint along the x-axis is imposed.

Manufacturing Constraints	Displ [mm]	Stress [N/mm^2]	Strain
Original Values	0.659	176	$1.09e^{-}3$
Free (upper bound at 30%)	0.480	243	$1.90e^{-}3$
Free (upper bound at 3%)	**0.491**	**146**	**$1.14e^{-}3$**
Draw Direction x-axis	0.479	172	$1.35e^{-}3$
Extrusion x-axis	0.469	198	$1.55e^{-}3$
Overhang Angle 45° x-axis	**0.544**	**137**	**$1.08e^{-}3$**

Table 4.3: Trade-off #2: static analysis results

From the modal analysis it emerged that the first frequency with modal participation along x is equal to 175 Hz, while in the original case it was 359 Hz. This result shows a large decrease in frequency, which should absolutely not occur. Indeed, the goal is to find an optimized solution that has higher resonant frequencies than the original ones. So a third optimization trade-off is necessary, with the aim of maximizing these frequencies.

4.4 Third Trade-Off

In this third trade-off, three separate load steps are considered, one for each inertial load of 25g along each of the three axes. A fourth load step is then introduced, no longer static but modal, which considers the frequencies.

Regarding the optimization constraints on the volume fraction, this time the case with an upper limit equal to 0.3 is always considered, since in the last trade-off, we obtain too low masses to be filled with a lattice structure. Three new types of responses are introduced: weighted compliance, compliance index and weighted reciprocal eigenvalue. These replace the compliance of the last trade-off, since in this new situation there are four different load steps, as we just say. Let's see them more specifically:

1. The weighted compliance is a method used to consider multiple load steps in a classical topology optimization. The response is the weighted sum of the compliance of each individual load step:

$$C_W = \sum_i W_i C_i = \frac{1}{2} \sum_i W_i u_i^T f_i \tag{4.1}$$

   where u_i^T is the transposed displacement and f_i the force. This is a global response that is defined for the whole structure.

2. The compliance index is a method to consider multiple frequencies and static load steps combined in a classical topology optimization. The index is defined as:

$$S = \sum_i W_i C_i + NORM \left(\frac{\sum_j (\frac{W_j}{\lambda_j})}{\sum_j W_j} \right) \tag{4.2}$$

this is a global response that is defined for the whole structure. The normalization factor, NORM, is used to normalize the contributions of compliances and eigenvalues. If NORM is not used, the linear static compliance requirements dominate the solution.

The quantity NORM is typically computed using the formula:

$$NORM = C_{max} \lambda_{min} \tag{4.3}$$

where, C_{max} is the highest compliance value in all load steps and λ_{min} is the lowest eigenvalue included in the index.

3. The weighted reciprocal eigenvalue (frequency) is a method to consider multiple frequencies in a classical topology optimization. The response is the weighted sum of the reciprocal eigenvalues of each individual mode considered in the optimization:

$$f_W = \sum_i \left(\frac{W_i}{\lambda_i} \right) \tag{4.4}$$

This is done so that increasing the frequencies of the lower modes will have a larger effect on the objective function than increasing the frequencies of the higher modes.

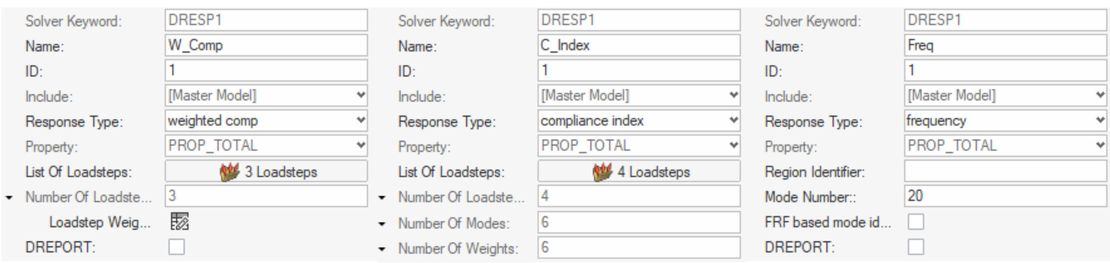

Figure 4.21: Trade-off #3: responses definition

Let's now take a look and analyze the various cases, in order to identify the definitive solution to be compared with the original structure, seen in Chapter 2.

The first response is used for those optimizations that aim at maximizing stiffness (i.e. minimizing compliance), for which the total compliance between three different loading steps will be calculated and then minimized. The free case (no manufacturing constraints) is not considered as it was already seen in the previous trade-off. So we have:

1. Draw direction along Z-axis

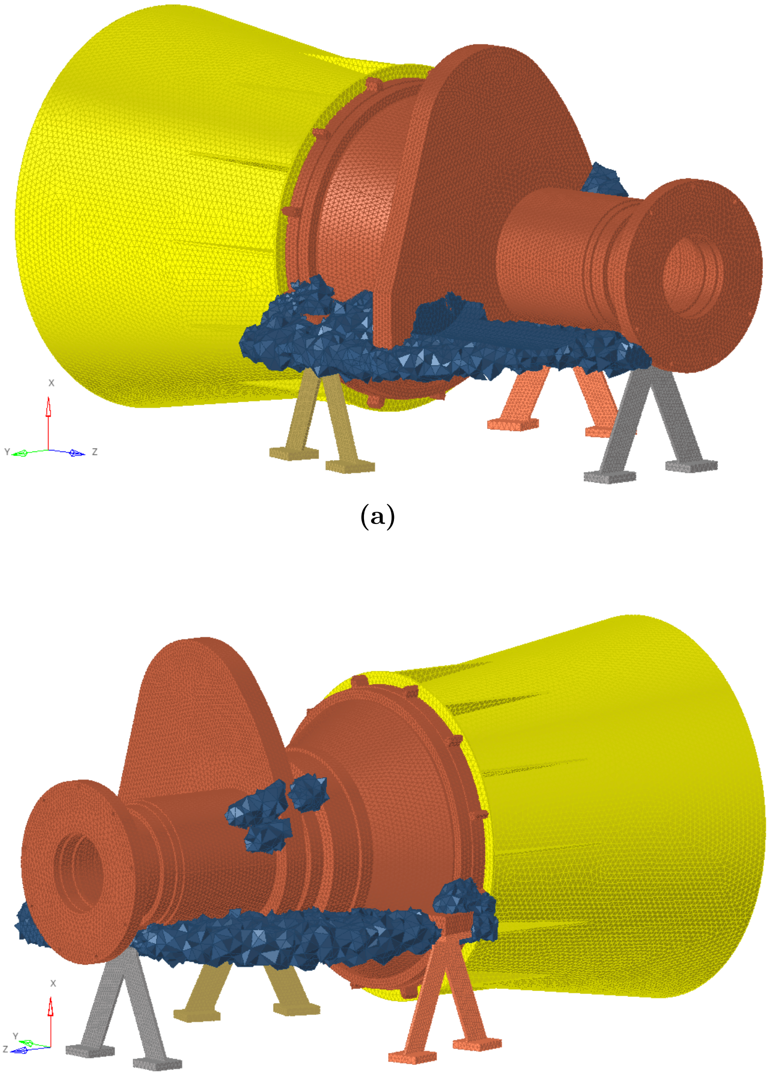

(a)

(b)

Figure 4.22: Trade-off #3: maximize stiffness with draw direction along z-axis

Mode #	Frequency [Hz]	X-TRANS	Y-TRANS	Z-TRANS
1	**206.4**	0.01%	**89.45%**	0.03%
2	**274.2**	0.87%	0.01%	**58.89%**
3	330.6	2.54%	0.31%	**28.03%**
4	347.0	0.13%	**7.84%**	0.69%
5	**535.1**	**5.53%**	0.04%	0.30%

Mass [kg]	**10.72**

Table 4.4: Trade-off #3: maximize stiffness with draw direction along z-axis

As we can immediately see from the second image, in this third trade-off there is the presence of a second arm on the side opposite to the SM. This allows us to have a greater stiffness, but also higher resonant frequencies than the baseline (see Table 2.3).

This second aspect can be easily seen in the table, where only the first five modes of vibrating are shown. In this case, however, there is a high increase in total mass, in fact it goes from 8.36 kg to 10.72 kg.

2. Overhang Angle of 45° along X-axis

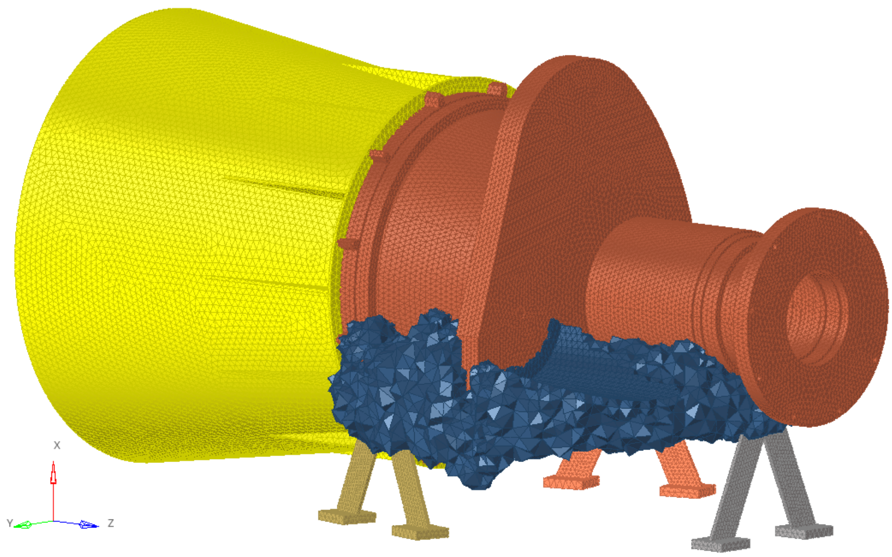

(a)

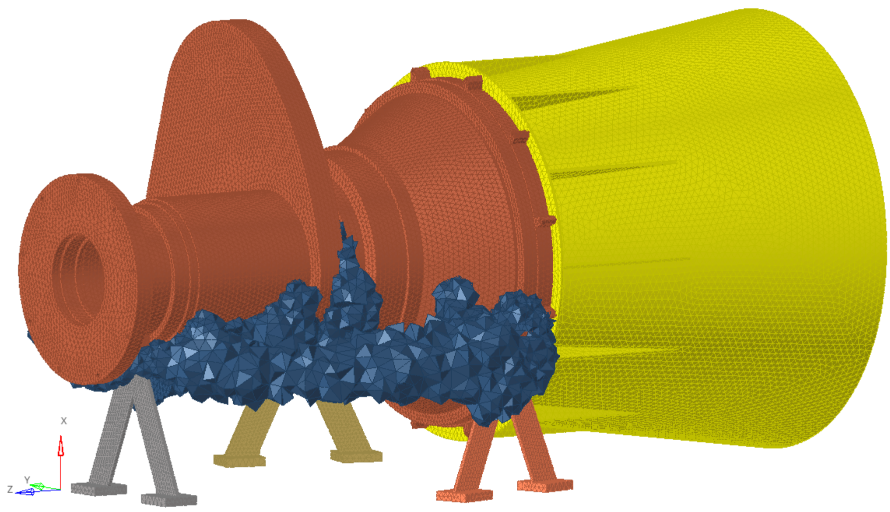

(b)

Figure 4.23: Trade-off #3: maximize stiffness with overhang angle of 45° along x-axis

Mode #	Frequency [Hz]	X-TRANS	Y-TRANS	Z-TRANS
1	**201.3**	0.02%	**89.10%**	0.01%
2	**272.6**	0.61%	0.07%	**62.44%**
3	326.8	2.33%	0.69%	**23.03%**
4	343.1	0.22%	**7.35%**	1.97%
5	528.4	2.24%	0.31%	0.01%

Mass [kg]	**11.02**

Table 4.5: Trade-off #3: maximize stiffness with overhang angle of 45° along x-axis

In this optimization a constraint has been imposed on the overhang angle along x-axis and as can be seen immediately from the images, there are always two arms along the two sides of the structure, but compared to the previous case there is more design material, in fact there is a higher mass.

Regarding the frequencies, however, there are lower values and no modal participation appears along the x-axis in the first five modes of vibration. So this case can be discarded immediately.

3. Overhang Angle of 45° along Z-axis

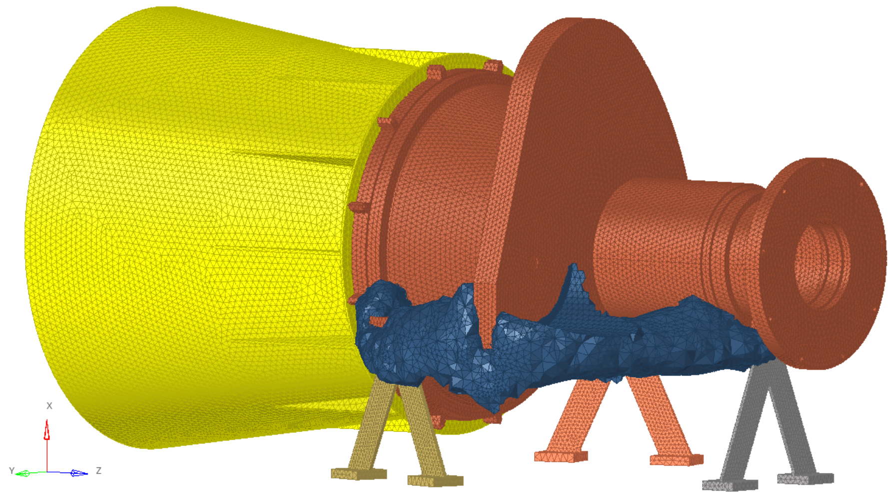

(a)

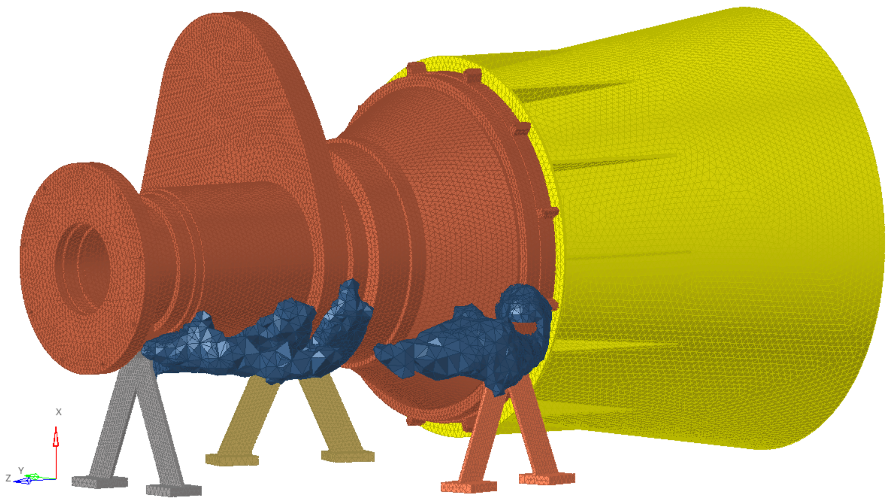

(b)

Figure 4.24: Trade-off #3: maximize stiffness with overhang angle of 45° along z-axis

Mode #	Frequency [Hz]	X-TRANS	Y-TRANS	Z-TRANS
1	**201.1**	0.26%	**80.05%**	3.58%
2	**231.2**	1.22%	**8.19%**	**25.87%**
3	330.8	1.05%	0.04%	**54.60%**
4	355.7	0.17%	**8.01%**	1.24%
5	**494.0**	**6.95**%	0.01%	1.06%

Mass [kg]	**8.90**

Table 4.6: Trade-off #3: maximize stiffness with overhang angle of 45° along z-axis

In this last optimization, we can immediately notice a lower mass than in the other two cases and this is clear as there is less optimized material. Unfortunately this is due to the presence of a discontinuity on one of the two arms. Then, the frequencies are the lowest among the three optimizations with weighted compliance, so if we have to choose a case among the three just seen, the first one would certainly be designated.

The second response, compared to the first, aims at the simultaneous maximization of stiffness and frequency, minimizing the compliance index. To do this, all four load steps are considered (the three static and the only modal one):

1. Free (no manufcturing constraints)

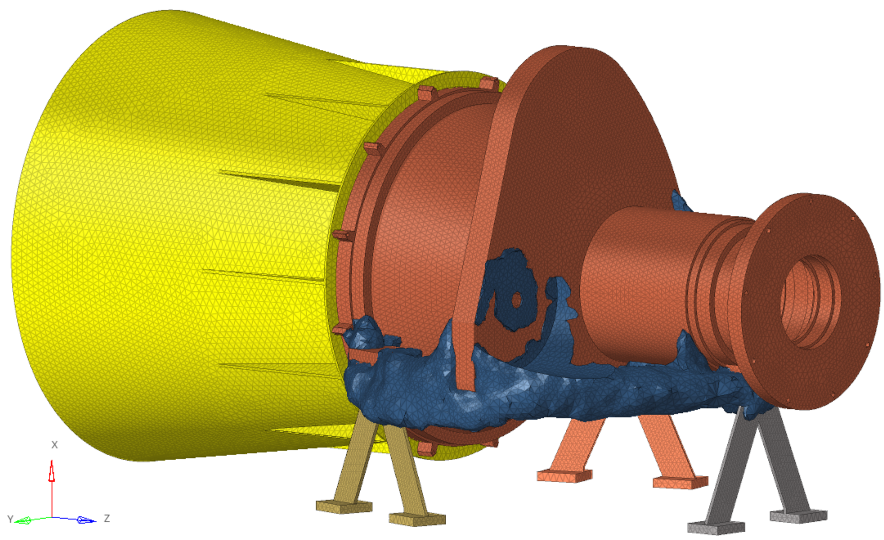

(a)

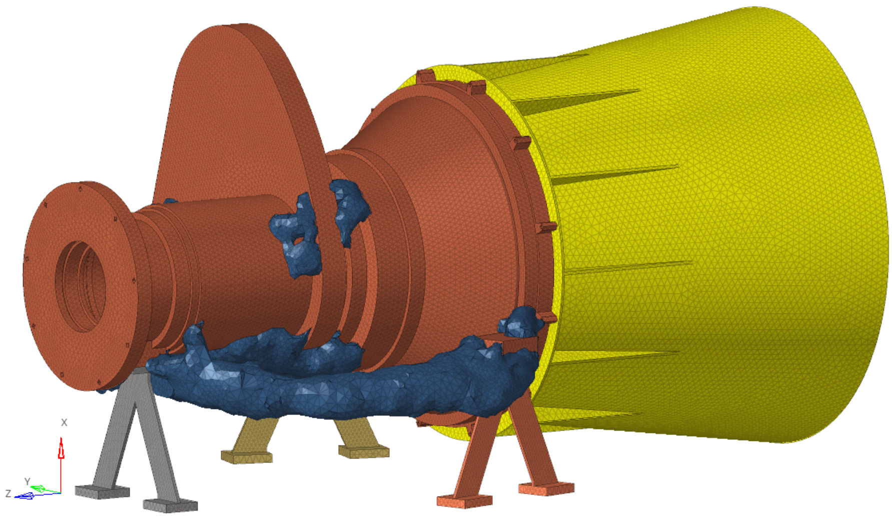

(b)

Figure 4.25: Trade-off #3: maximize stiffness and frequency without manufacturing constraints

Mode #	Frequency [Hz]	X-TRANS	Y-TRANS	Z-TRANS
1	**226.5**	0.02%	**90.88%**	0.25%
2	**298.7**	0.35%	0.44%	**87.60%**
3	427.7	0.13%	**6.17%**	0.02%
4	475.1	4.55%	0.34%	**9.02%**
5	585.9	0.85%	0.00%	1.67%
6	**689.5**	**49.51%**	0.37%	0.02%

Mass [kg]	**8.77**

Table 4.7: Trade-off #3: maximize stiffness and frequency without manufacturing constraints

In this single case with the objective of minimizing the compliance index, we see, as before, the presence of two arms along the sides of the structure, but now the material is inserted more neatly. Three independent mass blocks are then created: two that stiffen the upper part of the non-design space and one the base. Compared to the optimizations seen so far, this solution gives me the highest frequencies and the lowest mass.

The third response, finally, is used for those optimizations that have as their goal the maximization of frequencies and so only the one modal load step is considered, aiming at minimizing the weighted reciprocal eigenvalue:

1. Free (no manufacturing constraints)

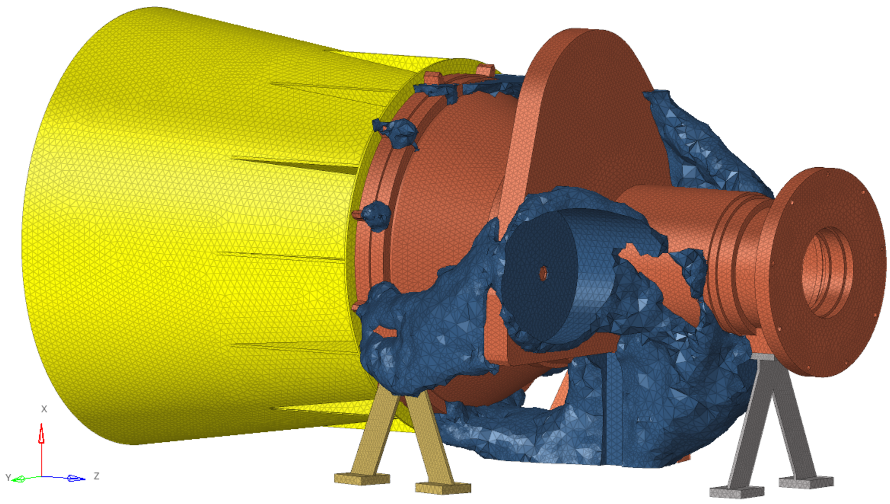

(a)

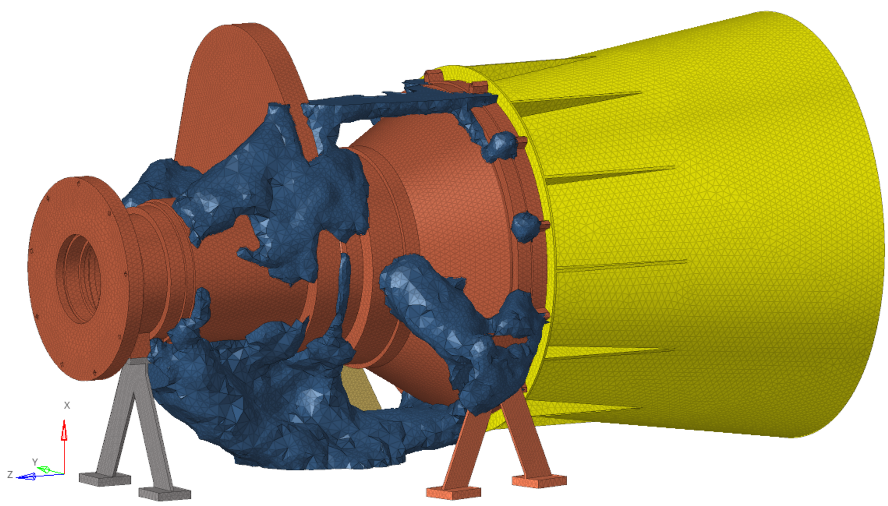

(b)

Figure 4.26: Trade-off #3: maximize frequency without manufacturing constraints

Mode #	Frequency [Hz]	X-TRANS	Y-TRANS	Z-TRANS
1	**201.3**	0.01%	**93.14%**	0.21%
2	**289.6**	0.06%	0.36%	96.56%
3	432.1	0.00%	**4.99%**	0.43%
4	**554.7**	**15.23%**	0.00%	1.64%
5	732.4	**73.62%**	0.07%	0.10%
6	759.9	0.01%	0.00%	0.00%

Mass [kg]	**11.02**

Table 4.8: Trade-off #3: maximize frequency without manufacturing constraints

As for this last optimization, which aims to maximize the weighted frequency, we can immediately notice a much higher mass than in the previous cases (about 11.02 kg in total). In addition to be much greater, the mass is arranged in an uneven and disordered way on the available volume and this would make its production difficult.

Speaking now of the measured frequencies, they are certainly greater than those seen for the first three cases, but remain lower than those of the previous case, so this case too can be excluded.

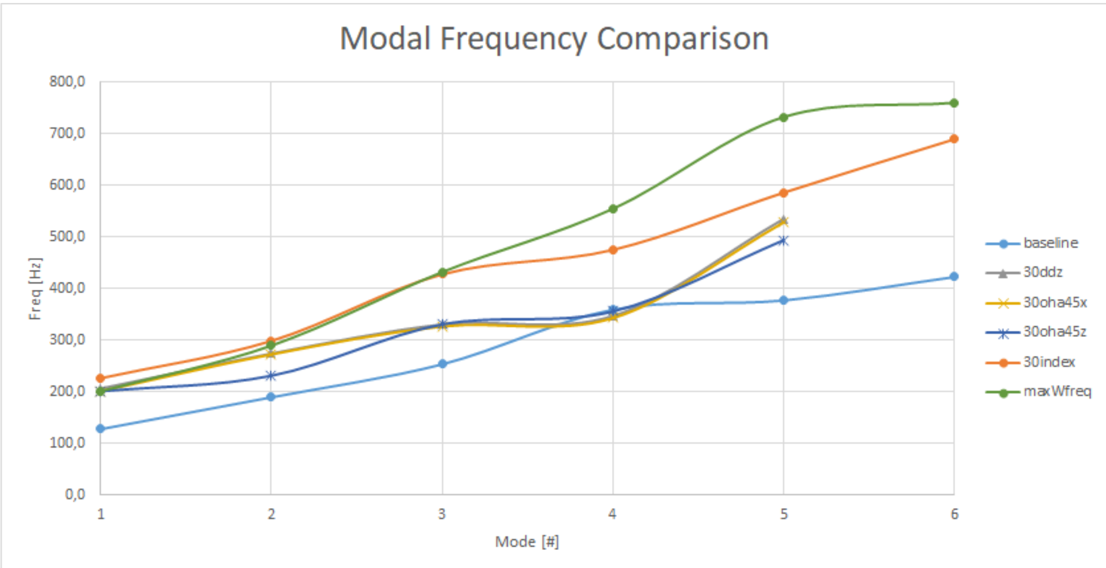

Figure 4.27: Trade-off #3: modal frequency comparison

Among the various optimizations seen in this third trade-off, for the good modal results obtained and for the structure with the best shape and mass, the free solution with the objective of minimizing the compliance index is chosen as the optimal case to be compared with the baseline. Let's go now to see the complete table of frequencies and modal participations:

Mode #	Frequency [Hz]	X-TRANS	Y-TRANS	Z-TRANS
1	**226.5**	0.02%	**90.88%**	0.25%
2	**298.7**	0.35%	0.44%	**87.60%**
3	427.7	0.13%	**6.17%**	0.02%
4	475.1	4.55%	0.34%	**9.02%**
5	585.9	0.85%	0.00%	1.67%
6	**689.5**	**49.51%**	0.37%	0.02%
7	736.8	0.06%	0.00%	0.00%
8	743.5	0.06%	0.00%	0.00%
9	870.4	**27.75%**	0.10%	0.00%
10	890.9	3.12%	0.08%	0.09%
11	954.3	0.39%	0.13%	0.02%
12	978.1	**9.84%**	0.25	0.03
13	1286	0.92%	0.00%	0.02%
14	1527	0.02%	0.01%	0.00%
15	1568	0.43%	0.01%	0.01%
16	1674	0.11%	0.03%	0.02%
17	1736	0.00%	0.00%	0.00%
18	1739	0.00%	0.00%	0.00%
19	1873	0.02%	0.00%	0.00%
20	1961	0.00%	0.01%	0.01%
Subcase Total		**98.14%**	**98.82%**	**98.79%**

Mass [kg]	8.77

Table 4.9: Trade-off #3: modal participation of the new twenty frequencies

As we can see from the previous table, the first three modal participations along the three axes are all greater than those of the baseline (from 359.1 Hz to 689.5 Hz along x, from 127.7 Hz to 226.5 Hz along y and from 189.5 Hz to 298.7 Hz along z). The only thing that changes is that the first frequency with modal participation along the x-axis greater than 5% occurs in the sixth mode and no longer in the fourth (where in reality there is a modal participation approximated by excess to 5%). Finally found the best optimization in terms of performance, we can proceed with the lattice optimization.

Chapter 5

Lattice Optimization

5.1 3D Modeling of the Optimized Design

The first thing to do, even before proceeding with the lattice optimization, is certainly to take the chosen result from the previous topological optimization and create a profile as uniform and smooth as possible. To do this we must export the mesh obtained from the optimization as a STL file, in order to define a geometry as well.

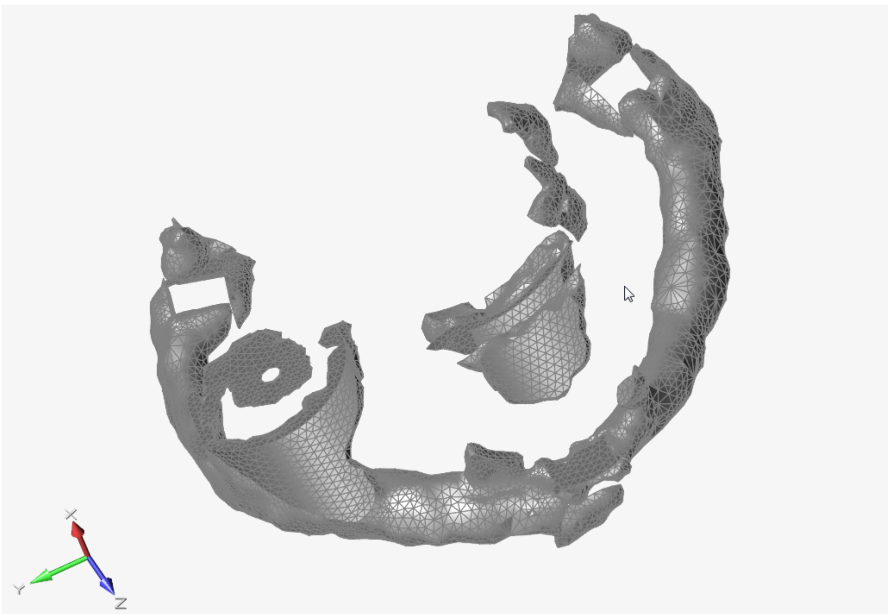

Figure 5.1: STL file imported in Inspire 2020

Intending to obtain a STL file, it is necessary to isolate the mesh of the optimized design and through the command "Validate > Faces > Find Faces" select all the displayed elements and proceed. At this point, once we get the skin of the designated mesh, we go to "File > Export > Geometry Model" and save the document as a STL file. Now all that remains to do is to open Inspire 2020 and import the new file.

At this point we have a geometry that we can model and smooth through Inspire's PolyNURBS functions, located in the Geometry command panel.

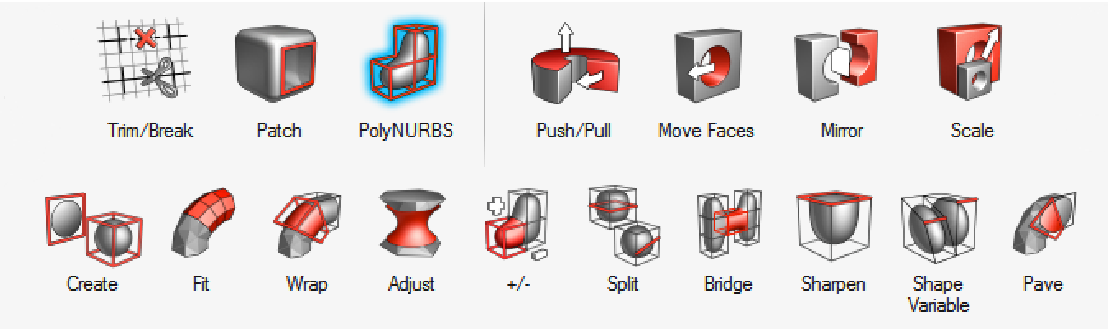

Figure 5.2: PolyNURBS commands panel

Through these functions it is possible to trace over optimized results with precision, ease and efficiency. The resulting model can be exported to other formats and is readily usable for manufacturing. The main command to create polyNURBS is the "Wrap" command, which allows us to view a preview during the modeling itself, helping to understand what the final shape of the structure will be. Through this command we can also create single cages that can later be connected each other. To connect a PolyNURBS with another, there is also the "Bridge" command.

If we want to create a PolyNURBS surface following an existing shape, all we have to do is use the "Pave" command. Through this command we can also blend two PolyNURBS surfaces, close holes in PolyNURBS geometry or convert PolyNURBS surfaces to solids.

Instead, if we want to build a PolyNURBS geometry without wrapping or paving, the "Create" tool is what we should start with. Using this function it is possible to create a single solid or PolyNURBS surface around a selected object or a starting point for a new model.

But if we do not need a specific shape and simply want to automatically derive the polyNURBS that schematize our optimized structure, we can proceed with the "Fit" command, then select the entire component and proceed with the automatic creation.

The remaining functions are used to modify existing PolyNURBS:

1. "Adjust" tool is useful for automatically shrinking or expanding PolyNURBS cages to fit them to an optimized shape;

2. "Add(+)/Remove(-)" tool is used for adding or removing blocks;

3. "Split" command splits a cage with a loop or splits a single PolyNURBS cage face;

4. "Sharpen" function can be used to control sharpness along the edges of a PolyNURBS (four levels of sharpness are available);

5. "Shape Variable" tool is used for the definition of moving directions of PolyNURBS cage points during PolyNURBS optimization.

After working with the different commands in order to obtain a structure as similar in mass and size as the original optimized one, but with a curved and rounded shape, the final result is shown in the following figures (including dimensions).

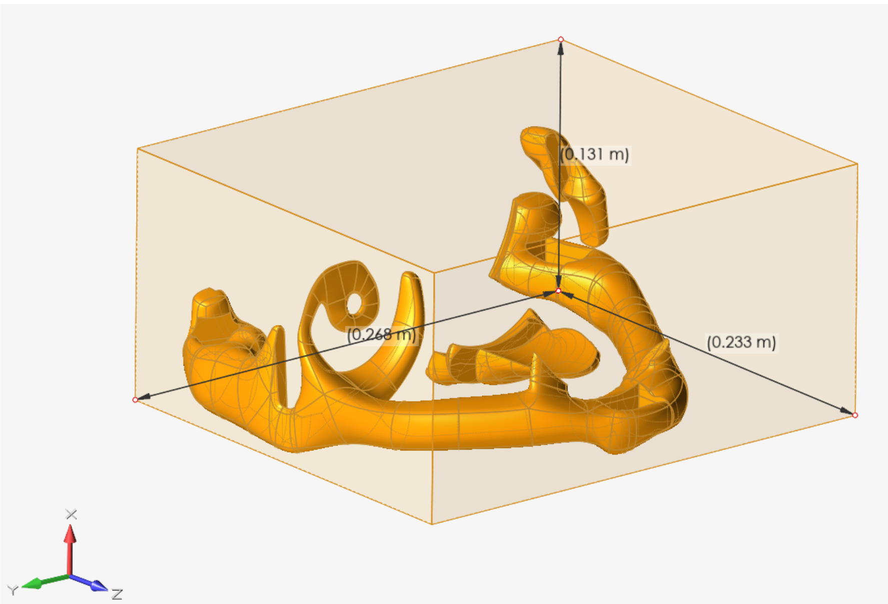

(a) *Maximum overall dimensions*

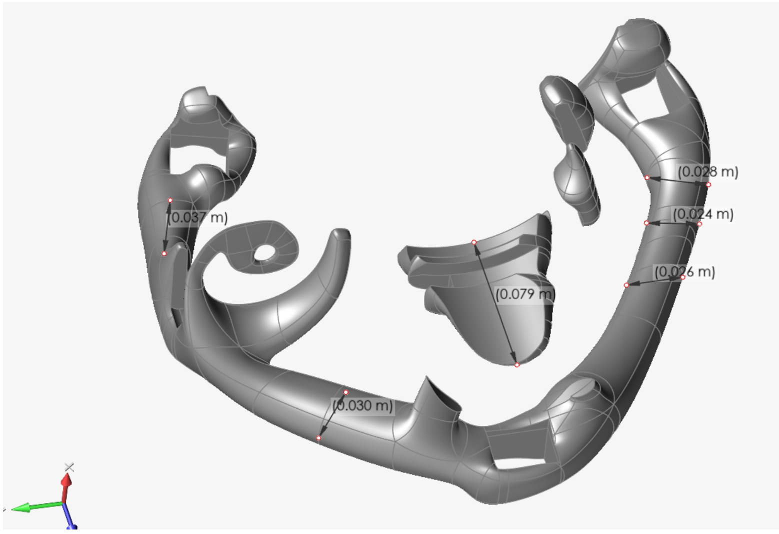

(b) *Some characteristic dimensions*

Figure 5.3: PolyNURBS structure with dimensions definition

As we can easily see, the structure maintains the same shape, but in this solution the surface is much more rounded and curved and has less discontinuity than the initial optimized geometry, so it is more suited to the application of the lattice. Now we just have to export the resulting geometry as a STMOD file and open it in Hyperworks X to be able to create a three-dimensional TETRA-mesh.

Figure 5.4: PolyNURBS structure three-dimensional TETRA-mesh

To create the three-dimensional mesh, we act in the same way we mesh the design and non-design space: we create a 3 mm two-dimensional TRIA-mesh of the external surface and then fill it with three-dimensional TETRA elements. At this point, we can import the new mesh into the file containing the entire structure mesh, replacing the original design space.

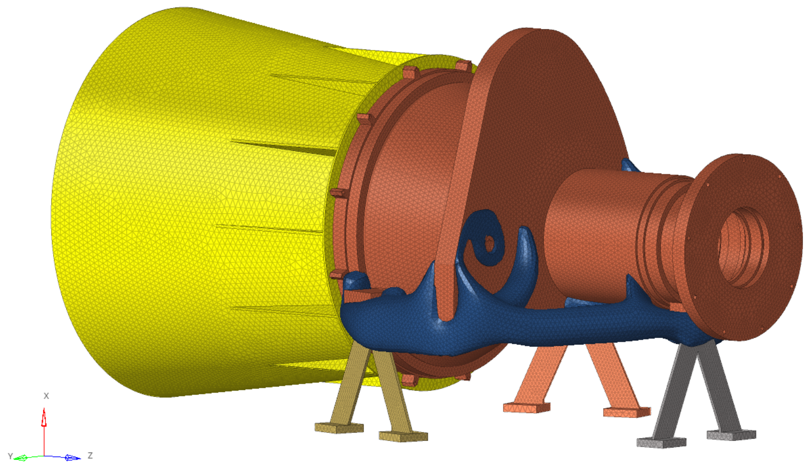

(a)

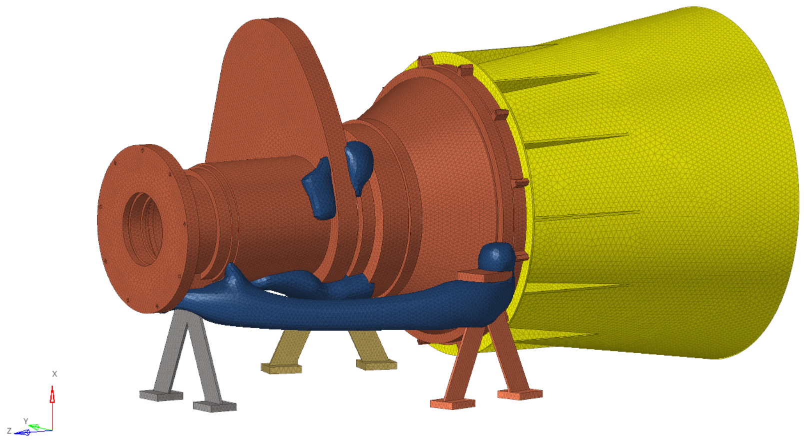

(b)

Figure 5.5: Optimized structure three-dimensional mesh including PolyNURBS

Once the mesh is done, we can perform a modal analysis to verify if the results correspond to the case without PolyNURBS and then carry out a static analysis to understand if this structure has any advantages over the baseline. Let's now see the results of the modal analysis:

Mode #	Frequency [Hz]	X-TRANS	Y-TRANS	Z-TRANS
1	**225.5**	0.02%	**90.82%**	0.34%
2	**297.0**	0.35%	0.57%	**87.27%**
3	424.4	0.10%	**6.17%**	0.02%
4	469.8	4.24%	0.28%	**9.75%**
5	610.3	3.71%	0.04%	1.14%
6	**689.3**	**49.09%**	0.33%	0.06%
7	734.4	0.00%	0.00%	0.00%
8	737.6	0.00%	0.00%	0.00%
9	856.6	**21.12%**	0.00%	0.01%
10	871.3	3.65%	0.22%	0.07%
11	940.2	**11.11%**	0.01%	0.06%
12	970.7	4.48%	0.33%	0.00%
13	1256	0.69%	0.00%	0.02%
14	1505	0.05%	0.01%	0.01%
15	1522	0.32%	0.01%	0.01%
16	1650	0.15%	0.02%	0.02%
17	1732	0.00%	0.00%	0.00%
18	1734	0.00%	0.00%	0.00%
19	1840	0.01%	0.00%	0.00%
20	1932	0.00%	0.01%	0.01%
Subcase Total		**98.08%**	**98.84%**	**98.79%**

Mass [kg]	**8.86**

Table 5.1: Modal analysis results for the PolyNURBS structure

Thanks to the table above we can compare these values with those seen in the previous chapter, concerning the optimized case without PolyNURBS: we can certainly say that they are almost the same. Not only frequencies and modal participations, but also the mass deviates very little and is not even exaggeratedly greater than the baseline, considering that with the lattice optimization we could reduce it.

We can see this similarity from the graph below, where a comparison between the frequencies of the two versions of the same optimized geometry and of the baseline is shown.

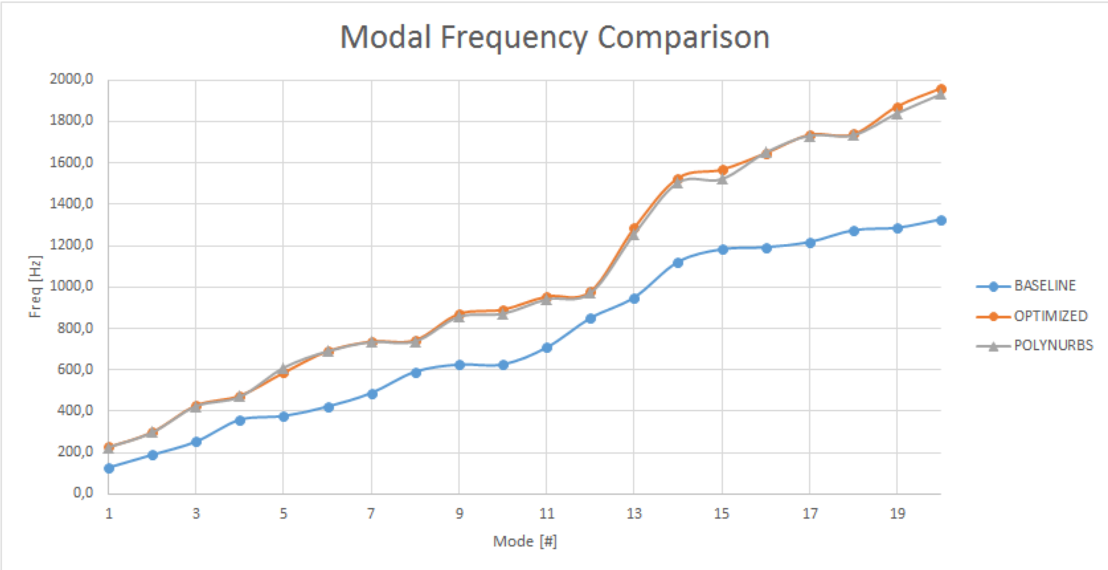

Figure 5.6: Modal frequency comparison: baseline and optimization

Now we just have to view the results of the static analysis, which, as in the previous case, is faced by considering the three gravitational loads (g_x, g_y and g_z) as three separate load steps:

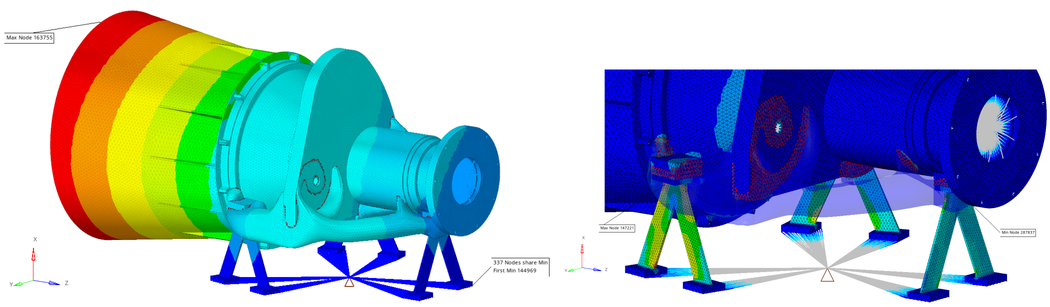

(a) *Displacement: 0.0368 mm* **(b)** *Von Mises Stress: 24.5 N/mm2*

Figure 5.7: Static results for g_x load step

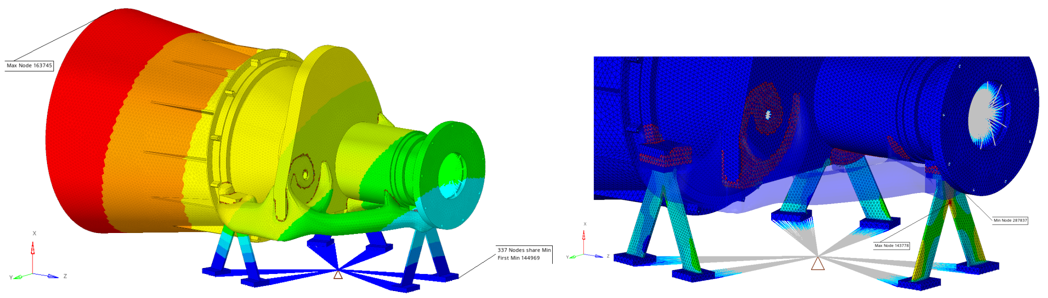

(a) *Displacement: 0.181 mm* **(b)** *Von Mises Stress: 98.3 N/mm2*

Figure 5.8: Static results for g_y load step

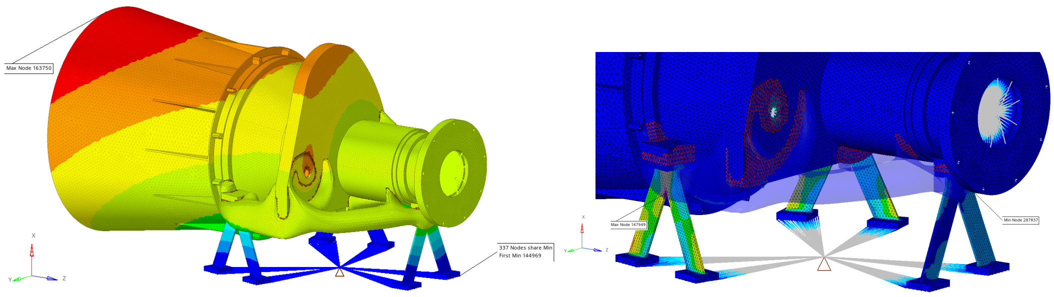

(a) *Displacement: 0.105 mm* **(b)** *Von Mises Stress: 68.7 N/mm2*

Figure 5.9: Static results for g_z load step

	Displacement [mm]			Stress [N/mm2]		
	x	**y**	**z**	**x**	**y**	**z**
Baseline	0.122	0.483	0.313	67.6	151	66.6
PolyNURBS	0.0368	0.181	0.105	24.5	98.3	68.7

Table 5.2: Static analysis results comparison

As we can see from the previous images, but more precisely from the table, both the displacements and the stresses of the three load steps never exceed the baseline values (except for the von Mises stress along z, but very little), which indicates advantages from the static point of view and not only from the modal one, as seen before. This analysis allows us to finally proceed with the lattice optimization, but first let's see what it consists of.

5.2 Basics for Lattice Structure Optimization

The lattice optimization is a new solution to create mixed solid and lattice structures from concept to detailed final design. This new technology is mostly used for structures that must be printed through additive manufacturing [6]. An optimization of this type involves two main phases:

1. Lattice structure creation (porous material definition);
2. Lattice structure optimization. In this phase, lattice members dimensions are optimized by imposing detailed constraints (e.g stress, displacements, etc).

The final result is a mixed solid and lattice parts structure of varying material volume. This optimization is initially similar to the topological one, but the design domain can include elements with intermediate densities. Theoretically, from a physical point of view, such structures can be more efficient compared to those resulting from the topology optimization. In our case, two types of lattice cell layout are available: tetrahedron and pyramid/diamond cells derived from tetrahedral and hexahedral meshes, respectively.

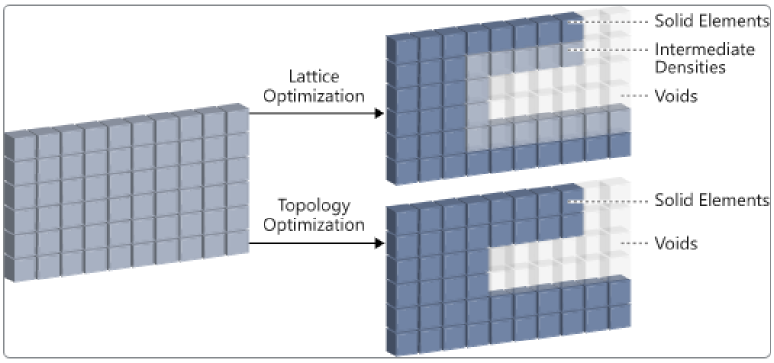

Figure 5.10: Lattice and Topology Optimization Comparison

A good application of Lattice Structure Optimization is, as it has been said before, Additive Manufacturing which can take advantage of the intricate lattice representation of the intermediate densities. Unfortunately, porous structures obtained from lattice optimization usually have a lower stiffness per volume unit than solid ones. For tetrahedron and diamond lattice cells , the homogenized Young's modulus to density relationship is approximately given as

$$E = \rho^{1.8} E_0 \tag{5.1}$$

where E_0 represents Young's modulus of the dense material.

Different levels of lattice domain in topology results can be controlled by the parameter POROSITY:

1. LOW porosity: the natural penalty of 1.8 is applied, which would typically lead to a final design with mostly fully dense materials distribution (or voids) if a simple 'stiffest structure' formulation is applied. However, we may have higher proportion of lattice areas in the design for buckling behavior, thermal performance, dynamic characteristics, and so on considerations;

2. HIGH porosity: no penalty is applied to Young's modulus to density relationship;

3. MED porosity: a reduced penalty of 1.25 is applied for a medium level of preference for lattice presence.

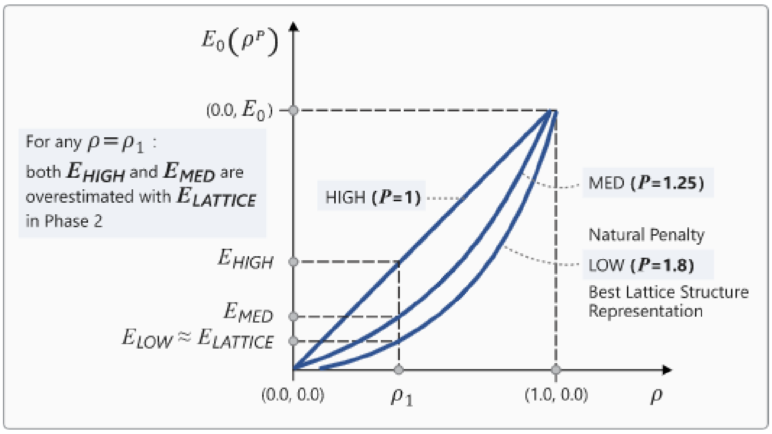

Figure 5.11: Difference between porosity options with regard to stiffness performance

Design constraints can be defined in both Phase 1 and 2 of the Lattice Optimization process. The second phase of the lattice optimization process should be viewed as the fine-tuning stage for the design since further manual manipulation of a lattice structure with hundreds of thousands cell members is almost impossible.

5.2.1 Phase 1: Lattice Generation

In the first phase, the design space is optimized like a regular topology optimization, except that intermediate density elements are preserved in the model. The intermediate densities in the optimized structure are represented by defined lattice types (micro-structures). The volume fraction of the lattice structure corresponds to the element density at the end of this phase. During the optimization process, stiffness of the intermediate densities corresponds to micro-structural homogenized properties.

In order to activates lattice optimization process, the lattice continuation line has to be included on all "DTPL Bulk Data Entries". Then, the Lower and the Upper Bound fields can be used to specify the range of densities for elements that can be converted into Lattice elements. Elements with densities lower than LB are removed from the model and those with densities above UB remain as solid elements.

The solid elements, first or second order, which stand between the LB and UB (intermediate densities) defined on the lattice continuation line are replaced by the corresponding Lattice Type. The lattice structures are constructed using 1D Tapered Beam (CBEAM) elements (Figure 5.11).

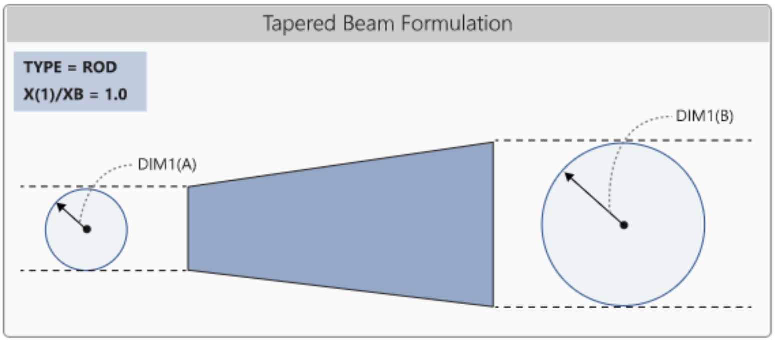

Figure 5.12: Tapered Beam Formulation

The initial radius of the lattice structure beam elements for each lattice structure cell is proportional to the density of the intermediate density elements which are replaced, such that the initial volume in phase 2 is equal to that at the end of phase 1. In phase 2, the concept of lattice beam element radius is interpreted as joint thickness. Thickness for each joint at the conjunction of lattice beam elements is determined and the radius of each element can vary across the beam length. The beam elements have the property PBEAML and TYPE = ROD is automatically assigned for each element. The thickness of this tapered beam element can vary along its length and only circular cross-sections are available. The X(1)/XB field on the PBEAML entry is always set to 1.0 for tapered beam elements.

Lattice Type	1	2	3	4
HEXA	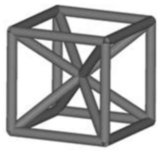	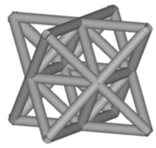	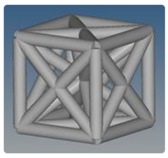	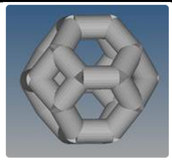
TETRA	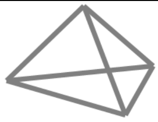			
PYRA	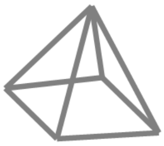			
PENTA	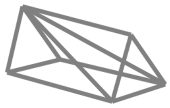			

Table 5.3: Lattice Types

5.2.2 Phase 2: Size Optimization

In the second phase, the Lattice Structure is optimized using Size optimization. The size (parameter) optimization phase is aimed at incorporating some anisotropy to the Lattice Structure, thereby making the structure more efficient. For a given load step, the newly created file "<name>_lattice.fem" includes sizing (parameter) optimization set-up. The optimization responses, constraints, and objective function should be reviewed and redefined (if necessary) in the second phase.

The contact sets should also be reviewed and possibly redefined if required. A single design variable (DESVAR) is automatically created for each conjunction of lattice tapered beam elements, representing the radius of all the beam cross sections at that point. The DESVARs are related to the radii of each tapered beam element by DVPREL entries in the size (parameter) optimization process. The lower bound of the sizing design variables is automatically set to a low value of $UB/10^6$.

At the end of the second phase, a new "<name>_lattice_optimized.fem" file is created, which includes optimized lattice structures. Beams with very small radii are automatically removed from the structure during this phase. Therefore, a verification analysis on the "<name>_lattice_optimized.fem" file is recommended to look at the final responses.

Compliance Management

During the lattice optimization, a compliance variation occurs based on several internal processes. Excessive reductions in compliance are the problems to avoid and it is a good thing to be careful during the phases of performance loss, that occurs:

1. At the end of Phase 1, by removing voids and low density elements in the model (elements with a density below LB);

2. During the transition from Phase 1 to Phase 2. If no penalty (high porosity) or low penalty (med porosity) is applied to the model, when intermediate density elements are replaced by lattices, the stiffness of the structure is overestimated.

Stress Constraints

In addition to the regular constraints, stress constraints can be used in lattice optimization. Stress constraints can be applied in two different ways:

1. The LATSTR field on the LATTICE continuation line in the DTPL entry can be used to define the stress constraint for the second phase. If "LATPRM > STRMETH > PNORM" (default) is specified, the Stress NORM method is used to calculate the maximum stress value that is constrained for a given set of CBEAM elements. Using the Stress NORM in this phase is important for the large number of beam elements. If stress constraints for all beams are considered as individual during the optimization, the size of the problem would be too large. Using Stress NORM improves efficiency of the handling of stress constraints in the second phase so it is recommended to retain the LATTICE parameter set to YES.

2. The STRESS field on the DTPL entry can be used to specify stress constraints for the first phase topology optimization, but this is not passed through to the second phase.

The Stress NORM method is used to approximately calculate the maximum stress value of all the elements included in a particular response. This is also scaled with the stress bounds specified for each element. So to minimize the maximum stress in a particular element set, the resulting stress NORM value (σ_{NORM}) is internally constrained to a value lower than 1.0:

$$\sigma_{NORM} = \left(\frac{1}{n} \sum_{i=1}^{n} \left(\frac{\sigma_i}{\sigma_{bound}} \right)^p \right)^{\frac{1}{p}} \tag{5.2}$$

where

σ_{NORM} = stress norm value
n = elements number
σ_i = single element stress value
σ_{bound} = stress bound
p = penality value (default 6.0)

The default penalty value is a reasonable approximation of the maximum ratio value and reduces instability. The Stress NORM feature creates two responses for a model, one stress NORM response for the elements with highest 10% of the stresses and a second stress NORM response for the rest of the model.

Contact

Typically, two types of CONTACT situations occur in Lattice Optimization:

1. Lattice structures at the interface between design and non-design are connected at the corner face nodes. However, in LT=2, floating grid points are present at the face centers of the lattice structure faces adjacent to the non-design solid elements at the interface. These floating grid points are connected using automatically generated Freeze contacts. If the CONTACT is not created, the center node on the faces connected to the solid elements is left hanging in the second phase.

2. The model contains preexisting contacts before Phase 1 is run. In such cases, it is recommended to review and update the contact interface, between the design, non-design and newly created lattice domains. The Lattice domain is always set as Slave and the non-design/solid domain in contact with the lattices is set as the Master.

Lattice Sizing+

It is an extended sizing optimization process at the end of the sizing optimization during the second phase of lattice optimization. Lattice Sizing+ is activated when "LATPRM > CLEAN > YES" (default) or "LATPRM > CLEAN > LESS" is present in the model. The "Beam Cleaning" procedure occurs after sizing optimization at the end of the second optimization phase to penalize beams with very low radii. The beams below MINRAD are pushed to 0 or 1 through a Topology optimization.

This topology optimization consists of two additional phases at the end of the sizing optimization phase. The first additional phase involves adding a penalty factor to the objective. This is equivalent to add a value equal to the objective at convergence of the sizing optimization to the objective. The second additional phase consists in adding a penalty of 1000 times the Objective.

The Lattice Sizing+ process allows the cleaning up of small beams without much loss in compliance when compared to the converged step of the sizing optimization. Since the cleaning process is now visible to the optimizer, there is no violation of constraints and performance drop is minimized. After the second optimization stage (sizing optimization), "*filename_oss_lattice_optimized.fem*" is created.

5.3 Lattice Optimization with Hyperworks X

5.3.1 Lattice Control Parameters Selection

We start by defining the optimization controls:

1. First of all, there is a LATPRM type control, thanks to which we define parameters that regulate the lattice optimization. The only parameter that is entered in this first moment is the one that controls the treatment of the rods that extend from the external surface after filling the unit cells through DLATTICE (BOUNDARY > PROJ);

Parameter	Values	Description
BOUNDARY	SHORTEST, PROJ, CUT	**SHORTEST (Default)** Rods which extend out of the external surface are cut off. There is no projection. **PROJ** Rods which extend out of the external surface are projected to the surface normal. **CUT** The shorter option of PROJ and CUT is picked automatically.

Figure 5.13: Lattice optimization control: BOUNDARY

2. Next we are going to define a DOPTPRM type control, which defines design optimization parameters by overriding the defaults. For this second control we define the characteristics of two parameters: the amount of intermediate densities in the model (POROSITY) and the Automatic Reanalysis process at the end of Phase 1 (LATLB). Porosity is set to MED, so it generates a relatively medium number of intermediate density elements, that is equivalent to set a penalty value (P) of 1.25. The LATLB is set to AUTO, so the Automatic Reanalysis is turned ON.

Parameter	Values	Description
POROSITY	< HIGH, MED, LOW >	**HIGH (Default)** Generates a relatively high number of intermediate density elements in the first stage of the optimization run. The penalty value (P) is set to 1.0 which is equivalent to no density penalization. **MED** Generates a relatively medium number of intermediate density elements in the first stage of the optimization run. This option is equivalent to a penalty value (P) of 1.25. **LOW** Generates a relatively low number of intermediate density elements in the first stage of the optimization run. This option is equivalent to a natural penalty value (P) of 1.8.

Figure 5.14: Lattice optimization control: POROSITY

Parameter	Values	Description
LATLB	<AUTO, USER or CHECK>	**AUTO** Turns ON the Automatic Reanalysis Process. **USER (Default)** Turns OFF the Automatic Reanalysis Process and the user-defined LB value (or default of 0.1) is used to generate Lattice Structures for Phase 2. **CHECK** This option can be used to run a single reanalysis iteration and a warning will be output which contains the percentage difference in compliance between the original and the reanalyzed structure. The CHECK option can be used to gain information about the compliance performance of the structure using the specified LB. If the compliance performance is not as expected, then you may consider rerunning Phase 1 using AUTO to possibly find a better density Lower Bound (LB).

Figure 5.15: Lattice optimization control: LATLB

At this point, in order to have a lattice optimization that works correctly, it is necessary to divide the optimizing volume into two components: one containing the solid TETRA mesh of the design space and another one containing the two-dimensional mesh of its skin.

This is done because in the definition of the lattice, the contact section between what could be the optimized volume (design space) and what could remain constant (i.e. the non-design space) is very important.

Four contact sets are then defined:

1. Lattice volume set, which represents the outer surface of the solid mesh of the design space;
2. Lattice skin set, which coincides with the two-dimensional skin of the design space;
3. Design Space set, which contains the solid (three-dimensional TETRA mesh) and shell (two-dimensional TRIA mesh) property;
4. Contact set, which contains the non-design space solid property.

Once the contact sets have been defined, all that remains is to identify a real contact between the design and the non-design space, then a contact group is created between the last two sets that we defined before, imposing a FREEZE type contact, which enforces zero relative displacements on the contact interface.

The last parameters on which you need to act to launch the lattice optimization, which are very important in order to just have such an optimization, are found in the DTPL interface of the design variable, under the lattice entry:

1. the lattice type, which is not selected as a customized cell is used for this optimization;
2. the lower and upper bounds to regulate the density of the resulting lattice (between 0.1 and 1);
3. the maximum stress value that the structure is able to withstand, imposing the yield strength of the titanium (about 800 MPa).

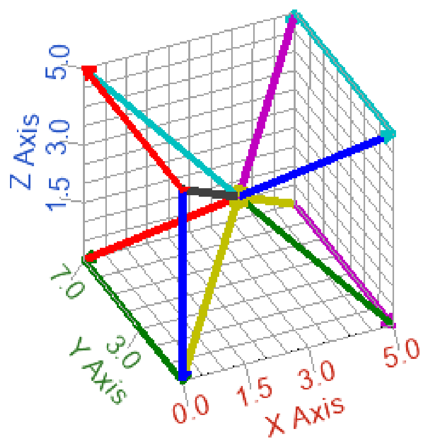

Figure 5.16: Custom cell plot in Altair Compose

As we said, the cell used for this optimization is implemented manually, as a text file, through the command "Panels > Analysis > Control Cards > Bulk Unsupported Cards":

```
DLATTICE,901,7,,900,1,3
,LAYOUT,1,1,1,5
CELL,900
,ROD,1,5
,ROD,2,6
,ROD,3,7
,ROD,4,8
,ROD,1,9
,ROD,2,9
,ROD,3,9
,ROD,4,9
,ROD,9,5
,ROD,9,6
,ROD,9,7
,ROD,9,8
,1,0.,0.,0.
,2,0.,0.,5.
,3,5.,0.,5.
,4,5.,0.,-0.
,5,0.,7.,0.
,6,0.,7.,5.
,7,5.,7.,5.
,8,5.,7.,0.
,9,2.5,3.5,2.5
```

The customized cell is meant to be an example to make clear how to proceed when we want a customized lattice structure. To visualize the shape of the cell we used the Altair Compose tool and made a plot of these lines (see figure 5.16).

(1)	(2)	(3)	(4)	(5)	(6)	(7)
DLATTICE	*ID*	*VOLSID*	*SURFSID*	*CELLID*	*MATID*	*CONTSET*
	LAYOUT	*S_X*	*S_Y*	*S_Z*	*CID*	
	ROD	*R1_ID1*	*R1_ID2*			

Figure 5.17: Bulk data entry: DLATTICE

The text lines above define the shape of the implemented cell, following the formatting of the HyperWorks DLATTICE function (figure 5.17) which defines parameters for filling a space with lattice-based unit cells. The presence of this entry also activates the creation of unit cells to fill the target volume.

- ID: identification number of the DLATTICE Bulk Data Entry;
- VOLSID: identifies an element set of CTETRA elements which define the inner volume that is to be filled with lattice unit cells;
- SURFSID: identifies an element set of shell elements which define the outer surface enclosing the volume that is to be filled with lattice unit cells;
- CELLID: identification number of a CELL Bulk Data Entry which identifies the unit cell structure;
- MATID:identification number of a Material Bulk Data Entry;
- CONTSET: identification number of a SET of elements which are used to create a TIE'd contact with the filled volume. The element SET defined on CONTSET is the master and the grids of the beams on the surface of the filled volume are the slave;
- S_X, S_Y, S_Z: scaling factors in X, Y, Z directions which allow scaling of the original unit cell;
- CID: coordinate system which identifies the orientation of the unit cell;
- Ri_ID1, Ri_ID2: identifies the first and the second point of the i-ROD.

If we have a blank space in the cell implementation text, it does not imply an error, but simply that particular parameter is not defined or the default value is considered (reference to the SURFSID space).

Now that all the parameters have been defined, we are ready to launch the lattice optimization, but after a check we notice an excessive RAM memory request (about 109GB). In order to ease the memory required for optimization, we decide to schematize the baffle with a concentrated mass and then go and reshape it once the lattice has been created.

5.3.2 1st Lattice Optimization without Design Space Skin

As can be seen from the following images, we obtain a very dense reticulated structure that replaces the full volume of design.

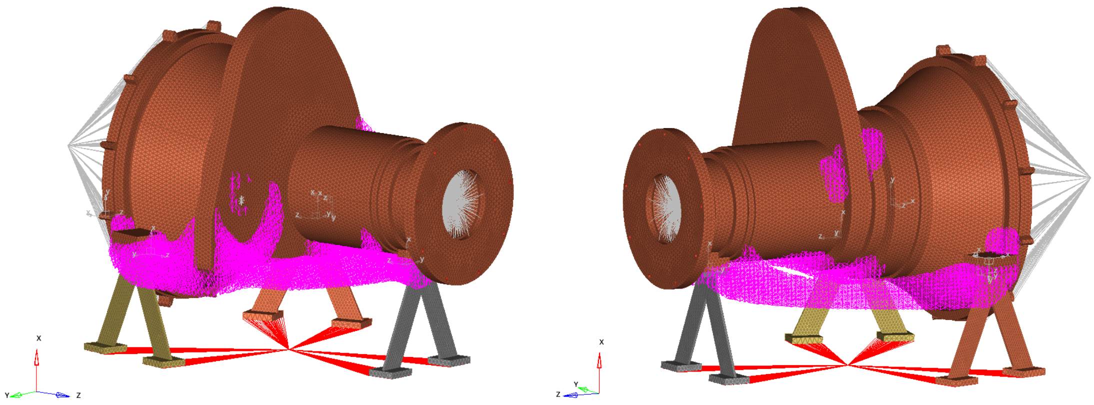

(a) (b)

Figure 5.18: Structural lattice optimization results (without baffle geometry)

Once we get this result , in addition to the classic optimization output files, this also gives me a file called ”$filename_{l}attice.fem$” that I can import and modify within HyperWorks X. Going to open and making the necessary changes, we can see the complete structure with baffle and lattice geometry in the following image.

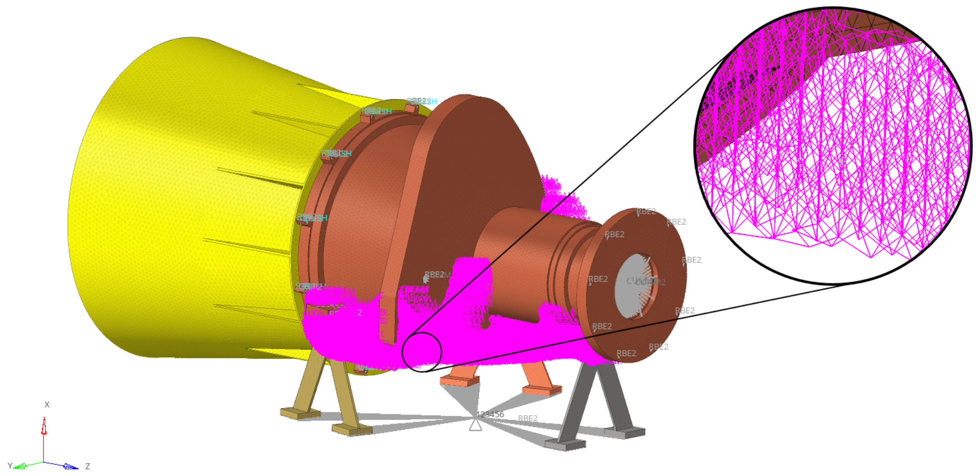

Figure 5.19: Structural lattice optimization results (whole structure)

However, we must keep in mind a very important detail: the lattice geometry that is created following the optimization is a set of two-dimensional BEAM elements of approximately 5x0.7 mm. So, although on a theoretical level we can carry out all the various static and modal analyzes, on a practical level we have to find a way to convert all these two-dimensional elements into three-dimensional solids that can be imported like a CAD or STL file.

We will deal with this problem later. Now let's check the performance of this solution in terms of stress, displacement and resonant frequencies. So let's carry out our usual three static analyzes with a gravitational load of 25g along the three directions and a modal analysis considering at least twenty resonant frequencies.

From the static analysis we obtain the following results:

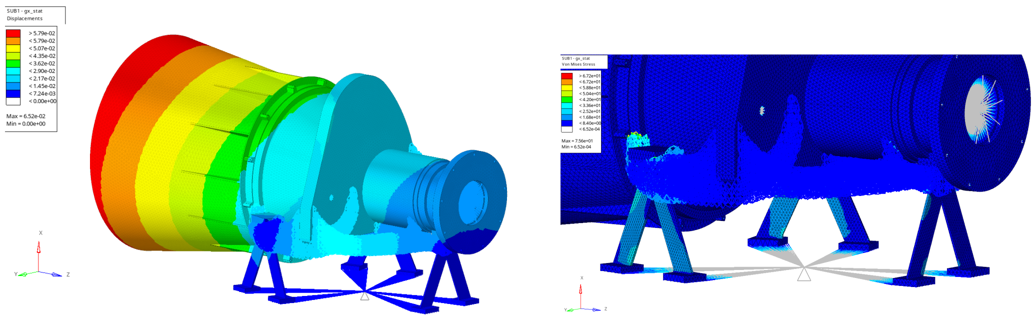

(a) *Displacement: 0.0652 mm* **(b)** *Von Mises Stress: 75.6 N/mm2*

Figure 5.20: 1st Lattice Optimization: static results for g_x load step

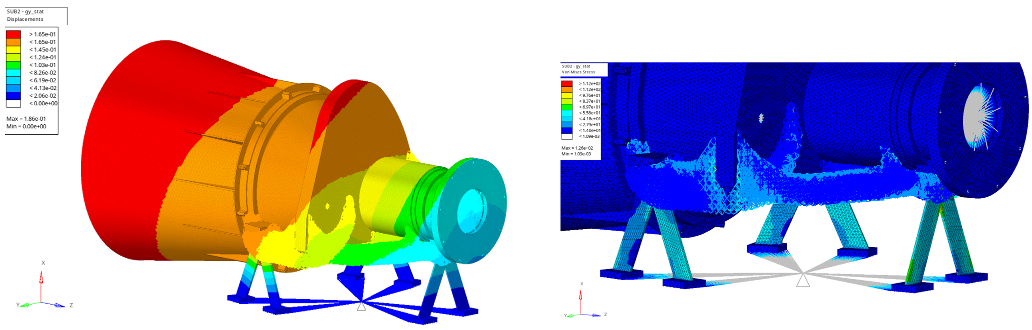

(a) *Displacement: 0.186 mm* **(b)** *Von Mises Stress: 126 N/mm2*

Figure 5.21: 1st Lattice Optimization: static results for g_y load step

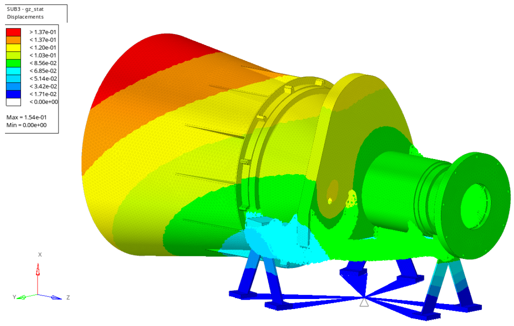

(a) *Displacement: 0.154 mm*

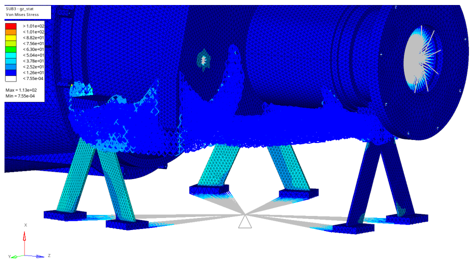

(b) *Von Mises Stress: 113 N/mm2*

Figure 5.22: 1st Lattice Optimization: static results for g_z load step

	Displacement [mm]			Stress [N/mm2]		
	x	y	z	x	y	z
Baseline	0.122	0.483	0.313	67.6	151	66.6
Lattice	0.0652	0.186	0.154	75.6	126	113

Table 5.4: 1st Lattice Optimization: static analysis results comparison

We can easily see from the images and the table above, that as regards the displacements we obtained lower values compared to the baseline and this is positive as there will be a higher stiffness. With regard to stress, however, we have the highest values for the case along x and along z (this last one is already higher than the baseline for the case of polyNURBS). This factor should not worry us too much since in any case they are all far below the yield point for titanium, set at 800 N/mm^2.

Now let's see the results of the modal analysis made on the first twenty resonant frequencies and compare them, as in the static case, with the baseline to understand if a lattice optimization allows to obtain better performances.

Mode #	Frequency [Hz]	X-TRANS	Y-TRANS	Z-TRANS
1	**206.2**	0.14%	**87.31%**	0.07%
2	**256.5**	2.42%	0.00%	**70.43%**
3	372.1	2.03%	2.57%	**11.35%**
4	414.9	0.01%	3.62%	**5.81%**
5	435.4	2.13%	1.09%	**6.18%**
6	**557.4**	**39.27%**	0.00%	3.70%

7	639.8	**11.88%**	2.62%	0.03%
8	734.8	**9.91%**	0.39%	0.20%
9	736.4	0.00%	0.00%	0.00%
10	741.1	0.04%	0.00%	0.00%
11	885.8	**6.05%**	0.34%	0.19%
12	946.7	**14.27%**	0.41%	0.00%
13	1043	**7.36%**	0.00%	0.01%
14	1147	0.39%	0.07%	0.00%
15	1169	0.00%	0.02%	0.26%
16	1311	0.05%	0.02%	0.02%
17	1314	0.20%	0.00%	0.01%
18	1493	0.15%	0.00%	0.01%
19	1564	0.00%	0.01%	0.09%
20	1713	0.17%	0.04%	0.00%
Subcase Total		**96.47%**	**98.53%**	**98.37%**

Mass [kg]	**7.76**

Table 5.5: Modal analysis results for the 1st lattice optimization

In the table we can see the frequencies and their modal participation along the three axes x, y and z. If we compare the values of the first three frequencies with modal participation along the three axes with those of the baseline (Table 2.3), we notice an increase (we go from 359.1 to 557.4 Hz in x, from 127.7 to 206.2 Hz in y, from 189.5 to 256.5 Hz in z). In the following images, however, the deformations of these first three frequencies are highlighted (scale factor of 1.5):

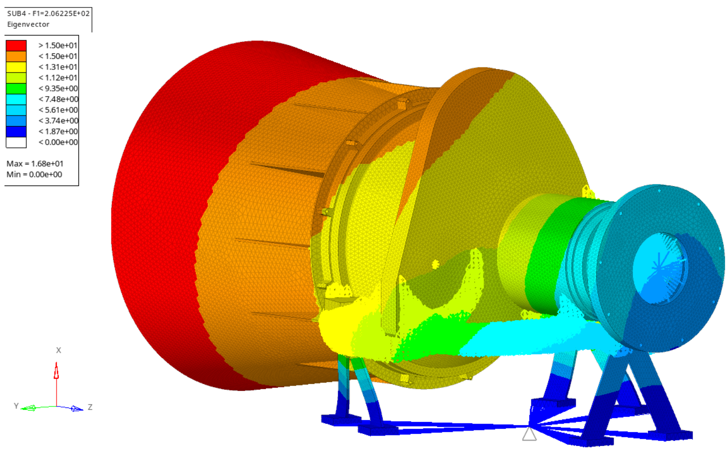

(a) *Frequency #1: 206.2 Hz (along y)*

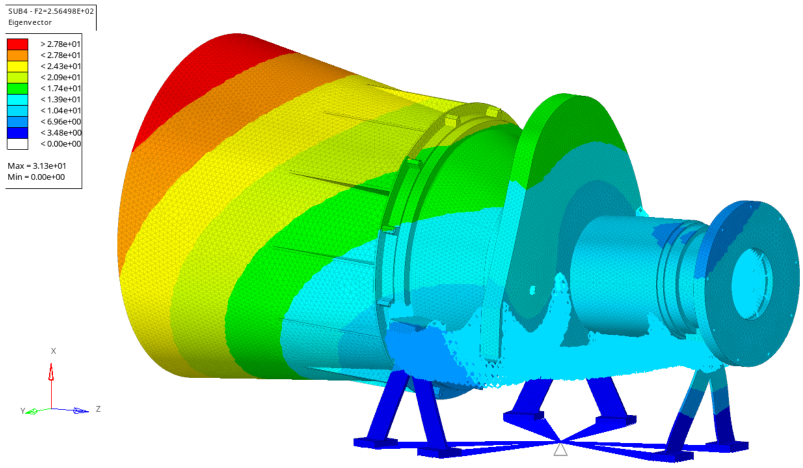

(b) *Frequency #2: 256.5 Hz (along z)*

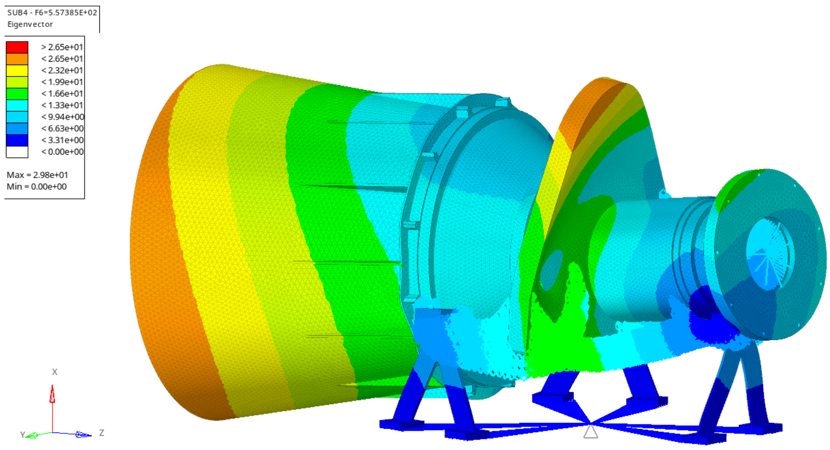

(c) *Frequency #6: 557.4 Hz (along x)*

Figure 5.23: 1st Lattice Optimization: modal participation along the three main directions

Comparing the previous images with those of the frequencies with corresponding modal participation on the baseline (Figure 2.19 (a), (b) and (d)), we notice quite similar deformations: the differences are due to the different structure, especially for the one along x-axis.

Thanks to the graphic representation below, it is easy to understand that the frequencies obtained from the structural lattice optimization are higher than the frequencies of the baseline, although they are lower than those obtained by using polyNURBS. This second aspect is not fundamental, as we are interested in having these frequencies always greater than the initial ones and therefore the only noteworthy comparison is that between the current case and the baseline.

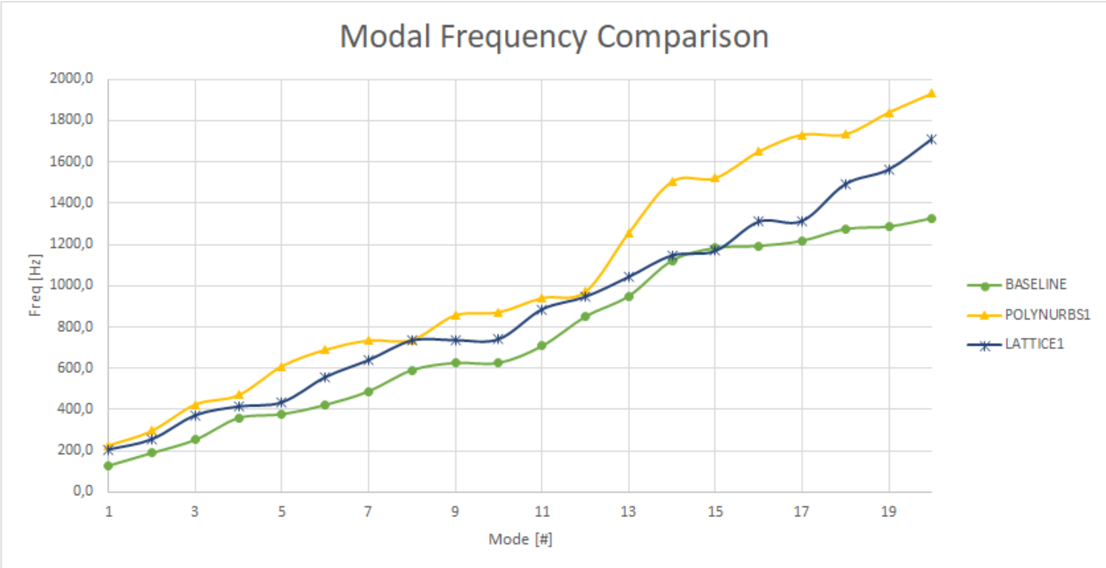

Figure 5.24: Modal frequency comparison: baseline, polyNURBS and lattice

The last parameter to measure and compare with the baseline and the case in polyNURBS, is the total mass of the structure. As we can see in the graph below, if in the previous case of topological optimization we have a slight increase in mass (from 8.36 kg to 8.86 kg), after the lattice optimization there is a decrease in mass (7.76 kg) compared to the baseline.

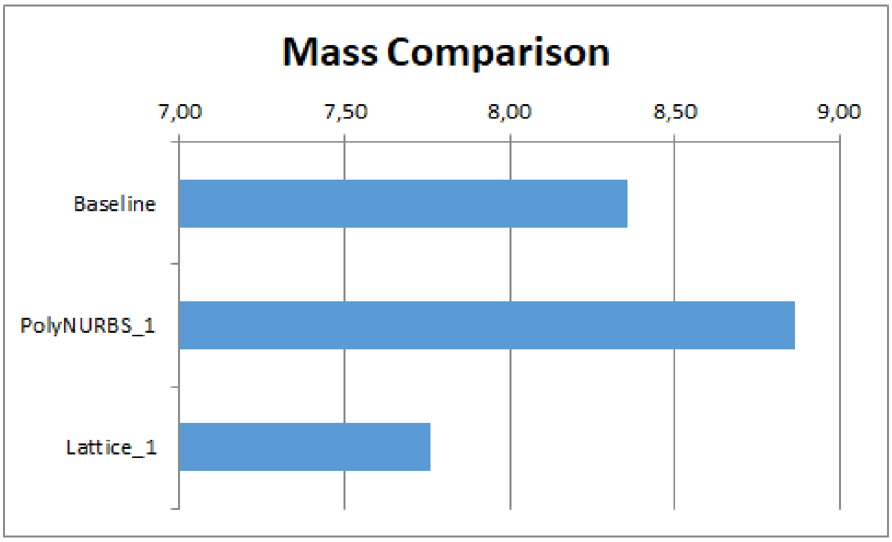

Figure 5.25: Mass comparison: baseline, polyNURBS and lattice

5.3.3 2nd Lattice Optimization with Design Space Skin

Before moving on to the second phase of the lattice optimization and so the sizing of the two-dimensional BEAM elements, in order to not exclude any variant, a second lattice structural optimization is performed, this time considering the external skin of the design space. Regarding the optimization set-up, there is nothing new to underline, except some lattice optimization control parameters (LATPRM) that are changed:

- the BOUNDARY parameter is set on the CUT option, to create a lattice structure that stops exactly on contact with the skin;
- the MINRAD patameter is introduced: it defines the minimum radius value for BEAM cleaning and it is set to 0.5 mm (beams with a radius less than this value are not considered in the Second Phase of Lattice Optimization);
- we have defined an aspect ratio, using the R2LRATIO command, which is used to set the minimum radius-to-length ratio for BEAM cleaning procedure in the Second Phase of Lattice Optimization (it is set to 0.1 mm);
- the TETSPLT command is also considered to turn on the splitting of all non-design or solid elements to TETRA elements for further usage in 3D printing software (this is performed during the second optimization stage in lattice optimization).

Considering a skin with a thickness of 1mm, we get the following result:

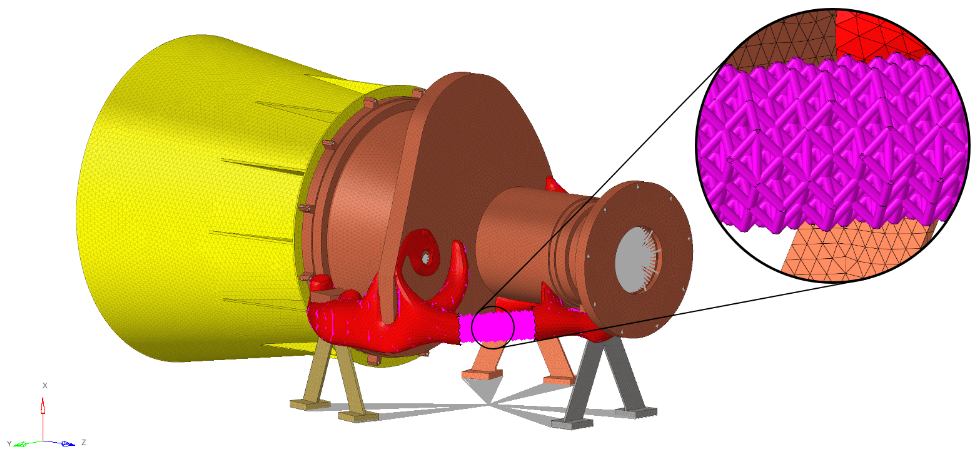

Figure 5.26: Topological lattice optimization results (with skin)

As in the previous case, in order to compare this solution with the baseline and the skinless case, we need to perform both the static and the modal analysis.

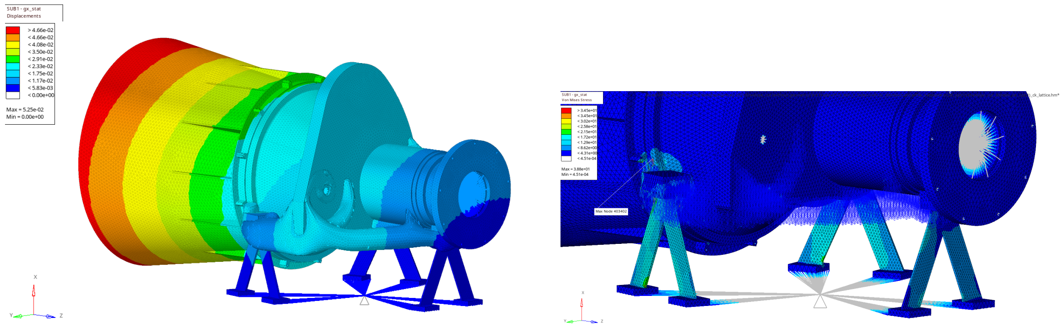

(a) *Displacement: 0.0525 mm* **(b)** *Von Mises Stress: 38.8 N/mm2*

Figure 5.27: 2nd Lattice Optimization: static results for g_x load step

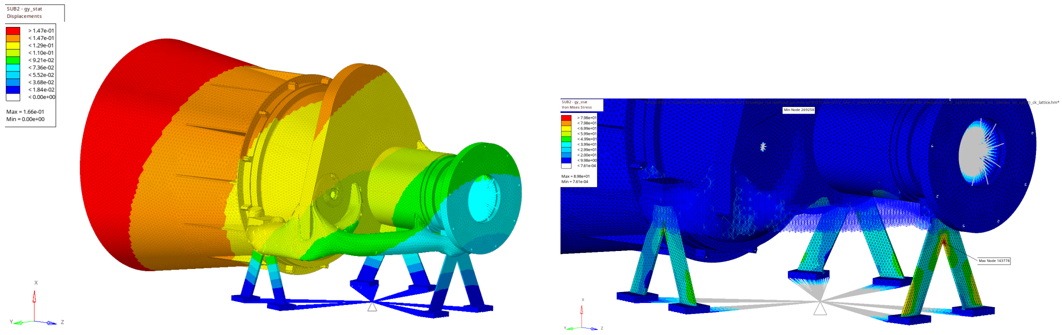

(a) *Displacement: 0.166 mm* **(b)** *Von Mises Stress: 89.8 N/mm2*

Figure 5.28: 2nd Lattice Optimization: static results for g_y load step

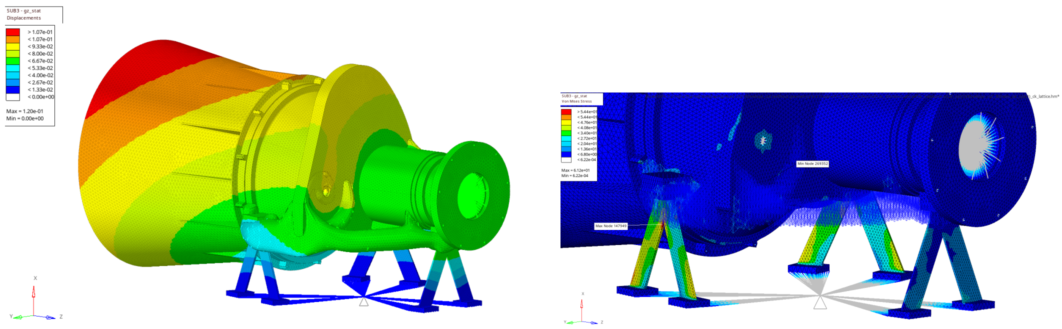

(a) *Displacement: 0.120 mm* **(b)** *Von Mises Stress: 61.2 N/mm2*

Figure 5.29: 2nd Lattice Optimization: static results for g_z load step

	Displacement [mm]			Stress [N/mm2]		
	x	y	z	x	y	z
Baseline	0.122	0.483	0.313	67.6	151	66.6
Lattice #1	0.0652	0.186	0.154	75.6	126	113
Lattice #2	0.0525	0.166	0.120	38.8	89.8	61.2

Table 5.6: 2nd Lattice Optimization: static analysis results comparison

The results obtained from the static analysis show evident improvements in displacement and stress, as they assume lower values than both the baseline and the previous case. This implies a better behavior of the structure when subjected to the inertial loads, so greater stiffness along the three directions. At this point, we just have to see how this structure behaves during a modal analysis:

Mode #	Frequency [Hz]	X-TRANS	Y-TRANS	Z-TRANS
1	**229.2**	0.06%	**89.20%**	0.757%
2	**289.9**	2.03%	0.72%	**75.90%**
3	433.0	2.48%	4.72%	**7.39%**
4	462.1	3.55%	1.90%	**10.85%**
5	555.8	2.87%	0.09%	2.43%
6	**645.2**	**42.62%**	0.13%	0.79%
7	740.2	0.08%	0.00%	0.00%
8	745.6	0.42%	0.02%	0.00%
9	769.9	**11.34%**	0.59%	0.05%
10	822.6	**5.52%**	0.55%	0.10%
11	951.5	**10.78%**	0.14%	0.13%
12	1007	**13.17%**	0.42%	0.00%
13	1182	1.57%	0.00%	0.04%
14	1361	0.10%	0.01%	0.07%
15	1405	0.14%	0.02%	0.03%
16	1581	0.03%	0.14%	0.03%
17	1734	0.00%	0.00%	0.00%
18	1737	0.00%	0.00%	0.00%
19	1748	0.01%	0.01%	0.00%
20	1834	0.01%	0.00%	0.01%
Subcase Total		**96.76%**	**98.67%**	**98.56%**

Mass [kg]	**7.97**

Table 5.7: Modal analysis results for the 2nd lattice optimization

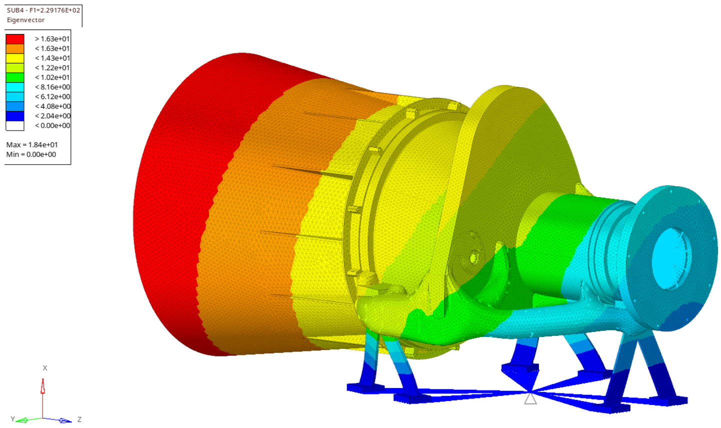

(a) *Frequency #1: 229.2 Hz (along y)*

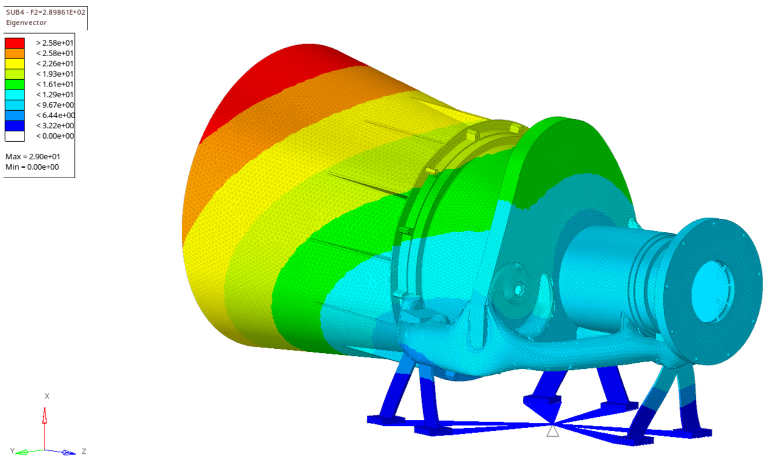

(b) *Frequency #2: 289.9 Hz (along z)*

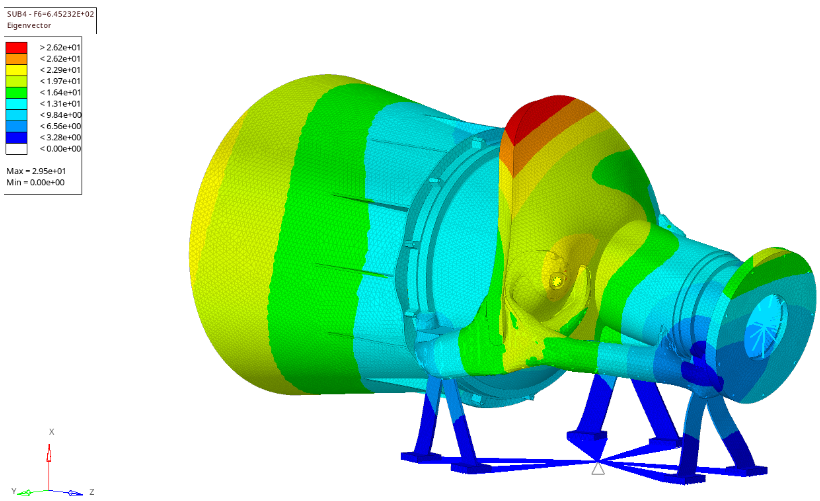

(c) *Frequency #6: 645.2 Hz (along x)*

Figure 5.30: 2nd Lattice Optimization: modal participation along the three main directions

As we can immediately see from the table above, both the values of the frequencies and their modal participation along the three axis increase considerably, even exceeding the results of the previous case and touching those of the topological optimization with polyNURBS. In fact, we went from 359.1 to 645.2 Hz in x, from 127.7 to 229.2 Hz in y, from 189.5 to 289.9 Hz in z).

The images show the behavior of the structure subjected to the first three frequencies with modal participation along x, y and z (scale factor of 2): there are evident similarities with those of the previous case and with the baseline, demonstrating the reliability of the results.

Thanks to the graph below, we have a more immediate and complete view on the values of the resonance frequencies for the cases seen so far. As previously mentioned, it is evident that the lattice optimization case considering the skin of the design space, has the highest frequency values, very similar to those obtained from the structure containing the polyNURBS.

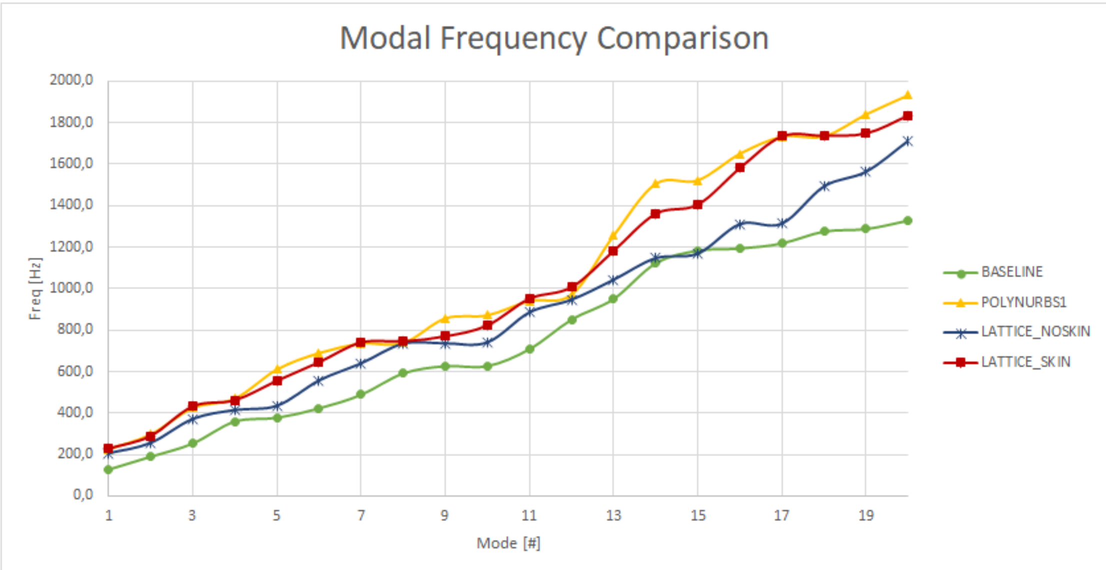

Figure 5.31: Modal frequency comparison: baseline, polyNURBS and lattice with and without skin

These results are really good, as this second lattice optimization shows great improvements both in terms of stiffness (displacement and stress) and in terms of resonant frequencies, compared to the baseline. This improvement is given precisely by the presence of the external skin of the lattice structure, which allows a more precise contact between the design and the non-design space.

The last data to consider, no less important than the previous ones, is the total mass of the structure. In the previous case we saw a reduction in mass due to the insertion of the lattice structure within the continuous volume of the design space.

Now, by considering the outer skin too, we certainly have a higher mass value: more precisely we get a total mass equal to 7.97 kg, which is in any case less than the starting value of the baseline. The image below highlights this comparison between the different mass values for the considered cases:

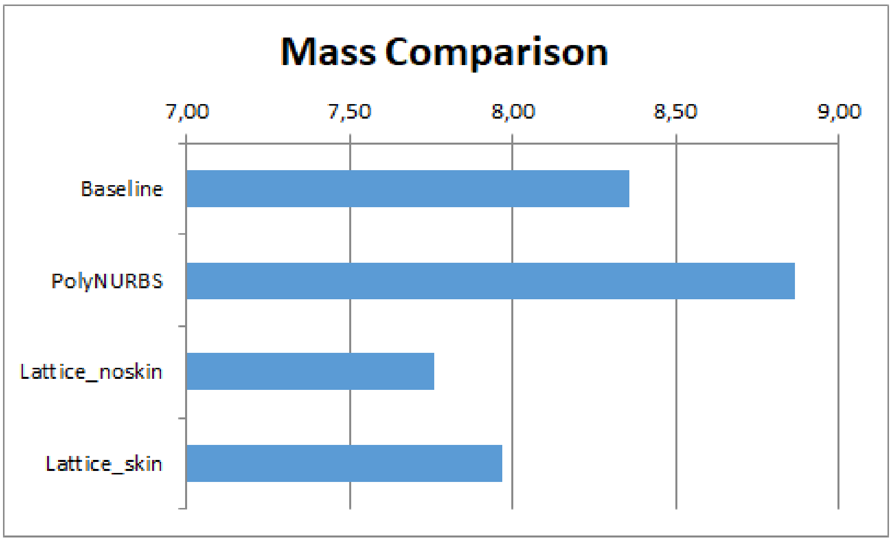

Figure 5.32: Mass comparison: baseline, polyNURBS and lattice with and without skin

Summarizing what has been said so far, this second lattice optimization allowed us to obtain a structure with higher performances and reduced mass compared to the starting one.

Once all the performances and characteristics of our new lattice structure are analyzed, all that remains is to carry out the second phase of the lattice structure optimization, with the aim of sizing the individual BEAM elements, so as to have different diameters and lengths. To do this, it would be enough to re-run an optimization on the file "*filename_lattice.fem*", but before we must review and redefine the optimization responses, constraints and objective, so a modification to some input data is necessary. These changes are made by directly editing the FEM file within a text reader. A single design variable (DESVAR) is automatically created for each BEAM elements representing the radius of all the beam cross sections at the joint.

In this case we act, above all, by modifying the responses (DRESP1 and DRESP2) which have syntax errors. This is because, after the first optimization, FREQ type responses is created with no indication of the number of modes to analyze: ten modes have been implemented. Besides, for the response on the compliance index, it is necessary to redefine the function that regulates the calculation, acting on the corresponding DRESP2.

After the necessary changes to allow the software to start the second phase and so conclude the lattice optimization, starting a second optimization process, we obtain an optimized lattice structure that presents BEAM elements with different properties. This is due to the fact that the previously defined parameters, relating to the dimensions of the one-dimensional elements, are now considered. We obtain a "*filename.prop*" file, which contains all these different properties and indicates, for each BEAM element, the radius values.

```
$HMNAME PROP                   29"PBEAML_29" 3
$HWCOLOR PROP                  29      37
PBEAML  29             1         ROD
+, .6921616, 0.0,, 1.0, .3543867392
$HMNAME PROP                   30"PBEAML_30" 3
$HWCOLOR PROP                  30      40
PBEAML  30             1         ROD
+, .57144861696, 0.0,, 1.0, .57144861696
$HMNAME PROP                   31"PBEAML_31" 3
$HWCOLOR PROP                  31      41
PBEAML  31             1         ROD
+, .57144861696, 0.0,, 1.0, .6921616
```

Figure 5.33: Some lines of the "*filename.prop*" file

For example, the BEAM 29 element has a radius of 0.6922 mm, the BEAM 30 element has a radius of 0.5714 mm and finally the BEAM 31 element has a radius of 0.5714. The length is calculated later, as we had defined an aspect ratio of 0.1, so the three BEAM elements measure respectively 6.922 mm, 5.714 mm and 5.714 mm.

One way to have an immediate view of the arrangement of the BEAMs based on the radius of the cross section, consist in mapping this parameter. To do this we need to import the "filename_optimized.fem" file, containing the lattice structure with the new properties, into HyperWorks.

Going to isolate the BEAMs and opening the Matrix Browser, we can view various parameters, including the radii of all these elements. Selecting all of them and following the selection path "elements> properties> pbeamlDIM1A" we obtain, for each BEAM, the value of the respective radius. At this point, going to perform a contour of this parameter, we obtain the distribution shown in the image below:

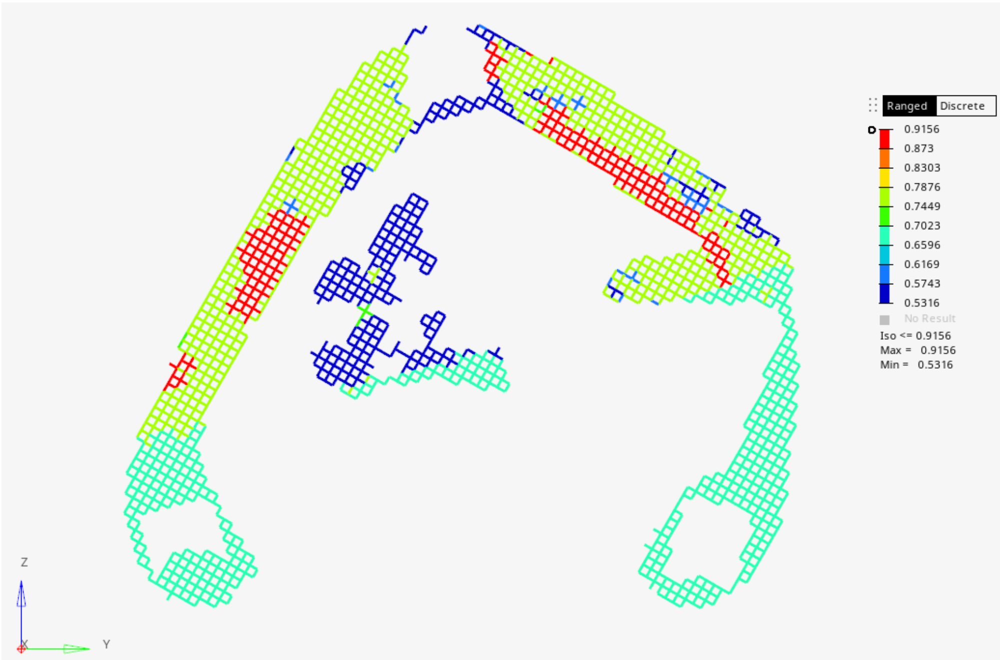

Figure 5.34: Radii distribution contouring after 2nd phase of lattice optimization

As can be seen from the image, the BEAMs radii range goes from a minimum of 0.5316 mm (blue zone) to a maximum of 0.9156 (red zone). This distribution indicates a presence of larger radius elements in the two central areas of the lattice arms. Instead, in the three parts of the lattice structure separated by the two main arms, elements with a smaller radius are inserted. We remind you that this arrangement follows the options entered during the optimization setup phase.

The final stage of the design is to find a way to make that structure printable. To do this we must find a way to convert all the one-dimensional BEAM elements into cylindrical solid elements, which can be exported like a CAD or STL file type.

For this last part of the project we will need another output file from the second phase of the optimization, that is the one with the name of "filename_optimized _tetsplt.fem". This file is the result of imposing YES to the TETSPLT option to turn on the splitting of all non-design or solid elements to TETRA elements for further usage in 3D printing software.

5.4 Preparation of the Lattice Structure for 3D Printing

As we see, the result of the optimization is a lattice structure formed by many one-dimensional BEAM elements, defined by their only length. The radii deriving from the size optimization are only the theoretical ones, so they do not have a practical function in the structure. In fact, if we try to export the geometry as an STL file, the lattice is not considered.

The ultimate objective of this study is to find a solution that allows us to derive a three-dimensional solid geometry from this set of one-dimensional BEAM elements. So it is necessary to develop a process, through one or more tools, to convert the FEM file into an STL file, that can be printed.

To achieve this goal we have thought of three possible alternatives, which have different aspects and methodologies:

- Altair Inspire, by taking the solid structure in polyNURBS and manually recreating the lattice structure, which will only be an interpretation of the one obtained following the lattice structural optimization seen in the previous paragraph;

- Materialise 3-Matic, through an automatic conversion of the entire one-dimensional lattice structure, which will then follow the results of the lattice optimization;

- Altair HyperWorks, by creating an STL file through a custom procedure in TCL language, using Altair Compose too.

Let's now analyze them in detail and then summarize the pros and the cons of these three different solutions.

5.4.1 Solution #1: Lattice Interpretation using Inspire

Regarding the creation of a solid lattice structure using Altair Inspire, we start from the polyNURBS structure deriving from the last topological optimization (see figure below).

As we have already said, in this case we cannot directly import the last seen structure determined by the lattice optimization, but we can create it manually, interpreting the original one.

Figure 5.35: PolyNURBS optimized design space structure

This lattice creation is done through the use of Inspire PolyMesh panel.

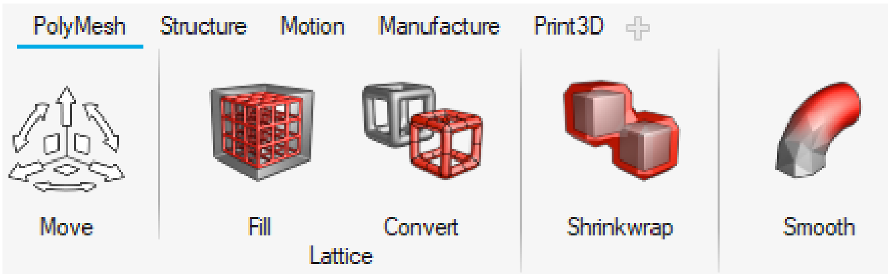

Figure 5.36: PolyMesh panel

We use the Fill tool to convert the solid part to a unit cell lattice and to do this we have to:

1. Select the solid part we want to fill with the lattice;
2. Select the shape of the reference system, in our case "Box shape";
3. Select a lattice cell type (SC-BCC: Simple Cubic Body Centered Cubic) and change the unit cell dimension (5 mm) and beam radius (0.5 mm) as desired (we made an average of the values obtained in the previous paragraph);
4. Click Create.

Then, we use the Convert tool to create polyNURBS surfaces from the unit cell lattice.

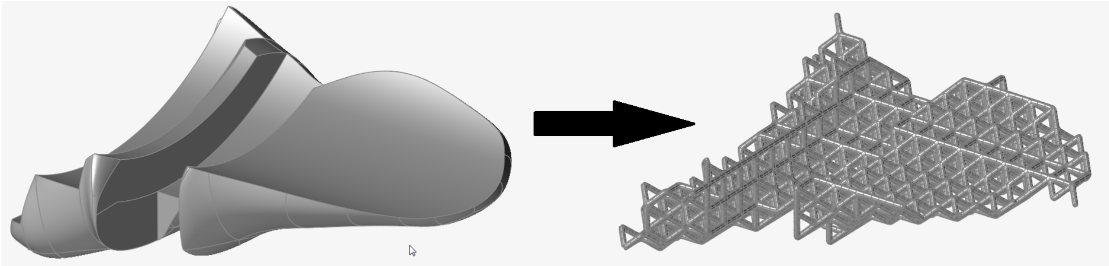

Figure 5.37: PolyNURBS structure to lattice

Once the lattice structure has been created, the polyNURBS are converted from solids to surfaces, which are connected with the lattice. Then the rest of the structure is imported and connected as well (i.e. everything that is not design space).

The PROS of this solution consist in:

- Easy control of lattice creation, by selecting shape and dimensions of the cell;
- It is a very intuitive process.

On the other hand, the CONS are:

- Manual conversion of the structure, with the possibility of making errors;
- Lattice structure is only an interpretation of the optimized one;
- We can't create elements of different sizes ora dimensions;
- Too large file to manage.

5.4.2 Solution #2: Lattice Conversion using 3-Matic

Let's now analyze the case in which Materialise's 3-Matic is used. Currently it is the only software that can read an OptiStruct FEM file and properly interpret our tapered BEAMS which are formed in lattice optimization. To use this tool properly, we need the "Remesh" license to open a FEM file and the "Lattice" license to convert the lattice structure into an STL file.

The solution procedure through the use of 3-Matic is described only for notional purposes: we know that it exists and that through simple steps we can obtain a structure ready to be printed in additive manufacturing. The steps to take are as follows:

1. Import the lattice FEM model "filename_optimized_tetsplt.fem" derived from previous sizing optimization, selecting the "Import graph mesh" option to read 1D elements correctly (if everything is done correctly, the solid elements are in the Surface List and the 1D lattice elements in the Graph List);

2. Convert the FEM file to an STL, by clicking on the tab labeled “Lattice” and going to "Convert Lattice to Mesh" button. Select the "Graph List" to convert the 1D elements in surfaces;

3. Improve the mesh quality and reduce the STL file size. There are different functions we can use to do this, starting from the "Smooth" option in the "Fix" tab, through which we can decrease “noise” in the mesh and make it smoother and then "Quality Preserving Reduce Triangles" in the "Remesh" tab to reduce the file size and number of facets;

4. Run an automatic mesh diagnostic following this path “Fix Tab > Fix Wizard > Diagnostics > Update";

5. Once 3-Matic finish to generate the surfaces for the lattice, we can export the STL file. Go to "File > Export > STL", select the newly created part that has the lattice geometry in the “Surface List” and click on Apply.

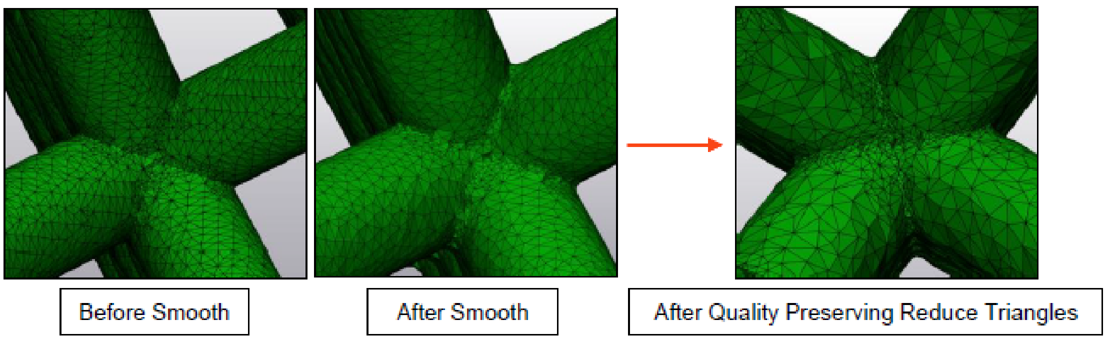

Figure 5.38: Mesh improving with 3-Matic tools

The PROS of this solution are:

- Automatic conversion of the structure, by directly importing it;
- Lattice shape is the same as the optimized one;
- Possibility to improve the mesh of the lattice structure, also going to reduce the size of the STL file.

The CONS, instead:

- There are a lot of controls for the lattice creation;
- A lot of licenses are required to use the software.

5.4.3 Solution #3: Custom Lattice using HyperWorks

1. Load "filename_optimized.fem" file derived from the second iteration lattice results and isolate BEAMs to convert;
2. Load TCL file «SolidConeData.tcl» in HyperWorks;
3. Export a CSV file from Matrix Browser (eg. Data.csv);
4. Update "Lattice_Macro.oml" in the I/O section and run Compose;
5. Update the name from "lattice.tcl.csv" to "lattice.tcl" and load this file in HyperWorks;
6. Check the output in the STL file.

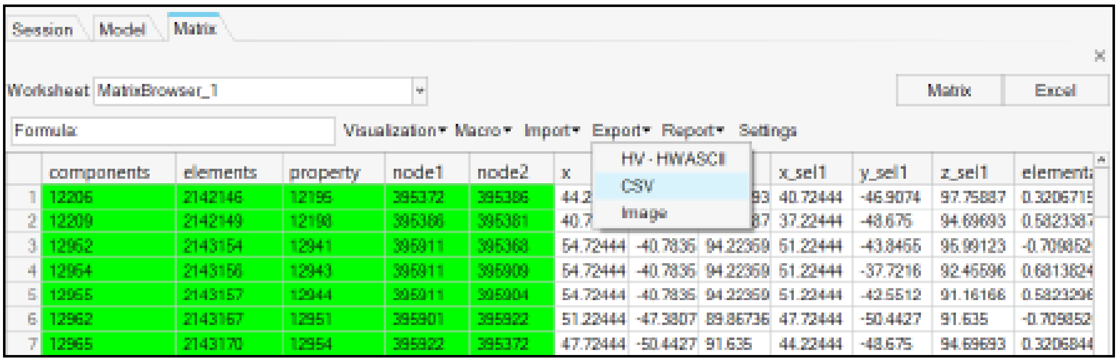

Figure 5.39: CSV file from Matrix Browser

If we want to obtain a CAD model, after these passages we have to:

1. Load the STL in Inspire and smooth the triangle mesh if needed;
2. Use "Fit" tool in PolyNurbs panel and export your model as CAD file.

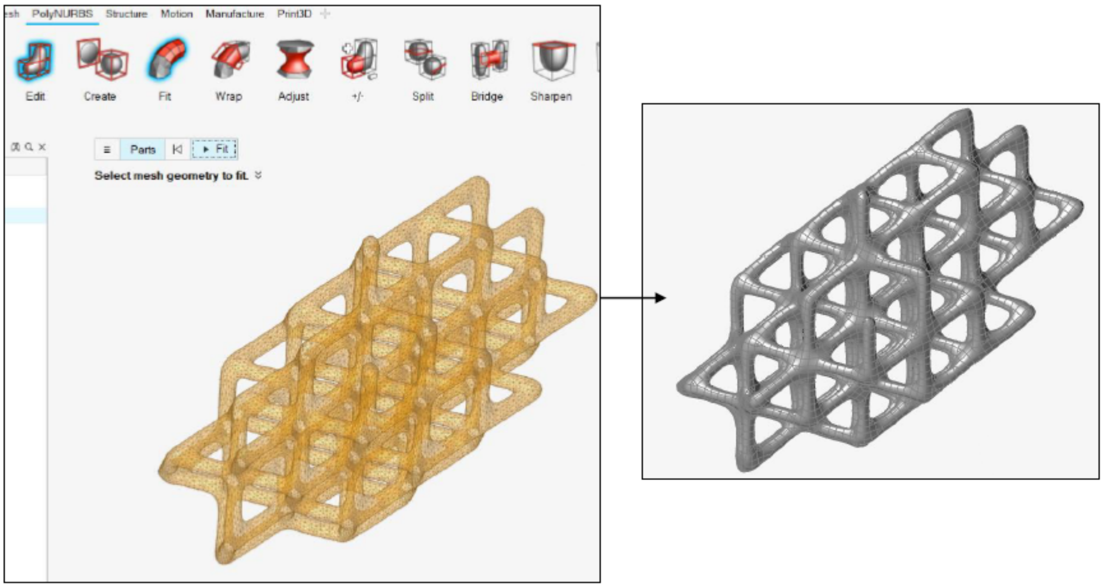

Figure 5.40: Fit tool in PolyNURBs panel

The PROS of this solution is that we have a customize and controlled procedure, but the CONS consists in the difficulty and intricacy of the process.

So if we want to draw a conclusion on the method to be used to give three-dimensionality to the BEAM elements, in order to print the lattice structure, the best method is certainly the second one by using 3-matic, for ease of use and results obtained. Immediately after, surely, we can opt for the third method, as it allows to obtain good results even if not in an immediate way. The last way to go is absolutely the first one with Inspire, as it does not allow us to have a faithful result to the optimization and the management of the structure becomes complicated, due to the large size of the output file.

Chapter 6

Conclusions

Once we see in detail all the steps that led us from the starting ribbed structure to the last result containing the lattice structure that we are now able to import into a 3D printing tool to be produced, let's try to make a summary of all the highlights and understand what are the advantages and disadvantages of using lattice optimization to achieve a lighter structure.

First of all, to get a complete picture of the situation, let's see how the mass and performances (displacement, static stress and resonance frequencies) of the various optimization steps vary, thanks to the summary table below:

Optimization Step		Baseline	PolyNURB	Lattice	Lattice (skin)
Mass [kg]		8.36	8.86	7.76	7.97
Displacement [mm]	**X**	0.122	0.037	0.065	0.053
	Y	0.483	0.181	0.186	0.166
	Z	0.313	0.105	0.154	0.120
Static Stress [$N/mm2$]	**X**	67.6	24.5	75.6	38.8
	Y	151.0	98.3	126.0	89.8
	Z	66.6	68.7	113.0	61.2
First Resonant Frequency [Hz]	**X**	359.1	689.3	557.4	645.2
	Y	127.7	225.5	206.2	229.2
	Z	189.5	297.0	256.5	289.9

Table 6.1: Performances and masses comparison

As is evident from the table, if our goal was only to maximize the resonance frequencies, we could have stopped at the topological optimization, that is, after having obtained the polyNURBS design. This is because for that step we obtain the highest frequency values ever.

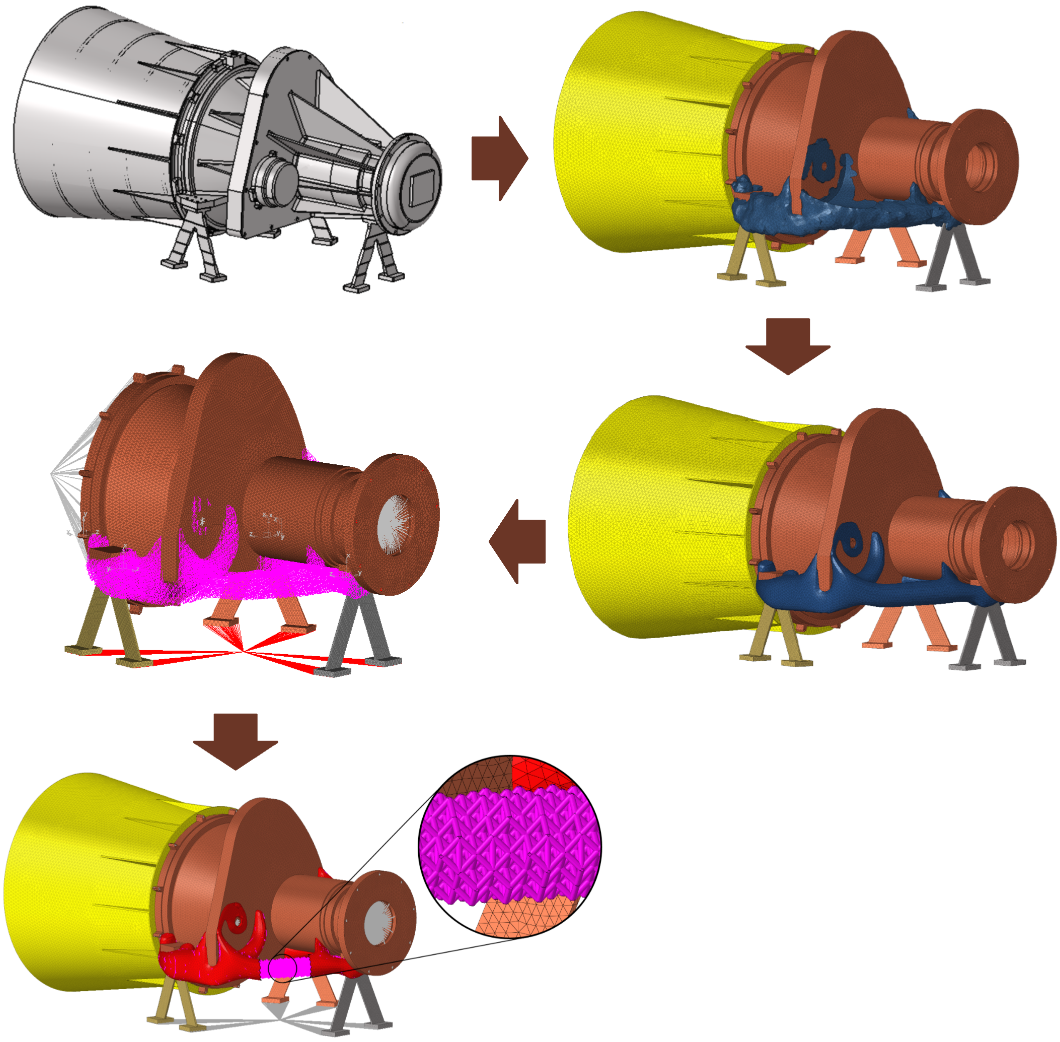

Figure 6.1: Main changes of the structure during the study

But since our goal is to maximize the resonance frequencies, minimizing the mass (most important factor in space structures) and increasing the stiffness of the structure, the best values are certainly those obtained from the lattice optimization considering the outer skin, i.e. the last result obtained. However, it must be emphasized that the values of the two results are almost the same.

In the previous image we can observe the five main optimization steps (on the table there are only four, as the second and the third have the same performance values), during which the structure undergoes significant geometric changes, which modify its mass and performance:

1. Baseline: the starting structure consists of two ribbed conical supports;
2. Topology optimization result: topologically optimized design space with a messy and jagged structure;
3. PolyNURBS application: topologically optimized design space with a smooth and rounded polyNURBS structure
4. Lattice optimization result: lattice optimized design space excluding the outer skin;
5. Outer skin application: lattice optimized design space including the outer skin as an interface to the non-design space.

So, at the end of the whole project, the lattice optimization is advantageous as it led to excellent results both from the point of view of performances and from the point of view of mass. Then, we find and define a way to convert one-dimensional BEAM elements into a solid structure that can be saved as an STL file and produced with additive manufacturing technology.

Regarding this last point, although already explained in the previous chapter, let's summarize the advantages and disadvantages of each method, putting them in order from best to worst:

	PROS	CONS
3-Matic	Automatic conversion of lattice Lattice shape is the same	Lots of controls and funcions
HW	Custom and controlled procedure	Intricate and difficult process
Inspire	Easy controls for lattice creation Very intuitive process	Manual conversion of lattice Lattice is an interpretation Too large file to manage

Table 6.2: Lattice production processes: pros and cons

So the best way to prepare a lattice structure for additive manufacturing is to use Materialise's 3-Matic tool. It allows us to maintain the same shape and dimensions obtained after the optimization.

Bibliography

[1] Istituto della Enciclopedia Italiana fondata da Giovanni Treccani S.p.A. *La Treccani*. URL: https://www.treccani.it/ (cit. on pp. 1, 9).

[2] Altair Engineering Inc. *Practical Aspects of Structural Optimization - A Study Guide*. 2018 (cit. on pp. 1, 13).

[3] M. Hirz W. Dietrich A. Gfrerrer J. Lang. *Integrated Computer - Aided Design in Automotive Development*. 2013 (cit. on p. 2).

[4] Altair Engineering Inc. *Practical Aspects of Finite Element Simulation - A Study Guide*. 2019 (cit. on p. 4).

[5] Axel Schumacher. *Optimierung mechanischer Strukturen - Grundlagen und industrielle Anwendungen*. 2013 (cit. on p. 10).

[6] Inc Altair Engineering. *Altair HyperWorks 2020.1 Help*. URL: https://2020.help.altair.com/2020.1/hwdesktop/altair_help/index.htm (cit. on pp. 17, 107).

[7] Wikipedia. *Wikipedia - The Free Encyclopedia*. URL: https://en.wikipedia.org/wiki/Main_Page (cit. on pp. 21–23).

[8] Vasili Karneichyk. *Infrared And Thermal Imaging Design*. URL: https://www.opticsforhire.com/blog/design-of-ir-lenses (cit. on p. 21).

[9] M. Ilkan K. Fuladlu M. Riza. «THE EFFECT OF RAPID URBANIZATION ON THE PHYSICAL MODIFICATION OF URBAN AREA». In: *S.ARCH 2018 - The 5th International Conference on Architecture and Built Environment with AWARDs*. Venice, Italy, May 2018 (cit. on p. 24).